CONTROLLING DYNAMIC TORSION LOADING

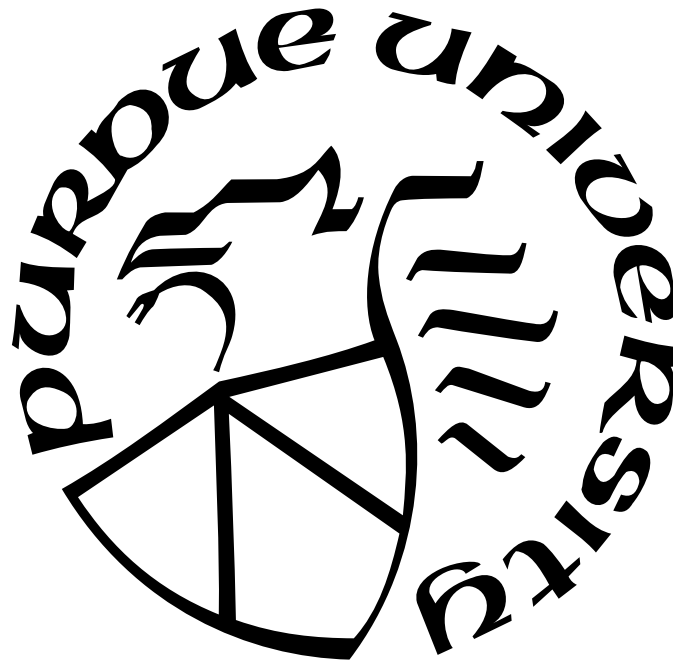by

Benjamin J. Claus

A Dissertation

Submitted to the Faculty of Purdue University

In Partial Fulfillment of the Requirements for the Degree of

Doctor of Philosophy

School of Aeronautics & Astronautics

West Lafayette, Indiana

December 2018

THE PURDUE UNIVERSITY GRADUATE SCHOOL
STATEMENT OF DISSERTATION APPROVAL

Dr. Weinong Chen, Chair

    School of Aeronautics and Astronautics

Dr. Michael Sangid

    School of Aeronautics and Astronautics

Dr. Wenbin Yu

    School of Aeronautics and Astronautics

Dr. Tyler Tallman

    School of Aeronautics and Astronautics

Approved by:

    Dr. Weinong Chen

        Head of the School Graduate Program

This work is dedicated to:

Those who believe in science and To the order of things,

Those who do things the correct way, and Those who believe in the truth;

Those who believe in the pursuit of knowledge, and The resulting happiness;

Those who express humility in their work, and do not push Their shortcomings onto others;

Those who are willing to help others, Even when there is no return;

and finally,

Those who face adversity in their work, and lose motivation to continue.

This work is also dedicated to my parents and my brothers, and my love.

Without her, I would not have continued.

Without her, I would not have finished.

ACKNOWLEDGMENTS

PREFACE

The full potential for research, science, mathematics, and engineering cannot be reached without an understanding that they are not separate concepts. While an engineer may be expected to be familiar with a single field, a scientist must be familiar with any and all fields related to their work.

An experiment might not be understood without mathematics or analysis. This idea applies to both the apparatus and the data measured during an experiment. Isolation to either purely experimental or purely analytical (or numerical) approaches will not result in a viable and sustainable solution. Isolated approaches often lead to the development of specialized applications that are inflexible and rely on assumptions that restrict the use to very specific cases.

A scientist must be willing to not only approach an unexplored problem, but also to expand their knowledge to account for the unknown, whether previously published in a different field, or wholly undiscovered. Denial of the need to understand other topics and other fields will ultimately lead to lost opportunities and stagnation of research.

TABLE OF CONTENTS

LIST OF TABLES

LIST OF FIGURES

Figure   Page

Figure   Page

SYMBOLS

C_B	Bar wave speed (also longitudinal wave speed)
C_S	Shear wave speed
ϵ	Normal strain
$\dot{\epsilon}$	Normal strain rate
E	Young's modulus
G	Shear modulus
μ	Shear modulus
σ	Normal stress
τ	Shear stress
γ	Engineering shear strain
$\dot{\gamma}$	Engineering shear strain Rate
R_O	Outer radius
R_{SO}	Specimen outer radius
R_I	Inner radius
R_{SI}	Specimen inner radius

NOMENCLATURE

CA   cyanoacrylate

PDMS   polydimethylsiloxane

PETN   pentaerythritol tetranitrate

ABSTRACT

Author: Claus, Benjamin J. PhD
Institution: Purdue University
Degree Received: December 2018
Title: Controlling Dynamic Torsion Loading
Committee Chair: Wayne Chen

Two new Kolsky bar techniques were developed to address a lack of capability in existing torsion Kolsky bar experiments. The side-impact torsion Kolsky bar provides for controllable duration, amplitude, and shape of the incident torsion wave, allowing for more ideal conditions during dynamic torsion experiments. The technique provides an ideal platform to study dynamic friction as well as dynamic shear of a material. The technique makes use of soft pulse shapers to convert longitudinal loading into torsional loading. The technique also brought forth a secondary technique to allow combined dynamic compression and dynamic torsion for soft materials. The combined loading was applied to study both shear properties and the friction behavior of a particle composite, which was imaged using x-ray phase contrast imaging. The same composite was studied with different surface conditions on the side-impact torsion Kolsky bar to discover the differences in behavior brought about by the choice of manufacturing method. The composite showed different friction behavior to metallic materials, and exhibited much more shear deformation during the experiment. The composite was also prone to surface evolution, leading to complex friction behavior.

1. INTRODUCTION

The Kolsky bar apparatus is an extremely flexible technique that has been used to characterize material properties and material behavior under dynamic conditions for nearly every type of material. Whether for stress-strain response at a given strain rate, attenuation of impulses, or propagation of failure, the Kolsky bar apparatus has been modified time and again to suit the needs of the study. Based upon the one dimensional wave equation, stress waves within the elastic range of the bar material may be used to not only load a specimen, but to also determine the response of the specimen. The one dimensional nature of the experiment allows for useful quantities such as stress, strain, strain rate, displacement, and force experienced by the specimen to be determined solely from the stress state in the Kolsky bar apparatus.

This type of apparatus is a necessity not only for studying material properties, but also for studying interfacial properties which are inherently dynamic. An interface is formed between two bodies that are in contact. How these bodies behave depends on the properties of the material of both bodies, which may be similar or dissimilar. Furthermore, advanced materials such as composites contain components that are different materials. These components are in contact and bound together, thus forming interfaces. In these materials, it is not only the material properties of the constituents, but also the interfacial properties that determine the bulk response of the composite.

1.1 The Kolsky Bar Technique

The Kolsky bar, also known as the Split-Hopkinson bar, is an apparatus designed to study the behavior of materials under dynamic conditions [1,2]. The premise of the experiment is that a wave is generated under controlled conditions and propagates

through an incident bar. After a period of time, the wave encounters the specimen at the end of the bar. Under this condition, a portion of the wave transmitted through the specimen and the remainder is reflected back into the incident bar. The portion of the wave that is transmitted into the specimen then propagates through the specimen and meets a transmission bar at the other end. Here, the same phenomenon occurs, and a portion of the wave is transmitted into the transmission bar.

Relative to the wave speed of the material, the specimen is short, requiring only several micro-seconds for a wave to traverse the length of the specimen. This means the waves within the specimen interact with the incident wave to produce a specific reflected waveform. Similarly in the transmission bar, the transmitted waveform is specific to the specimen. These three quantities, the incident wave, the reflected wave, and the transmitted wave are measured as a function of time and processed to produce the stress-strain response of the specimen.

1.1.1 The (One Dimensional) Wave Equation

The Kolsky bar experiment is firmly tied to the one dimensional wave equation (Equation 1.1). As opposed to higher dimensional theories with more degrees of freedom, the one dimensional wave equation has only one degree of freedom, one strain component, and one stress component. The application of this equation to the Kolsky bar experiment has several implications and restrictions on the exact method being employed. The most important restriction is that the waves within the apparatus are non-dispersive, or that the waveforms do not change shape or amplitude during propagation through a continuous section of material. In real materials, non-dispersive waves are non-trivial to generate, with the Kolsky bar being one of the simplest methods.

By requiring non-dispersive waves, the geometry of the apparatus itself becomes limited. Large diameter Kolsky bars tend to suffer from dispersion due to Poisson expansion and contraction at the outer surface of the bars. Furthermore, the length

of the striker is recommended to be no shorter than three times the bar diameter (as a rule of thumb).

The one dimensional wave equation relies on an assumption that drastically simplifies the constitutive equations. This assumption also results in the requirement that the measured waves be non-dispersive. For a linearly elastic material, the constitutive equation is simply a product of a matrix of stiffnesses and a vector of strains. Being one dimensional, the constitutive relation for this form of the wave equation has only one stiffness value, one strain value, and is dependent only upon the displacement (u) and the longitudinal wave speed (C_B).

$$\frac{\partial^2 u}{\partial t^2} = C_B^2 \frac{\partial^2 u}{\partial x^2} \tag{1.1}$$

The simplification of the constitutive relation has profound consequences for the behavior of a wave propagating through a one dimensional wave guide. Here, both wave speed relations in the frequency domain (phase speed and group speed) have identical values and are independent of frequency. In other words the waves described by the one dimensional wave equation are non-dispersive. Furthermore, with a simple solution, the waves within a real bar are easily described and processed using simple relations between stress and particle velocity, all thanks to the one dimensional wave equation.

The basic relation between stress and velocity is derived from simple manipulation of the wave equation and conversion into discrete quantities. Using the relationship between wave speed (C_B), stiffness (E), and density (ρ), the strain gradient ($\epsilon_{,x}$) may be converted into a stress gradient ($\sigma_{,x}$) (Equation 1.2). Considering the partial derivatives as discrete quantities provides a basic stress-velocity relationship that describes how a wave is generated within a one dimensional wave guide (Equation 1.3). Although this provides an approximation of the amplitude of a compression (or tension) wave as a function of the particle velocity, the shape and duration of the wave cannot be determined without contact laws and detailed geometric descriptions.

$$\rho\frac{\partial \dot{u}}{\partial t} = \rho C_B^2 \frac{\partial^2 u}{\partial x^2} = \rho\frac{E}{\rho}\frac{\partial^2 u}{\partial x^2} = E\frac{\partial \epsilon}{\partial x} = \frac{\partial \sigma}{\partial x} \tag{1.2}$$

$$\rho\frac{\Delta \dot{u}}{\Delta t} = \frac{\Delta \sigma}{\Delta x} \rightarrow \Delta\sigma \approx \rho\frac{\Delta x}{\Delta t}\Delta\dot{u} \approx \rho C_B \Delta\dot{u} \tag{1.3}$$

The interaction of a wave with an interface can be described using force equilibrium principles and the impedance of the materials involved. For an incident stress wave (σ_I), the reflected (σ_R) and transmitted (σ_T) stress waves (Equations 1.5 and 1.6) are determined using the impedance ratio (r) between the materials (Equation 1.4), which is the ratio of density (ρ), wave guide area (A), and wave speed (C). These equations clearly show that for a free end, the impedance ratio is near zero, and the wave will be fully reflected, with the stress amplitude changing sign. Following Equation 1.3, the change in direction accompanied by a change in sign of the stress wave means the particle velocity remains in the same direction. However, for an infinite impedance ratio, representing a fixed boundary, the particle velocity will reflect, producing a stress with the same sign. In this case, the particle velocity changes sign, meaning the bar is now traveling in the opposite direction. This is the principal behind the single loading device discussed in Section 1.1.4.

$$r = \frac{\rho_T A_T C_T}{\rho_I A_I C_I} \tag{1.4}$$

$$\sigma_R = \sigma_I \cdot \frac{r-1}{r+1} \tag{1.5}$$

$$\sigma_T = \sigma_I \cdot \frac{A_I}{A_T} \cdot \frac{2r}{r+1} \tag{1.6}$$

The Kolsky bar experiment itself does not require the previous equations, but the following data reduction process relies on observations from the equations. For a specimen between the incident and transmission bars, Equations 1.5 and 1.6 still hold. Thus, from the measured incident, reflected, and transmitted waves, the particle

velocities of the ends of the incident bar ($\dot{u}_1$) and transmission bar ($\dot{u}_2$) may be found using Equation 1.3. The strain rate of the specimen ($\dot{\epsilon}_S$) is then determined by the relative particle velocities of the bars and the length of the specimen (L_S, Equation 1.7).

$$\dot{\epsilon}_S = \frac{\dot{u}_2 - \dot{u}_1}{L_S} = \frac{\dot{u}_T - \dot{u}_I + \dot{u}_R}{L_S} = C_B \cdot \frac{\epsilon_T - \epsilon_I + \epsilon_R}{L_S} \tag{1.7}$$

The stress within the specimen (σ_S) is related to the transmitted wave through the ratio of areas between specimen (A_S) and transmission bar (A_T, Equation 1.8). Lastly, the strain in the specimen (ϵ_S) is determined through time integration of the strain rate (Equation 1.9).

$$\sigma_S = \sigma_T \cdot \frac{A_T}{A_S} \tag{1.8}$$

$$\epsilon_S = \int_0^t \dot{\epsilon}_S(\tau)\, d\tau \tag{1.9}$$

1.1.2 Compression

The most common type of Kolsky bar is the compression Kolsky bar which fundamentally consists of three components: a striker, an incident bar, and a transmission bar (Figure 1.1). There are many methods for launching the striker into the incident bar, with the gas gun being a common approach. Compression Kolsky bar experiments have an incident wave that is in compression, a reflected wave that is in tension, and a transmission wave that also in compression. The total particle velocity of the incident bar where the sample is located is higher than the particle velocity of the transmission bar where the sample is located. The result is that the sample is under a net state of compression. Real materials experience Poisson expansion, which may place certain regions in tension. However, assumptions that reduce the complexity of
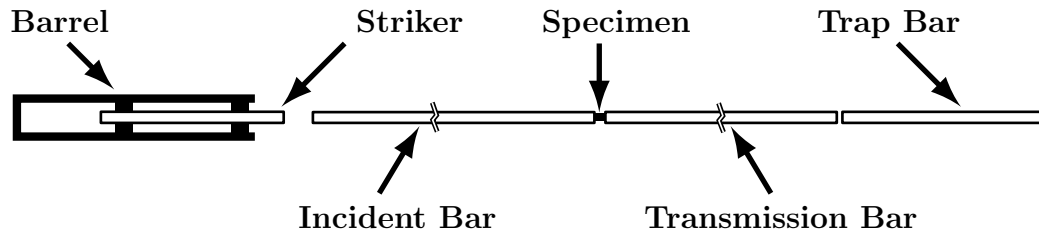
Figure 1.1. Simplified schematic of a gas-gun operated compression Kolsky bar.

processing experimental data prevent these states from being actively measured and studied.

The geometry of a compression specimen is simplistic, but has a restriction. Standards for material testing often require an aspect ratio greater than one, which provides a large region for measuring Poisson expansion and reduces the effect of stress concentrations from the ends. For Kolsky bar experiments, the length of the specimen directly influences the strain rate. Furthermore, the length of the specimen also directly influences the particle velocity of the incident and transmission bars. Logically, if the specimen were long enough, the time delay resulting from propagation of the wave across the specimen would cause the transmitted waveform to be out of sync with the incident and reflected waveforms. This concept is referred to as "dynamic equilibrium", where the particle velocity of the incident and transmission bars must be nearly equal. In the case of a long specimen, the particle velocities on each side of the specimen would not be indicative of the velocity gradient with the specimen. Rather, there would likely be a wavefront somewhere within the specimen. The result is a false determination of the strain rate. Similarly for an incorrect incident waveform, certain components of the wave may be absorbed or attentuated by the specimen. Such is the case for brittle materials, where the specimen will fail without reaching a constant strain rate when loaded with anything but a triangular waveform [2].

Soft materials require special treatment, as Poisson's ratio is typically a large value near the isotropic maximum of one half (an exception to this is foam-like materials which may have a Poisson's ratio of zero). Soft materials also tend to have a low wave speed, meaning even the shortest of specimens may not reach dynamic equilibrium. Since the stress state in a real material with low stiffness is inherently not uniaxial and cannot be measured, the excess stress must be relieved. An annular shaped specimen is the typical solution to this problem with soft materials, which relieves radial stresses in the center of the specimen and hoop stresses near the outer edge of the specimen, both of which are generated by Poisson expansion [2, 3].

Compression experiments are by far the simplest to perform. The specimens are often cylindrical and short in length, and easy shape to manufacture. The apparatus requires minor alignment, and does not require special fixtures to maintain the specimen's position.

1.1.3 Tension

The tension Kolsky bar is nearly the exact opposite of the compression variant. The tension apparatus also has a striker, incident bar, and transmission bar (Figure 1.2). However, the striker may vary significantly from the compression variant. The common approach to generating a tensile wave within a bar is by impacting a flange with a tube. Another means is by firing a cylindrical striker inside of a hollow incident bar, but this method poses other challenges that are not entirely relevant to the function of a tension Kolsky bar.

Tension Kolsky bar experiments are often regarded as the most difficult of the Kolsky bar experiments, as attaching a specimen to the bars is not trivial. Stiff materials tend to break adhesive bonds due to strain incompatibility, strong materials have no adhesive equivalent in terms of bonding strength, and grips disrupt the waveforms. Needless to say, proper design of the apparatus will yield successful experiments. There are thousands of types of adhesives, only one of which is required
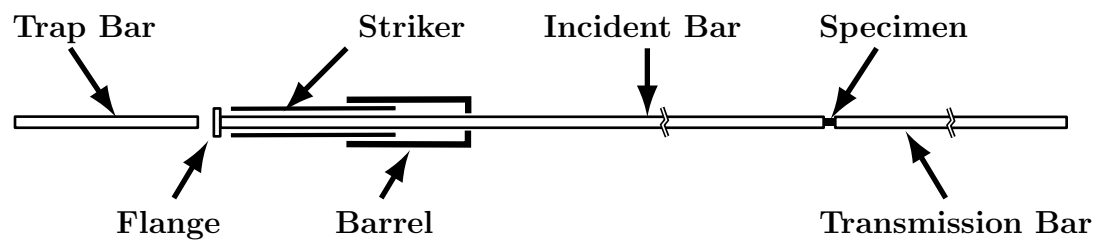
Figure 1.2. Simplified schematic of a gas-gun operated tension Kolsky bar.

for a successful experiment, this requires experimentation. Grips can be designed to have similar impedance to the bars, which means virtually all materials may be tested in the tensile mode. The exception, of course, is for very soft materials which will neither bond to adhesive nor stay within a grip when under strain. In this regard, torsion Kolsky bar experiments suffer from the same ailments when attaching a specimen to the bars.

1.1.4   Modified Kolsky Bars

The usefulness of the Kolsky bar apparatus has led to many developments to improve the effectiveness and usefulness of the experiment. An easy modification to make is to extend the length of the bars to prevent overlap of the waveforms. Unless cyclical loading is desired, techniques have been developed to stop loading of the specimen and to also prevent overlap of the waveforms.

While the length of the incident bar is fixed in relation to the maximum duration of loading as set by the maximum desired striker length, the transmission bar may be relatively short when coupled with a trap bar. This is possible because when the wave reaches the end of the transmission bar, the entirety of the wave is transmitted into the trap bar. Once at the other end of the trap bar, the wave is reflected into a stress of opposite sign, but the particle velocity remains in the same direction. Thus, the trap bar will separate from the transmission bar after the wave passes through. For tensile experiments, the trap bar is located at the striking end of the incident bar [2].

With a trap bar, the transmitted wave may be removed from the specimen, but the wave within the incident bar is still propagating. This wave may be either trapped with another trap bar, which is often impractical, or the particle velocity may be rectified into a particular direction. This technique is referred to as "dynamic recovery" and is achieved with a "single loading device". The single loading device has many purposes, the primary of which is to allow the specimen to be loaded only once.

However, the technique allows for tailoring the unloading of the specimen as well as controlling the duration of loading [4].

For a specimen with relatively low impedance as compared to the apparatus, the transmission bar may be removed entirely. This is a result of the fact that such a small portion of the incident wave is transmitted through the specimen that the particle velocity is immeasurable. Following with an assumption that the transmission side of the sample is fixed (i.e. the particle velocity is zero), the transmitted wave may be measured with a load cell. This modification significantly reduces the length of the Kolsky bar apparatus for facilities with limited space such as the Advanced Photon Source at Argonne National Laboratory [5].

1.1.5   Pulse Shaping

Despite state of the art practices, straight-on impact of two materials, even with perfectly parallel surfaces will generate non-dispersive waves. The dispersion is a result of wave propagation in real materials, where the speed at which any given frequency component of a waveform propagates is different. Thus, for bars made of stiff materials, the primary waveform contains frequency components at the lower end of the spectrum, but also contains high frequency components related to the stiffness of the material(s) [2].

Furthermore, achieving a constant strain rate as well as a state of dynamic equilibrium is non-trivial. However, these conditions may be met with the use of a pulse shaper. Unfortunately, not only is every material different, but most materials change behavior when the strain rate is changed [2,6]. For low impedance materials, a simple rectangular waveform is sufficient to produce a constant strain rate. The condition for dynamic equilibrium is inherently met with the use of a modified Kolsky bar, but must be double checked to prevent faulty conclusions.

For stiffer materials, the pulse shaper must provide the correct amount of elastic and plastic deformation to match the materials transmitted waveform. Some materi-

als require rectangular waveforms, some triangular, and others bi-linear. For elastic materials, the shape is determined by the response of the material, whereas brittle materials always require some form of triangular or bi-linear incident waveform.

Since controlling the loading conditions is desirable for developing new material models and validating numerical models, pulse shaping is all but required for Kolsky bar experiments. Furthermore, pulse shaping for tension and compression experiments is commonplace, but is nearly non-existent for the classical torsion Kolsky bars [7].

1.1.6 Imaging Techniques

New technology and the desire to understand how materials behave under dynamic conditions has led to the development and use of high speed imaging techniques. One rule of thumb is that as the sample gets smaller (or the magnification gets larger), the frame rate must increase proportionally. For moderately sized Kolsky bars (those with a diameter on the order of 20 mm or more), the required frame rate even for brittle materials does not exceed a few million frames per second. However, for smaller Kolsky bars, where the specimen is small, the frame rate must exceed the ratio of the event's speed to the specimen length. In other words, small samples may require frame rates in excess of two million frames per second. Examples are crack propagation and wave front tracking. On the other hand, bulk properties tend to occur on a longer time scale, only requiring up to a million frames per second. Phenomena that require this time scale include bulk motion, interfacial behavior, and rigid body motion (after a fracture event).

Conventional imaging makes use of a visible light source, whether from the front or back. For opaque materials, only surface detail may be examined. Thus, if a crack or other feature were to form internally, there is no way to observe the phenomenon. The Advanced Photon Source at Argonne National Laboratory provides a solution to viewing the inside of a specimen during dynamic loading. By generating x-rays,

which penetrate through the specimen, and converting those x-rays to visible light, the events that were otherwise hidden from view are now observable. The application of this imaging technique allows visualization of crack formation, wave propagation, and average interface motion. X-ray imaging can be tailored to form images or to study diffraction patterns in crystalline materials experiencing dynamic loading [5, 8–18].

1.2 Torsion Kolsky Bar Techniques

Torsion Kolsky bars differ greatly from the compression and tension variants. Although torsional loading involves rotation, the wave motion is still considered uni-axial. That is, the strain quantities exist along a single axis that is shared with the rotational quantities. Conventional torsion Kolsky bars also do not have a striker, and typically only have incident and transmission bars.

1.2.1 The Wave Equation in Shear

Unlike the wave equation for linear quantities (linear as in the quantities exist is Euclidean space), the wave equation in shear deals with rotational quantities (as in polar space, Equation 1.10). Similar to the one dimensional wave equation for linear quantities, torsional waves are non-dispersive. However, unlike real compression and tension waves, real torsion waves are also regarded as non-dispersive, where high and low frequency components of the bar rotation (θ) travel at the shear wave speed (C_S) [19].

$$\frac{\partial^2 \theta}{\partial t^2} = C_S^2 \frac{\partial^2 \theta}{\partial x^2} \tag{1.10}$$

The process of converting experimental measurements into meaningful quantities is identical to that for compression and tension experiments, except with a torque relation rather than a force relation. However, torsion experiments are more sensitive

to specimen geometry, as the shear stress and strain vary from zero at the center to the maximum at the outer radius of the specimen.

More details on data reduction of torsion Kolsky bar experiments are provided in Section 2.1.1.

1.2.2 Shear

One use for a torsion Kolsky bar is to study the shear properties of a material. These experiments require a single specimen to be fixed to the apparatus on both sides. The experiment is then performed and the data processed in the same fashion as compression and tension Kolsky bar experiments, where the transmitted wave represents the response of the specimen, and the incident and reflected waves represent the shear strain rate of the specimen.

1.2.3 Friction

The rotational nature of torsion Kolsky bars makes the apparatus favorable to studying friction as well. The duration of sliding is controlled by the total angle of rotation of the bar, which is in turn controlled by the duration and amplitude of the torsional wave. Compression may be applied to the specimen by either quasi-static or dynamic means to produce a desired stress state.

1.2.4 Compression-Shear

Friction inherently involves combined stress states (normal and shear) that may influence material behavior. Furthermore, real materials experience combined stress states in real applications. Thus, studying the effects of combined compression and torsion is of great interest, particularly for soft and/or volatile materials. Although a compression Kolsky bar may be modified to impart a static torsional stress, torsion Kolsky bars are better suited to providing either static or dynamic compressive

loading in combination with the dynamic shear loading. Adding this extra variable inherently complicates the experimental technique, but nonetheless provides more insight into the behavior of a material.

1.2.5 Pulse Shaping

Pulse shaping of conventional torsion Kolsky bars is virtually non-existent, and only used in a few cases for generating nominally rectangular waveforms [7, 20]. The rotational nature of the apparatus leaves little room for interfaces that would provide enough deformation of a pulse shaper to be useful. However, there is at least one technique that allows for pulse shaping torsional waveforms. This technique involves interrupting the wave guide with a tube [7]. Just like for the compression and tension Kolsky bars, the tube should provide a suitable amount of elastic and plastic deformation to appropriately shape the torsional wave. However, this technique does not work well with all forms of the torsion Kolsky bar, meaning many torsion experiments go without pulse shaping.

1.2.6 Types of Torsion Kolsky Bars

The Kolsky bar experiment, in any form, is highly flexible and may be modified to solve many problems. Specifically for the torsion variant, there are many possible ways to generate dynamic torsional loading. Some techniques depend upon quasi-static deformation or rigid body motion, while others utilize other dynamic phenomena such as longitudinal wave propagation or combustion of volatile materials to generate the torsional wave.

Stored-Torque

The stored-torque torsion Kolsky bar is perhaps the most fundamental of all of the torsion Kolsky bar variants, as only an incident and transmission bar are required
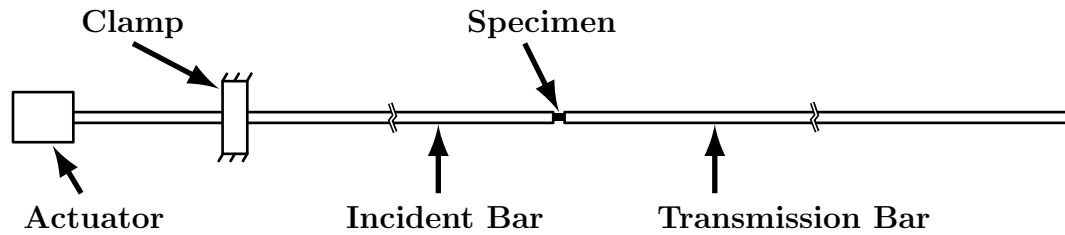
Figure 1.3. Simplified schematic of a stored-torque Kolsky bar. This apparatus relies on the quick release of a pre-torqued section of bar to generate a torsional wave.

[19–26]. This type of torsion Kolsky bar relies on a clamp to prevent the incident bar from rotating while a portion of the bar is being pre-loaded (Figure 1.3). Once the clamp is released, the torqued section releases the strain in the form of a torsion wave. The length of the pre-torqued section of bar directly determines the duration of torsional loading. Also, the amplitude of loading is determined by the amount of torque stored within the bar.

This method does not allow for fine control over the shape of the torsional wave. Different clamping methods may produce different rise times, but the wave form will be rectangular in nature unless the bar is physically shaped to produce a tailored waveform.

Eccentric Force

In mechanical systems, torque is often generated using one or more eccentric forces. The same is possible for dynamic experiments such as the torsion Kolsky bar, but loading must have a relatively fast onset in order to produce a sufficient rise time to elevate the strain rate within the specimen. An early approach to using eccentric forces made use of energetic materials and two tabs extending from the torsion bar (Figure 1.4a) [7]. Although the approach was capable of generating rectangular torsional waves with very fast rise times, timing the impact of reaction gases against the

Explosives

Torsion
Bar

Explosives

Impact
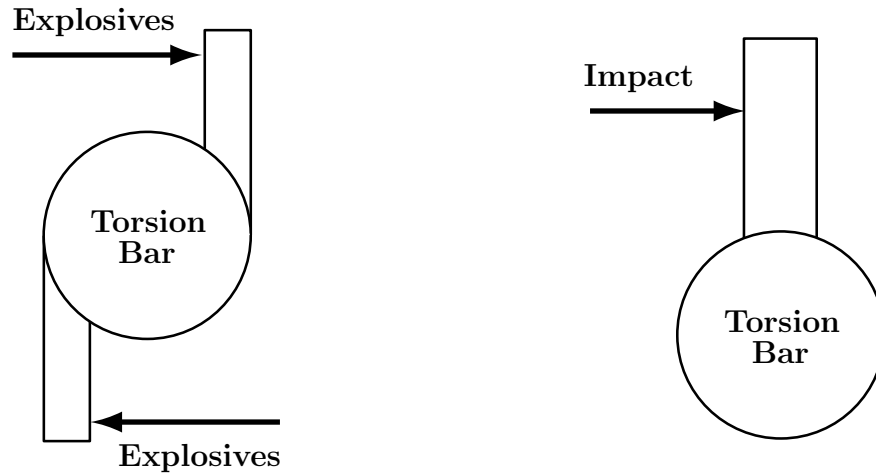
Torsion
Bar

(a) Simplified schematic of axisymmetric tabs that allow the detonation of explosives to generate a torsional wave.

(b) Simplified schematic of an eccentric tab that allows an external force (or stress wave) to generate a torsional wave.

Figure 1.4. Two styles of creating a torsion wave using eccentric forces.

two tabs proved to be difficult. The technique also made use of a special component to change the shape of the torsion wave before reaching the specimen.

A more mechanical approach to using an eccentric force to generate the torsional wave is to simply impact a striker against a tab affixed to the torsion bar (Figure 1.4b) [27, 28]. While acceleration of a striker in contact with the tab will not produce a sufficiently fast rise time, impact of an in-flight striker will. This is the premise of the side-impact torsion Kolsky bar, which originates from a desktop prototype experiment meant for studying the shear behavior of soft materials [27].

Mixed Stress States

Studying single mode loading is sufficient for many engineering material models. Furthermore, many material models do not include the effects of strain rate. However,
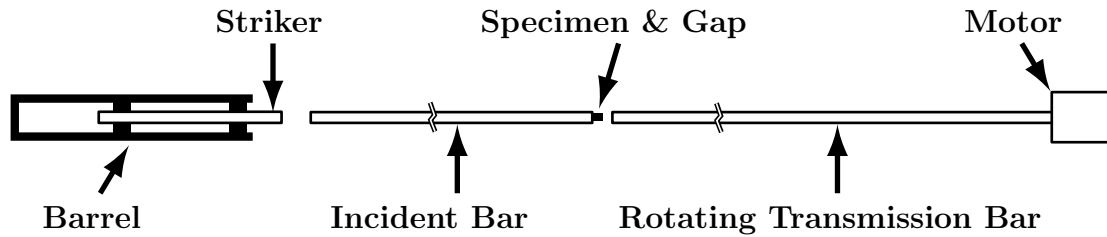
Figure 1.5. Simplified schematic of a modified compression Kolsky bar in which the transmission bar is spun at a desired angular velocity to induce dynamic torsion within a specimen during impact.

specialized applications often require knowledge of a material's behavior with a mixed stress state. For quasi-static experiments, mixed stress states are relatively simple. However, for dynamic experiments, where the time scales are short and the velocities may be large, studying the behavior of a material is non-trivial. The primary problem is related to how waves propagate, which is longitudinal waves and shear waves do not propagate at the same speed in common engineering materials. This means that for a given wave guide and a compression and shear wave generated at the same time, the compression wave will arrive at the destination first.

To circumvent the difference in shear wave speed, the compression Kolsky bar may be modified to deliver torsional loading in a different manner. While the experiment will run like a typical compression Kolsky bar experiment, the torsional wave operates in the opposite direction. This technique makes use of a transmission bar that is rotating at a pre-determined angular velocity (Figure 1.5) [29]. When the compression wave reaches the specimen, the specimen is pushed against the end of the rotating transmission bar, thus imparting angular momentum to the specimen. The transmission bar is in essence the torsion incident bar, and the incident bar is the torsion transmission bar.

An experimental technique involving a marriage of a compression Kolsky bar and a stored-torque Kolsky bar was developed to overcome this problem. The technique is particularly well suited for the study of friction under dually dynamic stress states [30].
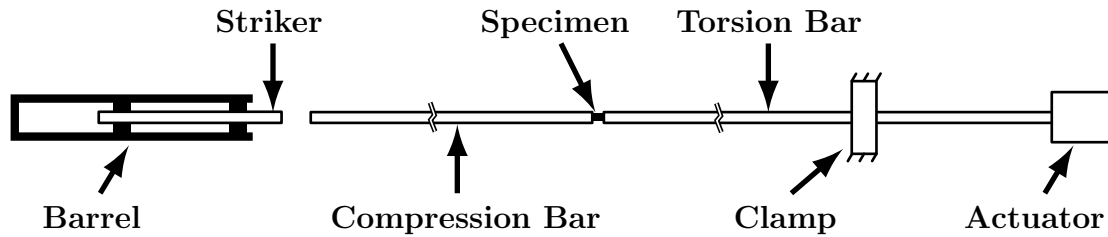
Figure 1.6. Simplified schematic of a modified Kolsky bar where one end is impacted with a striker to generate a longitudinal wave and the other end is pre-torque to generate a torsional wave. Timing between the impact and release events is critical.

This apparatus consisted of a torsion incident bar and a compression incident bar, where the two incident bars later serve as the transmission bars for the opposing stress waves (Figure 1.6). This technique also introduced flexural waves into the system, for which a simple solution was devised: the flexural waves could be damped using a thin acrylic sleeve. The primary shortcoming of this technique is related to how the torsion wave was initiated. The compression wave was monitored by an oscilloscope, once the amplitude reached a predefined value, the oscilloscope trigger the release of the torsion wave by discharging a capacitor through foil that retained the stored torque. The foil however may not always release at the same time, where micro-second accuracy is needed, but so long as the system is consistent, the arrival times of the two types of waves would be withing ten micro-seconds.

The shortcomings of the two previous techniques provide an avenue for improvement to the concept of combined compression-torsion loading. Instead of using a rotating transmission bar to impart torque to the specimen, the compression loading itself may be used [16]. This technique relies on mechanical conversion of a portion of the incident compression wave, meaning the compression loading experienced by the specimen may be lower than expected (Figure 1.7). However, this technique is also not without shortcomings, as the amount of torque generated depends upon the specimen. For example, friction experiments will not see much torque, as the speci-
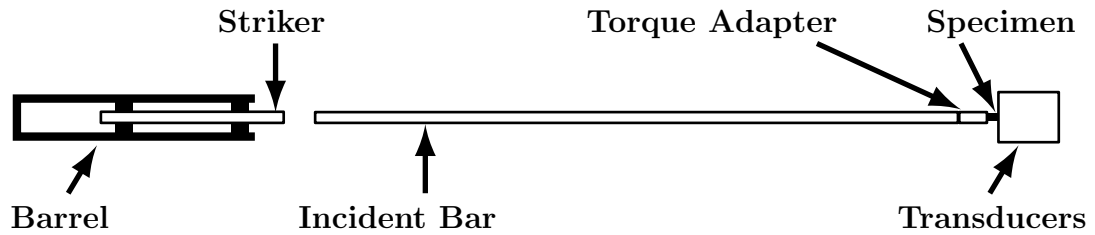
Figure 1.7. Simplified schematic of a modified compression Kolsky bar where simultaneous dynamic compression and dynamic torsion are applied to the specimen through a torque adapter.

men will experience more rotation because the interface is not fixed. The opposite is true for shear experiments, where the specimen will resist rotation.

1.3   Other Forms of Dynamic Shear Loading

Dynamic experiments involving shear are not limited to torsion Kolsky bar experiments. In fact, shear properties may also be studied using either a compression or tension Kolsky bar. These experiments include punch-out and pull-out experiments [31, 32], force fit experiments [33–35], and inclined plane experiments [36–40].

1.3.1   Punch-Out

Punch out experiments place a region of a specimen into pure shear. The goal of this type of experiment is to determine the shear strength, as opposed to the shear properties of a material [31, 32]. This type of experiment makes use of a compression Kolsky bar, which is capable of delivering very high stresses with little need for fixtures (Figure 1.8). The waveforms measured from the incident bar and transmission bar then provide an detailed picture of the shear failure processes under dynamic conditions.
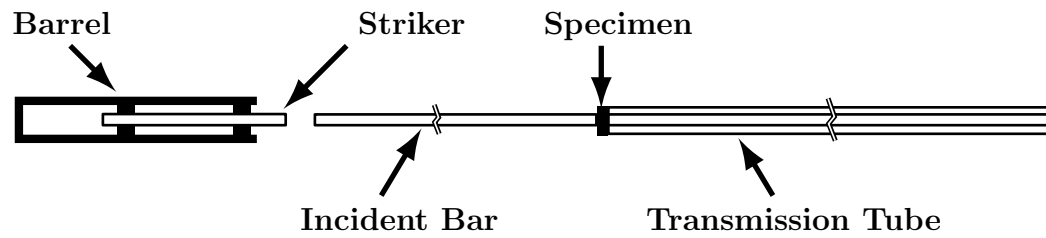
Figure 1.8. Simplified schematic of a modified compression Kolsky bar where a portion of the specimen is punched into the transmission tube to measure the dynamic shear strength of a material [31, 32].
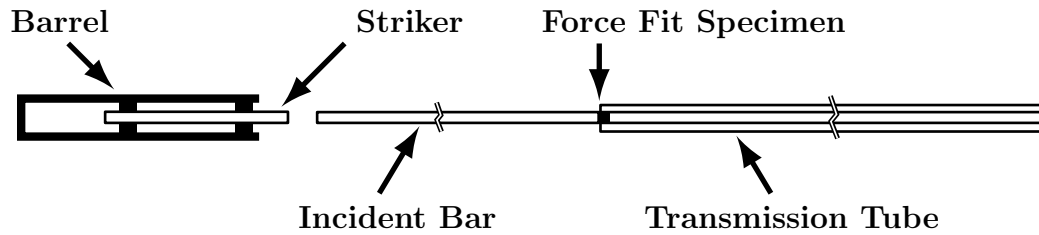
Figure 1.9. Simplified schematic of a modified compression Kolsky bar where the specimen is force fit into a fixture that applies a pre-determined amount a compression. The specimen is then pushed by the incident bar to induce a state of sliding for which interfacial properties may be measured [33, 34].

1.3.2 Force Fit Friction

A common technique that uses a minimum of space an makes use of the ever flexible tension and compression Kolsky bar apparatus is a force-fit friction experiment [33–35]. Essentially, the specimen is either pushed or pulled through an opening that has been sized to apply a predetermined compressive force to the specimen (Figures 1.9 and 1.10). The shear stresses in this type of experiment are measured as compressive or tensile stresses in the transmission bar. The amount of compression on the friction interface is not directly measurable within the tension or compression apparatus and depends upon addition sensors. One approach is to use a dynamometer ring, which measures hoop stresses induced by variations in compressive stress applied to the friction interface [33]. Piezo-electric films such as PVDF (polyvinylidene difluoride) may also be used to measure the stresses applied to each of the individual components [35]. Of course, analytical methods may also be used to determine the stresses based upon a predetermined force fit [34].

The advantage of the compression and tension techniques over torsion techniques relates to material behavior. Torsion techniques will work well with isotropic and transversely isotropic materials. However, the radial nature of the specimen in torsion experiments places the same requirement on the material properties. That is, if a material that is more anisotropic than a transversely isotropic material is to be
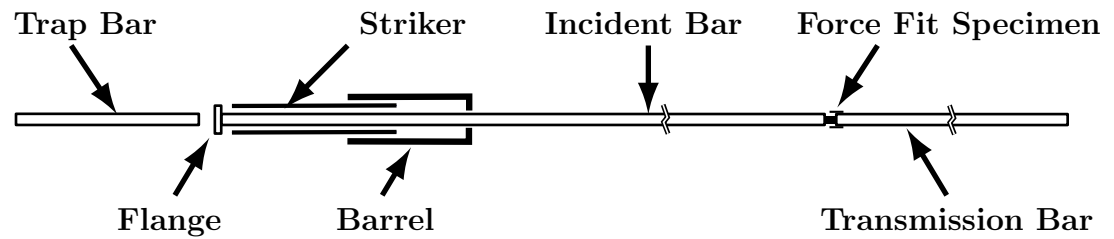
Figure 1.10. Simplified schematic of a modified tension Kolsky bar where the specimen is force fit into a fixture that applies a pre-determined amount a compression. The specimen is then pulled by the incident bar to induce a state of sliding for which interfacial properties may be measured [35].

studied, the torsion experiment will mask direction dependent behavior. Whereas the tension and compression types of experiments will allow friction and shear to be studied in a single specific material direction. However, interaction between the fixtures and the waves may partially mask the specimen's true response for these compression and tension experiments, requiring extra care when analyzing experimental data.

1.3.3 Inclined Compression

The usefulness of inclined planes has extended into the Kolsky bar experiment as well. These experiments may be symmetric or non-symmetric, both with their advantages and disadvantages. The non-symmetric experiments involve a specimen with two inclined planes. The inclined planes are facing each other such that applied compression will result in transverse shearing of the specimen. The specimen may be a single piece of material (Figures 1.11a, 1.11b, and 1.11c) or a fixture that contains the material inside (Figures 1.11d and 1.11e) [36, 37, 40]. This type of experiment produces transverse forces as a result of the inclined planes, a fact that may or may not be compatible with conventional Kolsky bar concepts, as the specimen experiences a significant amount of rotation.

Keeping the specimen aligned is more important for friction experiments than for shear experiments. Reversing the inclined planes to form a wedge is one solution (Figure 1.12) [38, 39]. This type of Kolsky bar experiment thus has two transmission bars, each with a separate specimen. This technique is compatible with both friction and shear experiments.

Regardless of the type of technique, shear waves do not propagate as nicely as longitudinal waves, as the shear waves tend to induce flexural waves which are highly dispersive. As a result, these experiments depend upon transducers to measure the transverse loading experienced by the specimen, as the shear waves do not propagate very far even in an ideal waveguide.

(a) Compression-shear specimen [36, 37].

(b) Round cross-section [36].

(c) Flat cross-section [37].

(d) Confined specimen [40].

(e) Confined cross-section [40].
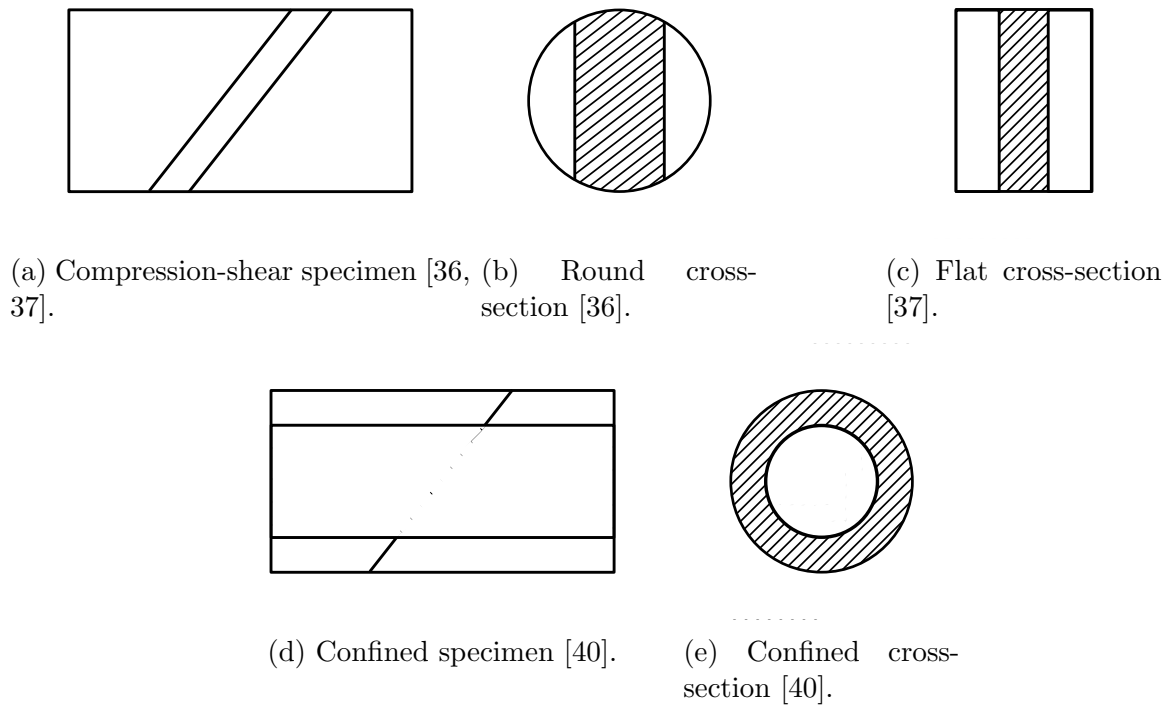
Figure 1.11. Specimen geometries that induce compression and shear via inclined places [36, 37, 40].
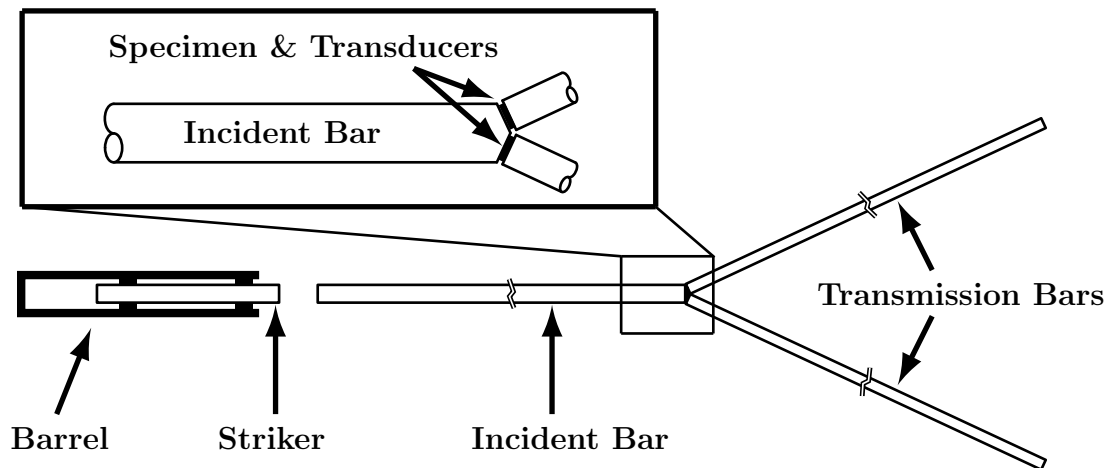
Figure 1.12. Simplified schematic of a modified compression Kolsky bar where the incident bar end is cut with two inclined planes. Each direction has an accompanying transmission bar to measure combined compression and shear loading [38, 39].

1.4   Requirements for More Detailed Material Testing

There are some basic considerations and concepts related to the Kolsky bar experiment and the uses for data obtained from the experiment. These include the type of data being measured and analyzed, the true (as opposed to assumed) state of stress of the specimen, the micro-structure of the specimen material, and how the specimen is loaded.

1.4.1   Is It Strain Rate or Velocity Gradient?

The one dimensional data reduction method for Kolsky bar experiments relies on a discrete derivative across the length of the specimen to determine the strain rate. From a continuum mechanics or an elasticity point of view, these quantities are identical for the linear modes of deformation (linear as in Euclidean space). Furthermore, real materials are often characterized in terms of engineering stress and strain; and here, the strain rate is also the engineering strain rate.

Many material models make use of the strain rate as a parameter, but the distinction between engineering strain rate and true strain rate is not made apparent. For lower strain rates, the two are nearly indistinguishable, but for higher strain rates, the two may differ drastically [41]. This fact means a material model that is intended to cover a large range of strain rates must make the distinction between the engineering strain rate and true strain in order to be accurate, as the experiment may need modification to account for one or the other.

1.4.2   State of Stress

Real materials are rarely exposed to simple states of stress. Whether friction or compression-shear of a uniform specimen with parallel surfaces or interaction between multiple stressed bodies, the real stress state in a specimen may not have an analytical solution [11,13–16]. Composite materials also experience complicated states of stress,

even if the macro-scale stress state is simple [17, 18]. These situations require some form of analysis (typically numerical) to make heads or tails of experimental data. The evolution of high speed imaging has also played a major role in discovering and observing these stress states and their corresponding deformation fields [5, 8].

1.4.3 Micro-Structure

The micro-structure of material may have a profound effect on the material response and may also place a lower limit on the size of a specimen. This can be a point of contention for Kolsky bar experiments, which often require a small specimen with an aspect ratio less than one (i.e. the specimen length is less than the diameter of the bar). In these cases, the behavior may become more anisotropic, where an axis-aligned strain in the specimen produces an off-axis stress state. In the case of brittle materials, the internal stress state may be strongly influenced by the ends of the specimen [11, 13–15]. Conventions for material testing typically require specimens for these materials to have an aspect ratio of at least two, creating a source of conflict for the Kolsky bar experiments [42].

Another case for the study of micro-structure is in high performance fibers. These fibers are drawn to such an extent that the ultimate tensile strength exceeds that of even the strongest metals and ceramics. However, their small size and non-metallic nature makes studying the micro-structure difficult. Furthermore, these fibers are often utilized in composite materials, making them a part of the micro-structure of another material, where interfacial properties become important [17, 18]. These fibers, though part of the micro-structure of a macro-material, also have their own micro-structure. The scale of high performance fibers, often with a diameter less than ten microns, places the scale of relevant micro-structure on the order of nano-meters, leading to different behavior: polymeric fibers tend to show fibrillation, whereas glass fibers experience brittle fracture [43]. Furthermore, understanding how the micro-

structure degrades is also important, particularly for ballistic applications, where the material may change due to mechanical and environmental effects [44].

1.4.4 Pulse Shaping

Pulse shaping of the incident wave, whether compression, tension, or torsion, has been shown to be necessary in order to ensure that the specimen is in a uniform state of loading [2, 6, 28]. Without pulse shaping, the particle velocity on either end of the specimen may not match, and wave propagation within the specimen will result in a non-uniform stress state across the length of the specimen. Thus, the measured material response will only be a portion of the real response of the material, a potentially large problem for size dependent materials.

1.4.5 Overall Strain

The overall strain of a specimen may be determined with respect to two different variables. The first is strain rate, where an integral with respect to time will produce the strain. However, strain rate is not typically a quantity that can be measured. For dynamic experiments, particularly Kolsky bar experiments, the particle velocity (which may be used to determine strain rate), is more suitable. Since the Kolsky bar experiment deals explicitly in particle velocity, the axial deformation may be determined as a function of time based on quantities measured from the incident and transmission bars. Thus, there are three important variables to consider when striving to reach a target strain during a Kolsky bar experiment: loading duration, loading amplitude, and the length of the specimen.

The length of the specimen and the amplitude of loading are relatively simple to change. However, the duration may not be so trivial. A longer loading duration requires a proportionally longer striker. Similarly, in order to avoid overlap of the incident and reflected wave measurements, the incident bar must be sufficiently long to prevent this overlap. Lastly, the trap bar must also be at least the same length as the

striker, otherwise a portion of the wave may become trapped within the transmission bar, potentially causing problems if the specimen must be recovered for observation after the experiment. Ultimately, larger strains for a given strain rate require a longer Kolsky bar.

Supposing the apparatus cannot be extended because of limitations on space, the specimen geometry must change with a corresponding change in impact velocity. However, some materials exhibit size dependence, where the response of the material becomes more dependent on individual micro-structural components as the specimen becomes smaller. These effects are especially important for brittle materials such as concrete and drawn materials such as high performance fibers [2, 42, 45].

1.4.6   Resolution of Measurements

Some materials and phenomena occur at such small stress levels that the wave within the transmission bar is not readily measurable. In these cases the transmission bar may be altered without disrupting the function as a wave guide. For compression and tension experiments, a solid bar may be replaced with a tube; and for torsion experiments, the diameter of the bar need only be reduced [46]. For a sufficiently small specimen, the transmitted particle velocity may be assumed to be zero. Thus, the transmission bar would not move at all, and may be replaced with a transducer. Both of these techniques serve to naturally amplify the data obtained from the experiment and reduce the signal to noise ratio.

1.4.7   Modes of Loading

Most materials and their properties become known to the scientific community through quasi-static experiments. These experiments are largely single mode experiments, with the material experiencing a single state of stress (either axial or shear). The extent of analytical material models stops with the quasi-static experiments. However, all materials are intrinsically strain rate dependent, the most sensitive of

which typically require iterative or numerical methods to predict the material's state for a given form of loading. These types of models depend on data obtain from dynamic experiments such as the Kolsky bar experiment.

Kolsky bar experiments are however limited to single modes of loading without major modification. The types are compression, tension, and torsion. Although, the Kolsky bar experiment is extremely flexible, allowing for virtually any type of experiment that involves elastic wave propagation. These experiments include mixed mode loading (axial and shear loading) if the apparatus is constructed from isotropic materials, as the axial and shear terms are independent.

The dynamic nature of the Kolsky bar experiment also presents some challenges with regard to mixed mode loading. The main challenge is timing, with the wave speeds in common metals are on the order of several thousand meters per second. Thus, not only do events occur within micro-seconds of generating a wave, but events involving different modes will occur at different times for any set of waves generated at the same instance in time. This temporal separation of events is a result of the fact that not all waves propagate at the same speed. Even within a single-mode waveform, the various components will propagate at different speeds. However, the largest difference in wave speed, and the most important for mixed-mode Kolsky bar experiments, is the difference between axial and shear wave speeds. For these types of experiments, the wave generating events either must occur at the same instance in time, but separated by an appropriate distance; or must be generated at different instances in time. This type of experiment is non-trivial, but not impossible.

1.4.8 Interaction with Other Materials

The interaction between different materials is also an important matter to investigate. A common interpretation of the interaction between materials relates to friction, but this also applies to composite materials, strain compatibility, and to applications that attempt to tailor failure modes to produce a specific response.

Regardless, the interaction between different materials inherently involves mixed stress states. Although the experiment may not be required to supply mixed mode loading, the response of the specimen may in fact be mixed mode. Such is the case with friction experiments, but also with soft materials, composites that involve anisotropic materials, and even interaction of the specimen with the experimental apparatus [10, 16, 17, 28].

1.5 Introduction to Friction

Friction is a simple concept to understand and many examples exist in every day life. The term is also widely used to explain losses in a system that would otherwise be unexplained. While it is true that friction may be directly responsible for some losses in a system, the term is often used to generalize other concepts in order to explain something unknown that was not given any attention. In general, friction is dependent on nearly every variable ranging from stress state, total strain, strain rate, relative velocity (which is not directly proportional to strain rate), surface quality, temperature, lubrication, total wear, and obviously, material.

1.5.1 Surface Description

An interface between two bodies inherently involves two surfaces. The means through which the material of each body interacts is dependent upon the quality of the surfaces. Surface quality, or surface roughness, describes the presence, size, and frequency of asperities [47]. In layman's terms, asperities form peaks and valleys on a surface, it is these peaks and valleys that interact, interlock, and result in friction. This mechanical explanation for friction is not the only explanation, atomic scale interactions such as Coulomb and Van der Waals forces also play an important role in the friction behavior of a material. The mechanical explanation however, is more applicable when dissimilar materials are involved. Whether the materials are compliant or stiff, or elastic or brittle will highly influence the amount of friction

at the interface. Lastly, the degree to which the surface evolves over the course of friction loading also contributes to the total response.

1.5.2   Compliant Materials

Compliant materials, also referred to as soft materials, tend to be more "sticky" than stiff materials. The stickiness is explained by a higher amount of friction that is a result of how the material deforms. Mechanically, compliant materials are capable of filling spaces between and forming around asperities [48–51]. The local stresses around the asperities may be sufficient to retain the deformed shape at the interface, producing the appearance of adhesion to a surface. This however, is a static explanation, where there is no sliding velocity.

In a dynamic case, where the soft material is sliding across a surface, the material will deform and relax depending on the local surface conditions. This propensity to deform will reduce the local sliding velocity until the deformation exceeds what can be maintained by the friction with the interface. At this point the soft material will release from the surface and relax, only to start the process again. This stick-slip behavior may also occur at the global level, where the entire specimen exhibits periodic variations in sliding velocity and interfacial stress levels [47, 52, 53].

1.5.3   Stiff Materials

Stiff materials, in contrast to compliant materials, are not capable of actively filling between or forming around asperities. Rather, the asperities across the two surfaces may engage mechanically and provide temporary resistance until the asperities are permanently deformed. In addition, some of the asperities may break free of the surface and become debris within the interface which also influences the how the friction behavior evolves [47].

1.5.4 Elastic-Plastic Materials

Elastic-plastic materials behave somewhat similarly to elastic materials in that the material will return intact to a strain relieved state that will resemble the original. However, an interface that experiences plastic deformation will be permanently deformed. Some materials will appear to have a smoother surface texture, as the asperities have been deformed and crushed into the neighboring voids. Other materials will experience galling, which is the creation of large asperities which prevent even surface contact and cause stress concentrations which result in further surface evolution. Prolonged deformation may also result in the separation of these large asperities which results in further deformation of the surfaces at the interface [47].

1.5.5 Brittle Materials

Brittle materials behave somewhat differently than elastic and elastic-plastic materials. The primary difference is that when material failure occurs, portions of the materials separate from the main body. At an interface experiencing friction loading, these portions become debris within the interface which may contribute to further surface evolution or act to preserve the surfaces in their current state [47].

1.6 Introduction to Particle Composites

Particle composites are materials that are made up of one or more type of particle and a binding material. Some examples of particle composites are concrete, which is a mixture of one or more types of aggregate bound together with cement; asphalt, which also may contain multiple types of aggregate bound together with bitumen; and polymer bonded energetic materials, which are some form of volatile crystal bound together with polymer.

Each of these materials may be classified as either high-volume fraction or low-volume fraction composites, for which the distinction is typically made based on

their engineering use and composition. The reason for this is that classical theories do not handle the odd geometries encountered in real materials [54, 55]. Rather, classical theories are typically limited to spherical (or elliptical) and linearly elastic aggregates [56–58]. However, the theories themselves may be applied using iterative methods which do permit non-spherical geometry and non-linear materials [55,59,60].

The application of these theories is typically not so clear, as many numerical methods are capable of providing an appropriate solution using the governing equations of elasticity if the geometric solution is also appropriate. For example, methods that make use of simplified geometry will produce an accurate solution if certain geometric parameters are in order; other methods that make use of realistic geometries do not require additional parameters. Ultimately, each numerical method may be classified into one of these two categories, the first of which is essentially a curve fit, while the has the potential to provide realistic predictions for not-yet-existing materials. However, fully detailed numerical models with correct material properties and crystal orientations are not trivial to create or solve [61–63]. Rather, popular methods such as the finite element method have benefited from the inclusion of classical theories such as Eshelby's inclusion theory, the Mori-Tanaka method, and the Generalized Self-Consistent Model [61].

1.6.1 Difficulties of Particle Composites

The primary difficulty with particle composites is related to the shear number of interfaces between the individual particles and binder material. To further complicate matters, the particles are usually small enough to be composed of only a single grain: i.e. the particle is a single crystal that is not isotropic. Although the bulk response of the composite may be isotropic due to the random orientation of the aggregate, the local interactions between the aggregate and binder are not isotropic. Thus, the stress state at any given point in the composite may vary drastically from that of the macroscopic specimen.

Particle composites are also difficult to manufacture in a consistent manner. Although the distribution of particle sizes may be similar between batches, the physical distribution of particles may not be. Furthermore, the particles may be too small to break the surface tension of the binder material, resulting in pockets of aggregate that are not held together with binder. These materials require aggressive mixing with large shear stresses that may also break down the size distribution of particles in order for all of the particles to be bound by the binder.

Another difficulty related to the manufacture of particle composites is caused by the particular manufacturing method. A specimen that is produced using subtractive processes will have surfaces with the same properties as the bulk material. However, a specimen that is cast will have surface properties that are more similar to the bulk properties of the binder material. This is caused by capillary action between the aggregate and the walls of the mold, resulting in excess binder material on the outer surfaces of the composite specimen [28].

1.6.2 Relationship to Energetic Materials

The most common form of energetic material is a particle composite. These composites are composed of a crystalline aggregate (that is extremely volatile) and an inert binder. The binder often supplements the chemical reaction to produce a desired effect, but is primarily used to contain and protect the aggregate. These materials are called polymer bonded explosives, their inert counter parts are often called polymer bonded simulants. The term simulant refers to the fact that the inert form of the composite does not have the potential for a violent chemical reaction, yet the material behavior is similar to that of the volatile composite.

Energetic materials are typically rated in terms of volatility on a go, no-go basis. These tests are open-ended as the results depend only upon whether there were signs of chemical reaction [64]. Although, there is the possibility to take measurements

involving thermal, stress, and strain state of a sample of material, this is typically not performed.

There are a variety of tests that simulate real world scenarios that have led to accidental reactions and personal injury in the past. These include a drop-weight test, to simulate an object being dropped on an energetic material; a puncture test, to simulate the perforation of an energetic material or a warhead; a friction test, to gage sensitivity to shear loading; and many others [64].

An important test is the friction test, which exposes an energetic material to not only rubbing, but also shear. Friction has been proven to be a leading cause of hot-spot formation within energetic materials [65–69]. A hot spot is a region with elevated temperature, whether caused by mechanical loading, thermal loading, or minor chemical reaction. For energetic materials, there is a threshold (that is yet unknown), where the material will experience a cascading reaction as a result of a hot spot. The relevance to friction is that the go-no-go friction test does not address the state of the material.

An important factor for particle composites is how they are produced, specifically for composites that are cast using a liquid binder that later cures into a solid. Since these materials typically have a high volume fraction of aggregate, a cast component will be composed mostly of the aggregate. Near the walls of the mold, the aggregate produces strong capillary effects, drawing the liquid binder toward the surfaces of the part. This effect results in surfaces that are composed mostly of the binder. In contrast, a part that is mechanically processed (i.e. machined, formed, or pressed), will have surfaces with more aggregate and a composition identical to the bulk composition.

The differences between these two manufacturing methods may have a drastic effect. One may hypothesize that the extra binder on the surfaces of a cast part will protect the underlying volatile components. Yet, knowing that friction and shear are the leading causes for hot spot formation, one may expect that the cast part will experience more hot spot formation than the mechanically processed part. Thus,

understanding friction alone is not sufficient, and a more detailed analysis of surface conditions is necessary.

2. MATERIALS & METHODS

In order to address the many shortcomings of state of the art torsion Kolsky bars, advances from the compression and tension variants were applied to the torsional concept. A desirable Kolsky bar apparatus has the following traits: adjustable loading duration, controllable waveform, and adjustable wave amplitude. The conventional torsion variants only provide for adjustable duration and amplitude. The development of a new technique was necessary in order to control the waveform in a more detailed manner.

During the development of the torsion pulse-shaping capabilities, the study of torsional interfaces also became a necessity. This study produced a concept that had the potential to allow for simultaneous compression-torsion loading, providing a means to study materials in dually dynamic states of compression and torsion.

2.1   Side-Impact Torsion Kolsky Bar

The side-impact torsion Kolsky bar is a marriage between modern compression Kolsky bar technology and the torsion Kolsky bar. The design of the apparatus allows not only for control of the duration and amplitude of the incident torsional wave, but also of the shape of the wave. Furthermore, the duration of the torsion wave is determined by the single loading device located on the loading bar. Unlike stored-torque torsion Kolsky bars which require a long length of pre-torqued bar as the source of the wave, a much longer torsion wave may be generated by the loading bar as the impedance ratio between the tab and the loading bar does not reduce the motion of the loading bar by a significant amount.

The side-impact torsion Kolsky bar has five waveguides: the striker, the loading bar, the impact mechanism, the incident bar, and the transmission bar (Figure 2.1).
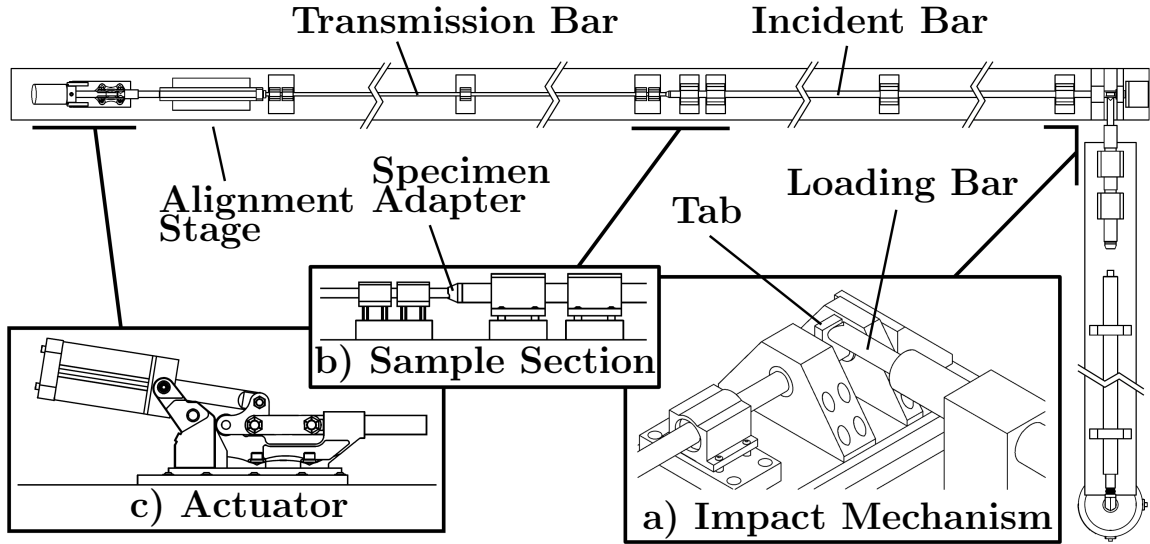
Figure 2.1. An overview of the side impact torsion Kolsky bar. a) The incident bar is impacted by the loading bar through a tab. b) The sample section is adapted for materials that exhibit small coefficients of friction. c) The system is compressed axially using an actuator through an alignment stage to prevent unintentional bending.

Details of the function and properties of the components are discussed in detail in Section 3.1.

The striker is launched using a low pressure gas gun with a recoil dampener. The dampener prevents the striker from impacting the loading bar multiple times. The loading bar is a bar of nearly equal length to the striker. On one end, the loading bar is flanged, and on the other, the bar has a cylindrical face which provides a line contact with a tab. The tab is a permanent feature of a component referred to as the impact mechanism, which is produced from a single piece of material to reduce the total number of interfaces within the system. The impact mechanism is supported on both sides of the tab by sleeve bearings which limit the lateral motion and thus reduce the propensity for the generation and propagation of flexural waves. The impact mechanism is mated to the torsion incident bar through a key-slot joint. The key-slot design is simplistic and can be easily produced with tight tolerances, which improves overall waveform quality.

The incident bar and transmission bar are simple round cross-section bars. For experiments with relatively high transmitted wave amplitudes, the transmission bar may be the same diameter as the incident bar. However, for low amplitude transmitted waves, the transmission bar must have reduced inertia to that of the incident bar. For example: the primary variable related to inertia in compression and tension Kolsky bar experiments is the cross-section area. Reducing the area increases the amplitude of the stress and also of the overall measurement. The most stable method to accomplish this is to use a hollow bar (or tube), as decreasing the diameter may lead to buckling of the bar. For torsion, the primary variable related to inertia is the polar moment of inertia. using a hollow bar in this case would not significantly decrease the moment of inertia. Rather, the diameter must decreased.

Just as in compression experiments, decreasing the diameter has implications related to buckling, particularly during friction experiments that require an axial load. Furthermore, the specimen must be mated in such a manner that the stress may flow from the larger incident bar, through the specimen, and into the transmission bar. One way to accomplish this is with an adapter mated to the transmission bar with another key-slot interface.

For experiments that require axial compression (friction experiments or compression-shear experiments), the apparatus may be outfitted with an actuator. Since the torsion generating mechanism is not axially aligned with the incident and transmission bars, axial compression may be applied without worry of influencing how the torsion wave is generated. For these types of experiments, the bar must be outfitted with a thrust bearing to support the impact mechanism and prevent axial motion of the entire torsion apparatus. Furthermore, to prevent from inducing flexural stresses, the force of the actuator should be applied through alignment apparatus which contains another thrust bearing that allows the transmission bar to rotate.

2.1.1 Data Reduction

Data obtained from torsion Kolsky bar experiments may be in processed several ways with the two most important factors being shear and friction. Shear experiments required determination of stress and strain within the specimen, whereas friction experiments require determination of the sliding velocity and interfacial stresses. The general process between these two experiments is identical except for how the specimen is treated. Furthermore, the nature of torsion experiments also places restrictions on specimen geometry, a factor which should be considered when developing material models.

General Approach

The process of reducing experimentally obtained measurements depends upon the geometry of the apparatus and of the specimen. This process assumes that the incident and transmission bars are homogeneous, have a circular cross section, and share the same density (ρ) and shear modulus (G). However, the transmission bar may be required to have a different radius than the incident bar. Thus, the radius of the transmission bar is R_T and the radius of the incident bar is R_I.

The incident shear stress (τ_I), reflected shear stress (τ_R), and transmitted shear stress (τ_T), are obtained from the respective measured shear strains (Figure 2.2). The individual quantities are extracted from time-based measurements using the one dimensional wave equation. With known bar lengths, the ratio with the wave speed provides time offsets for each of the waves.

With these quantities in place, the angular velocity induced by each of the measured waveforms is simply related through the shear wave speed (C_S) and the measured strain (or stress) of each of the waves. These angular velocities are then used to determine quantities within the specimen such as shear strain rate and sliding velocity (Equations 2.1, 2.2, and 2.3).
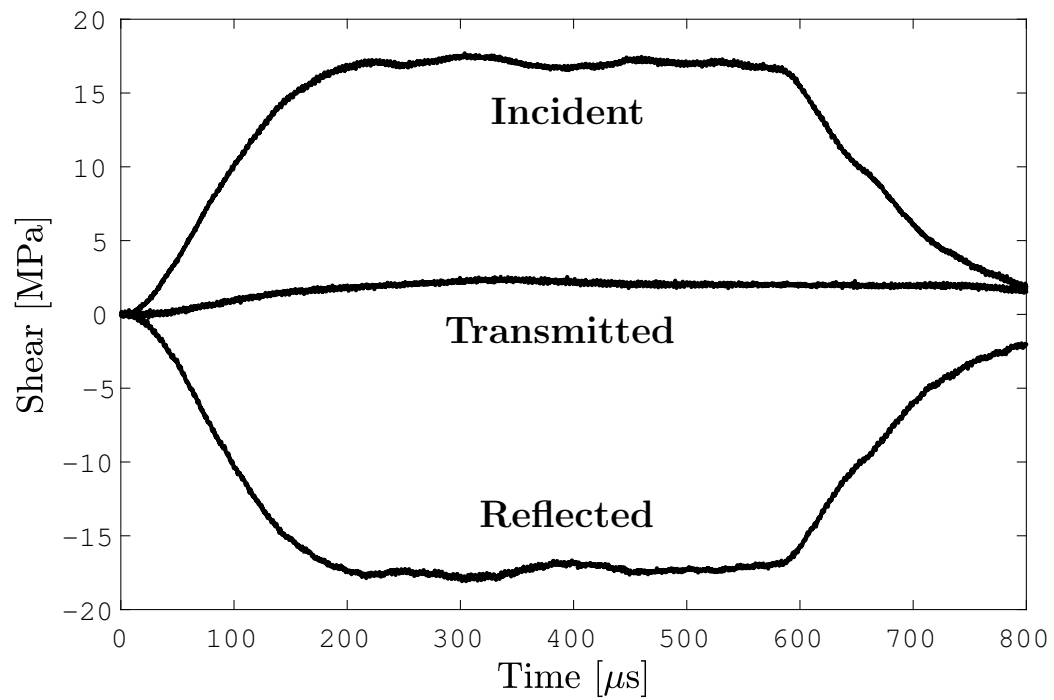
Figure 2.2. Example of incident, reflected, and transmitted waveforms from a side-impact torsion Kolsky bar experiment. The signals are extracted from an oscilloscope trace at times specified by the one dimensional wave equation.
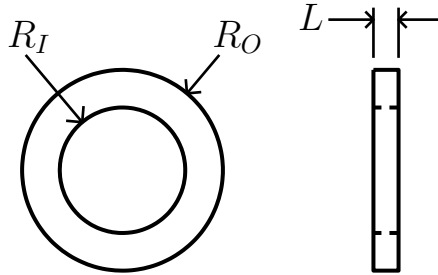
Figure 2.3. The specimen is annular in shape in order to obtain well defined shear quantities on the cross section. Reproduced with permission from [28]. Copyright (2015) Experimental Mechanics.

$$\dot{\theta}_I = \frac{\gamma_I}{R_I}C_S = \frac{\tau_I}{R_I}\frac{C_S}{G} \tag{2.1}$$

$$\dot{\theta}_R = \frac{\gamma_R}{R_R}C_S = \frac{\tau_R}{R_R}\frac{C_S}{G} \tag{2.2}$$

$$\dot{\theta}_T = \frac{\gamma_T}{R_T}C_S = \frac{\tau_T}{R_T}\frac{C_S}{G} \tag{2.3}$$

However, before converting to these measured quantities to quantities that represent the specimen, the geometry of the specimen must be known. Typically, right circular cylinders are not acceptable for torsion experiments. Rather, an annulus is required in order for the quantities to have a well defined relationship with the measurements (Figure 2.3). An annulus is essentially a disc, except with the center portion removed such that the average quantities across the specimen surfaces do not deviate drastically from the minimum and maximum. The average quantities are defined at the average radius (R_A). Rather than using the outer radius of the specimen (R_{SO}), all of the equations for a disc should simply make use of the average radius.

The relationships between the average radius and average values are more complex than a simple substitution of variables. For an analytical representation of a system, the stress, strain, and velocity are field variables. For a real system, the real values are

also field variables, but limitations associated with taking measurements means the values are scalar (but still a function of time). In other words, the integrals become independent of the measured quantity and produce a simple relation for the average radius (R_A, Equation 2.4), where the outer radius (R_O) and the inner radius (R_I) define the annulus in Figure 2.3. However, it is a coincidence that this equation may be used directly with the other equations that depend on the radial ordinate. For a generalized field, these integrals will not necessarily produce this solution.

$$R_A = \frac{2}{3} \frac{R_O^2 + R_O R_I + R_I^2}{R_O + R_I} \tag{2.4}$$

For a given quantity that is linearly dependent upon the radial ordinate (r, Equation 2.5), the error between quantities at the null (zero), minimum (R_I), maximum (R_O), average (R_A), or arbitrary (R) ordinate can be determined (Equation 2.6). This relationship is also linear, meaning that the inner and outer radii of the annulus must be within the same percent of error that is tolerable for the measured quantities. However, this is not practical, as some studies require a bulk of material, or make use of a pre-defined contact area.

$$F(r) = r \cdot G(\gamma, \tau, \dot{\theta}) \tag{2.5}$$

$$E(r, R) = (R - r) \cdot G(\gamma, \tau, \dot{\theta}) \tag{2.6}$$

Shear Experiments

Similar to compression and tension experiments, shear (torsion) experiments make use of the relative incident and transmission bar velocities. For the torsion bar, these velocities are angular in nature, and are converted to shear strain rate. The transmitted waveform is then used to determine the shear stress within the specimen. These quantities describe the stress-strain response of the specimen in shear.

The general equation for the shear strain rate of a specimen (γ_S) with length L_S experiencing torsion illustrates the necessity of an annular specimen point quite well, where the radial ordinate (r_S) within the specimen is present. Here, the shear strain rate varies from zero at the center to a maximum at the outer radius (R_S, Equation 2.7); the same of which is true for all quantities that may be calculated for the specimen.

$$\dot{\gamma}_S = \frac{r_S}{L_S}(\dot{\theta}_I - \dot{\theta}_R - \dot{\theta}_T) \tag{2.7}$$

$$\dot{\gamma}_S = \frac{1}{L_S} \frac{\displaystyle\int_{R_{SI}}^{R_{SO}} r_S(\dot{\theta}_I - \dot{\theta}_R - \dot{\theta}_T)dr_S}{\displaystyle\int_{R_{SI}}^{R_{SO}} r_S dr_S}$$

$$= \frac{2}{3}\frac{R_{SO}^2 + R_{SO}R_{SI} + R_{SI}^2}{R_{SO} + R_{SI}}\frac{1}{L_S}(\dot{\theta}_I - \dot{\theta}_R - \dot{\theta}_T) \tag{2.8}$$

The average strain of the specimen (γ_S) is then determined through a time integral of the shear strain rate (Equation 2.9). Supposing that Equation 2.8 was used to determine the shear strain rate, both the shear strain and the shear strain rate are then defined on the mean radius (Equation 2.4). The minimum and maximum values of the these quantities can be determined using Equation 2.7, but this is not required.

$$\gamma_S = \int_0^t \dot{\gamma}_S(\tau)\, d\tau \tag{2.9}$$

The average shear stress in the specimen can be determined solely from the transmitted waveform. The process follows the same approach as the compression and tension Kolsky bar data reduction, except with shear quantities. First, the measured quantity must be converted into torque (T_T, Equation 2.10), which then must be integrated over the cross section and converted to stress to determine the average shear stress (τ_S) on the specimen (Equation 2.11).

$$T_T = \frac{\pi R^4 \tau_T}{2r} \tag{2.10}$$

$$\tau_S = \frac{\displaystyle\int_{R_{SI}}^{R_{SO}} \frac{2 T_T r_s^2}{\pi (R_{SO}^4 - R_{SI}^4)} dr_S}{\displaystyle\int_{R_{SI}}^{R_{SO}} r_S dr_S} = \frac{2}{3} \frac{R_O^2 + R_O R_I + R_I^2}{R_O + R_I} \frac{R_O^4}{(R_{SO}^4 - R_{SI}^4)} \tau_T \tag{2.11}$$

Friction Experiments

Unlike shear experiments, friction experiments make use of the relative angular velocity between the incident and transmission torsion bars to determine the sliding velocity at the interface between the two halves of the specimen (also called a tribo-pair). Friction experiments conducted on a torsion Kolsky bar are required to be annular in shape. This is a direct result of the relationship between sliding velocity and angular velocity. Since the friction coefficient is known to be dependent upon sliding velocity, it is important that this quantity be well defined. Thus a cylindrical specimen, with sliding velocity varying from zero at the center, is not fit for this type of experiment.

Similar to the shear experiment, the transmitted waveform represents the amount of shear supported by the interface. However, this quantity does not have an accompanying shear strain rate or shear strain. Rather, the opposing quantity is the sliding velocity, which is related to the relative angular velocity between the incident and transmission bar. The equations for a disc (Equation 2.12) and annulus (Equation 2.13) are provided for comparison. The sliding velocity is similar to the shear strain rate in that the quantity is defined by the relative angular velocity.

$$v_S = r_S \cdot (\dot{\theta}_I - \dot{\theta}_R - \dot{\theta}_T) \tag{2.12}$$

$$v_S = \frac{\displaystyle\int_{R_{SI}}^{R_{SO}} r_S(\dot{\theta}_I - \dot{\theta}_R - \dot{\theta}_T)dr_S}{\displaystyle\int_{R_{SI}}^{R_{SO}} r_S dr_S}$$

$$= \frac{2}{3}\frac{R_{SO}^2 + R_{SO}R_{SI} + R_{SI}^2}{R_{SO} + R_{SI}}(\dot{\theta}_I - \dot{\theta}_R - \dot{\theta}_T)$$

(2.13)

The friction experiment would not be complete without a friction law. Friction laws may be a function of many variables, such as compressive stress, shear stress, sliding velocity, material properties, surface quality, material strength, and environment. While a complex friction law may be used to aid data reduction and determine the stress state in a material, a more simplistic approach is of benefit to unstudied materials. The most basic friction law is the Coulomb friction law (Equation 2.14), which relates the friction coefficient (μ) to the current state of compression (σ or F_N) and shear (τ or F_S), whether represented as forces (F_N and F_S) or stresses (σ and τ).

$$\mu = \frac{\tau}{\sigma} = \frac{F_S}{F_N}$$

(2.14)

Although the stress state supported by the interface is known, the state of the components of the specimen (i.e. the tribo-pair), are not. Supposing the material properties are known, the strain in the specimen may be determined in an open-ended fashion. This is a result of the definition of sliding velocity, which describes all relative angular motion between the incident and transmission bars. For stiff materials, a significant amount of torque is required to produce noticeable shear deformation. However, for soft materials, a small amount of torque may produce a large amount of shear deformation. Suppose that the materials at the interface never truly slide, then the experiment is essentially a shear stress-strain experiment. Unfortunately, the data reduction process assumes there is sliding, and the sliding velocity will reflect this assumption, and produce a non-zero quantity. This issue is discussed more in Chapter 4.

2.1.2   Specimen Geometry

In torsion, the stresses (or strains) vary from zero at the center to the maximum value at the surface of the specimen. Thus whether the experiment is intended to study shear or friction, the transmitted wave will be influenced by the average state across the entire cross section of the specimen. For a specimen that is disk shaped, the measured quantities may have large variations from the measured values depending on the location within the specimen.

To rectify this issue, the cross sectional area of the specimen may be reduced in a manner that provides a minimal variation from the mean. In other words, the specimen must be annular (or ring shaped, Figure 2.3)). By removing the center section of the specimen, the areas with less deformation (or stress) will not influence the measurements. Thus, the measured values will more closely reflect the true state of the specimen.

Using an annular specimen is more important for non-linear materials and friction experiments, where the behavior of the material may vary drastically with variables such as strain rate, velocity, and total strain.

Specific information on specimen geometry is discussed in Section 2.3.

2.2   Combined Compression-Torsion Kolsky Bar

The combined compression-torsion Kolsky bar is in essence a compression Kolsky bar with a modified bar end to generate torsional stress within the specimen. While the experimental technique described here is meant for soft materials with low amplitude responses, the approach may be applied on a larger scale for materials that respond with a higher amplitude with some modifications. However, this technique was developed for use at the Advanced Photon Source at Argonne National Laboratory, where space is at a premium and conventional Kolsky bars simply do not fit within the alloted space.

The current approach is based on a modified compression Kolsky bar with an assumption that the materials in question are sufficiently small and with low stiffness that any transmitted response will be immeasurable. For this assumption, the transmission bar is replaced with a set of static transducers. For materials that do not satisfy this assumption, a transmission bar should be used. In either case, the experiment follows the same process. Initially, an incident compression wave approaches the sample, upon interaction with a torque adapter, a portion of the compression wave is converted to torsion (Figure 2.4). The specimen's response is then transmitted to the sensing apparatus (whether transmission bar or force transducers). This response will be a stress state involving both compression and shear components. Regardless of whether a set of force transducers are used or a transmission bar is employed, the two waves (compression and shear) travel at different speeds, meaning even the length of the force transducers will introduce a slight delay. Depending on the distance to the sensing components this delay may be on the order of one micro-second or one hundred micro-seconds. For previous techniques, this difference in wave speed posed a serious problem when attempting to load a specimen simultaneously with compression and shear waves.

Unlike previous techniques, the incident wave is only a compression wave, meaning there is no shear wave that must arrive at the same time. However, the response of the specimen not only influences the reflected wave, but also generates a torsional wave within the incident bar. For materials with a low amplitude response, this quantity will be nearly immeasurable, but for stronger responses, this torsional wave describes specimen rotation near the incident bar. This technique also has a limitation, where the torque adapter must be in an opened position in order for any torque to be generated (Figure 2.5). In the closed position, the torque adapter will transmit all compression, and will not induce any torque in the specimen.

68
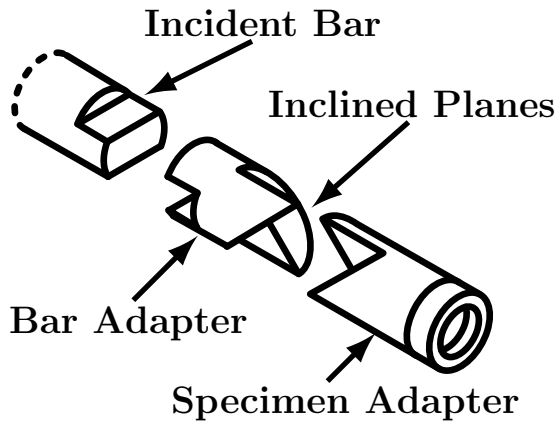
Figure 2.4. Assembly of torque adapter with specimen and incident bar. Adapted with permission from [16]. Copyright (2017) Experimental Mechanics.
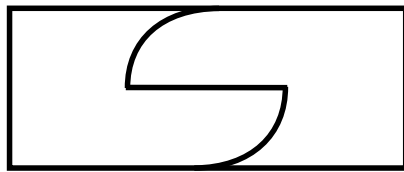
(a) Closed.
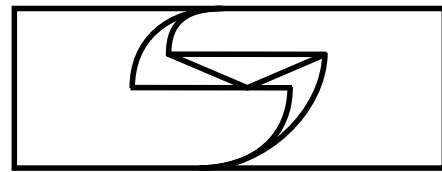
(b) Opened.

Figure 2.5. The torque adapter in the (a) closed position and (b) opened position. The adapter does not produce torque in the closed position. Reproduced with permission from [16]. Copyright (2017) Experimental Mechanics.

2.2.1 X-Ray Phase Contrast Imaging

The Advanced Photon Source at Argonne National Laboratory places many restrictions on an experimental apparatus due to the use of high energy x-rays. Each sector of the the facility has their own beam line equipment and a small hutch in which the x-rays are confined. The x-ray beam is typically on the order of one square millimeter, meaning an entire specimen cannot be observed during a single experiment. These restrictions mean the Kolsky bar apparatus must be remotely operated, remotely positioned, and small in scale.

X-Ray Facility

The Advanced Photon Source consists of a linear acceleration, electron storage ring, and thirty five beam lines, each with several experimental facilities. An individual experiment will make use of a hutch which is typically only a few hundred square feet. For hutch B in sector thirty-two, the actual space for an experiment is smaller, and must either fit on a small optical table, or within a three foot wide by ten foot long area. As with all of the beam lines, the x-ray source and beam line equipment are provided. The primary mode of operation used was the standard top-up operation mode which consists of twenty four singlets.

The general setup for phase contrast imaging makes use of a scintillator, which converts x-rays into visible light (Figure 2.6). The visible light is then reflected into a high speed camera. Integration of any dynamic experiment with the system requires accurate timing and remote operation in order view the events under investigation.

Remote Apparatus

Space limitations within the hutch require the Kolsky bar apparatus to be self contained and miniature in scale. The apparatus contains all power and control systems, and only needs to be supplemented by the appropriate data acquisition
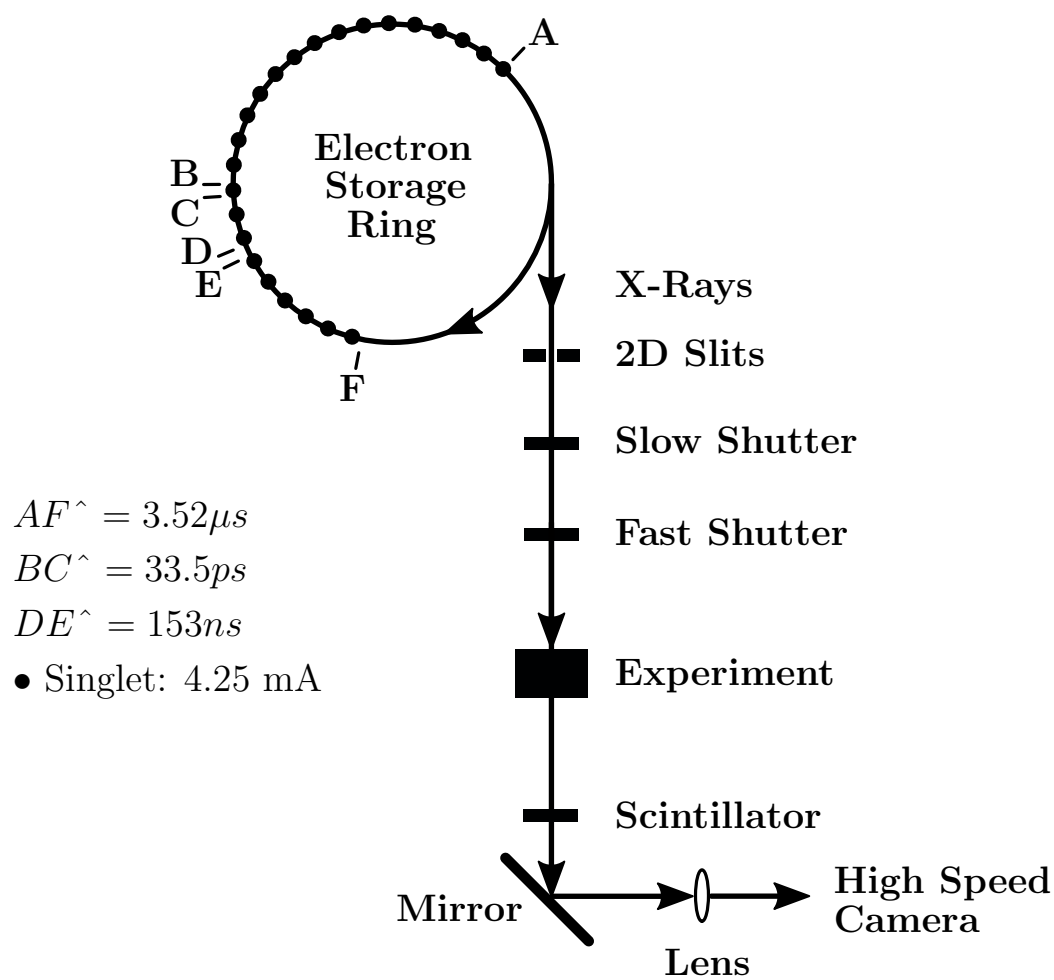
Figure 2.6. Schematic of a typical phase contrast imaging experiment at the Advanced Photon Source in Argonne National Laboratory.

equipment (Figures 2.7 and 2.8). The limited size of the x-ray beam means the specimen must be small, and an assumption was made that the impedance ratio between the specimen and bar materials is sufficiently small that the load may be measured with a transducer.

The size of the x-ray beam is on the order of one millimeter. The apparatus is composed of three mobile components: the table, which only needs to be positioned to within a few centimeters; the stands, which are manually positionable; and the top plate, which may be remotely positioned to within ten microns in directions transverse to the x-ray beam. The apparatus is capable of performing experiments for either phase contrast imaging, diffraction, or both. Positioning of the apparatus and the stands allow steep angles up to sixty degrees to the x-ray beam.

The general procedure for preparing an experiment is to load the specimen, prepare the Kolsky bar for firing, and seal the hutch. Once the hutch is sealed, the operations are fully remote. The x-ray shutter may be opened and the intensity tailored to suit the material of the specimen through a series of tests, during which the position of the specimen may be adjusted. Ensuring that the x-rays, high speed camera, and dynamic loading are time synced is a fairly complicated process.

The remote apparatus is modular in that the top plate may be replaced with another. This allows the entire system to be host to multiple other experiments. The primary use is for compression and tension Kolsky bar experiments, but another top plate, with a compression-torsion Kolsky bar was substituted to perform friction and shear experiments on particle composites (Figure 2.9).

X-Ray Integration

The Kolsky bar apparatus is integrated with the beam line in two fashions: by position, and in time. Positioning is a relatively simple process that may be accomplished manually in large steps, or remotely in precise steps. Controlling timing between each of the systems is not so simple. The beam line and the Kolsky bar
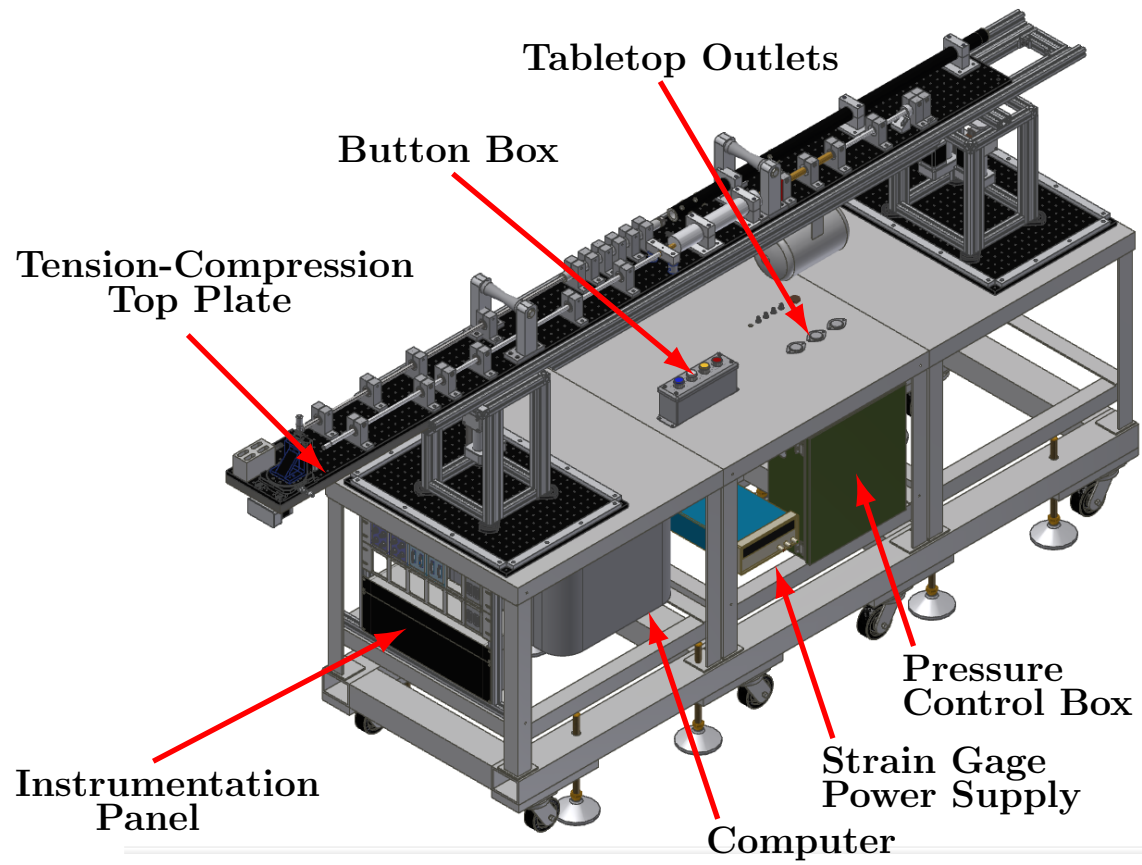
Figure 2.7. Left side of the remotely operated Kolsky bar system.
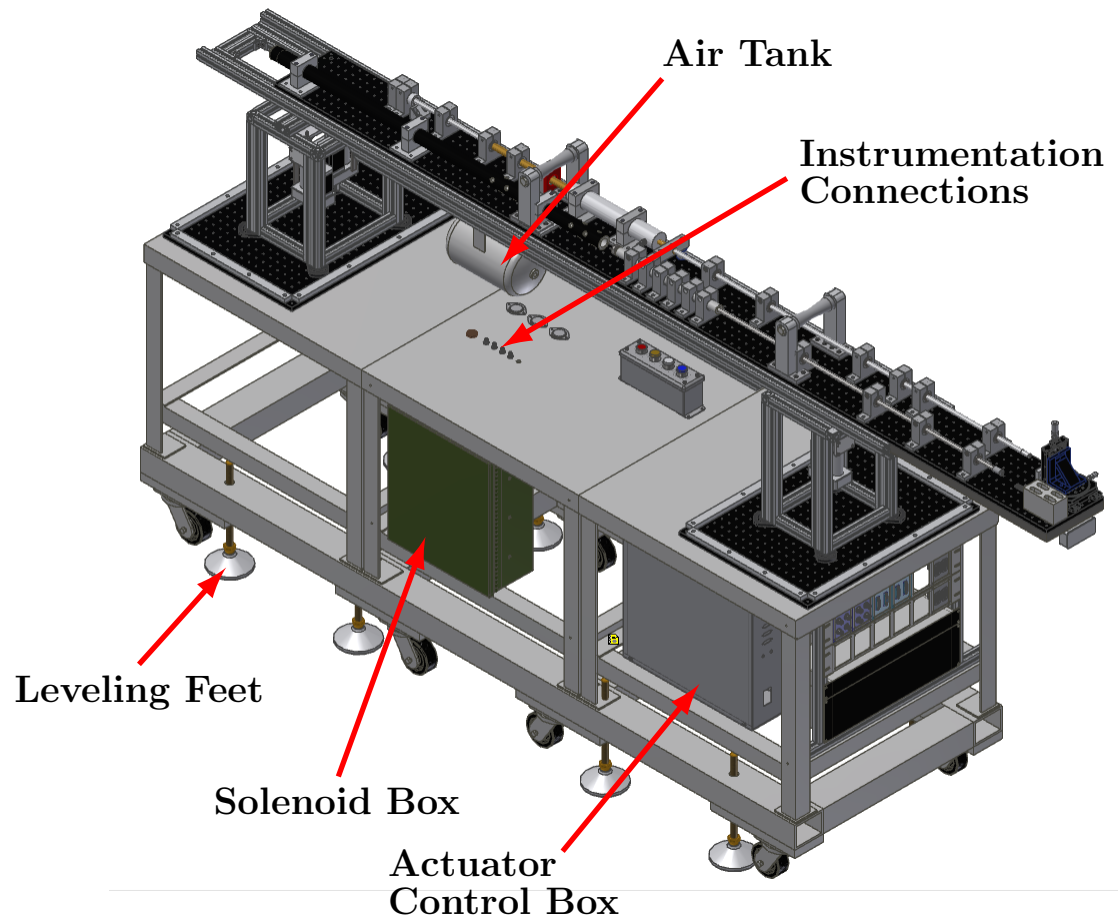
Figure 2.8. Right side of the remotely operated Kolsky bar system.

(a) Tension & Compression   (b) Combined Compression-Torsion
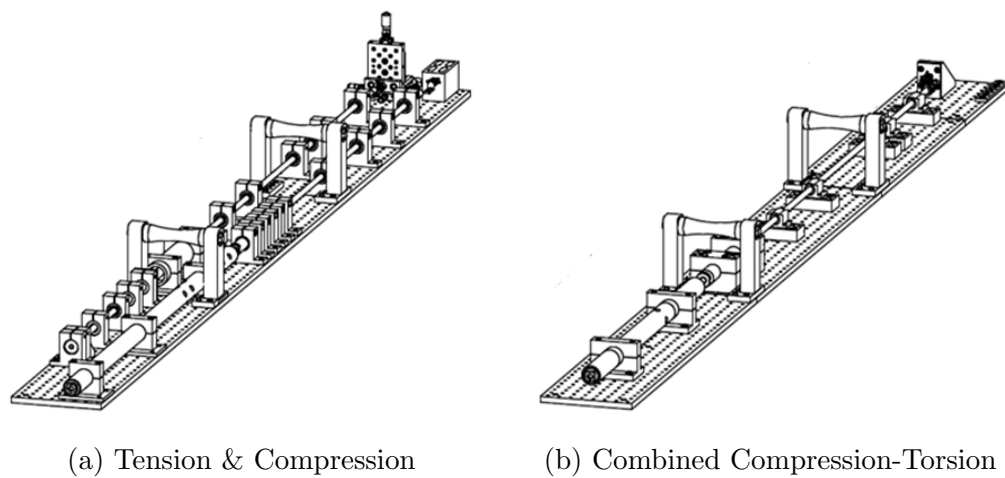
Figure 2.9. Comparison of modular top plates with different Kolsky bar experiments.
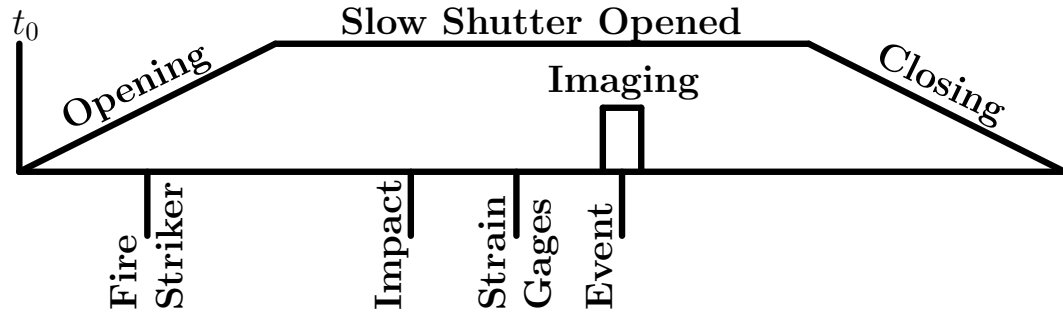
Figure 2.10. Sequence of events for a fast system, where the transit time of the striker is shorter than the opening time of the slow shutter.

apparatus contain two key components that define how the system operates and the quality of imaging: the gas gun, and the slow shutter.

The slow shutter at the sector thirty-two beam line is capable of opening or closing within sixty milli-seconds, this value is relatively fixed, and is expected to be consistent in order for the beam line to function. The gas gun for a small Kolsky bar is capable of firing the striker within one hundred milli-seconds, but the exact time depends on the firing pressure and cleanliness of the barrel. An average time must be calibrated for each nominal firing pressure, as small changes in pressure will result in small changes in striker velocity, and hence small changes in the timing (Figures 2.10 and 2.11).

To compensate for inconsistencies in gas gun operation, the slow shutter is moved to the open position a few milli-seconds before impact of the striker with the incident bar, and remains open for a few milli-seconds after impact. Once the data acquisition system is triggered by passage of the incident wave, the camera and fast shutters are activated with a time delay corresponding to the time of arrival at the specimen. This setup requires multiple delay generators to produce a successful imaging experiment, but once the parameters are known, the start time of the high speed camera may be fine tuned to view any point within an event.

75
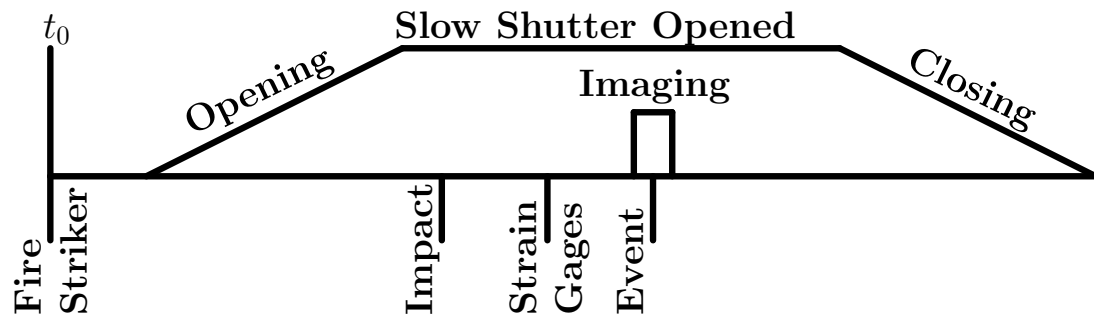
Figure 2.11. Sequence of events for a slow system, where the transit time of the striker is longer than the opening time of the slow shutter.
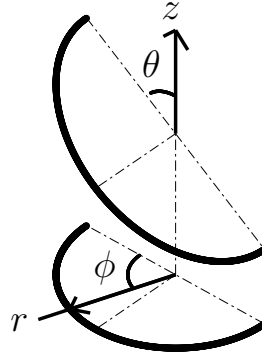
Figure 2.12. Projection of the circular bar cross-section onto the inclined plane at angle θ. The coordinate system is polar (r,z,ϕ), with the z axis aligned with the bar axis. Reproduced with permission from [16]. Copyright (2017) Experimental Mechanics.

2.2.2   Data Reduction

Processing data from a combined compression-torsion experiment is fairly straight forward. Although, the motion of the entire system is coupled, including the torque adapter, the data reduction process is mostly decoupled. This process is also based upon the assumption that the specimen has such low mechanical impedance, that the force and torque must be measured using transducers, as the particle velocity on the transmitted side is nearly zero.

For the data reduction process to be valid, two conditions must be satisfied: the torque adapter must not be closed (Figure 2.5b), and the two parts of the torque adapter must remain in contact. Supposing the two parts remain in contact, the point of contact follows an elliptical profile (Figure 2.12). The contact condition can be all but guaranteed if a specimen is present and provides resistance to the loading. However, an initial gap between the two parts or between the specimen and the transducers will produce erroneous results.

The elliptical profile (Equation 2.15 and Figure 2.12) can be described by the angle of opening (ϕ) and the angle of inclination (θ), where the bar radius (R_B) is

relevant only for the absolute path. The data reduction process requires the tangent vector (Equation 2.16) in normalized form (Equation 2.17).

$$\vec{p} = R_B \left\{ \begin{array}{c} 1 \\ \cos(\phi)\cos(\theta) \\ \phi \end{array} \right\} \tag{2.15}$$

$$\vec{p_t} = R_B \left\{ \begin{array}{c} 0 \\ -\sin(\phi)\cos(\theta) \\ 1 \end{array} \right\} \tag{2.16}$$

$$\vec{p_t} = \frac{1}{\sqrt{1+\sin^2(\phi)\cos^2(\theta)}} \left\{ \begin{array}{c} 0 \\ -\sin(\phi)\cos(\theta) \\ 1 \end{array} \right\} \tag{2.17}$$

The opening angle is related to the contact point by the half angle. That is, since both parts of the adapter are inclined, the contact point lies at the average ordinate of the two, which is precisely half of the opening angle. Thus, through a trigonometric identity (Equation 2.18), the tangent direction can be modified to provide the transmitted components of compression and shear as a function of the opening angle (Equation 2.19).

$$\sin(\frac{\pi}{2} - \frac{\phi_0}{2}) = \cos(\frac{\phi_0}{2}) \tag{2.18}$$

$$\vec{p_t} = \frac{1}{|\vec{t}|} \left\{ \begin{array}{c} 0 \\ -\cos\left(\frac{\phi_0}{2}\right)\cos(\theta) \\ 1 \end{array} \right\} \tag{2.19}$$

Two important quantities are measured by transducers: the axial force (F_S) on the specimen, and the torque (T_S) on the specimen. These quantities describe the axial stress (σ_S) and the shear stress (τ_S) of the specimen (Equations 2.20 and 2.21). Assuming the specimen is an annulus, the shear stress may defined at the average radius

(Equation 2.22). For friction experiments, the friction coefficient may be calculated using the Coulomb friction law (Equation 2.23).

$$\sigma_S = \frac{F_S}{A_S} \tag{2.20}$$

$$\tau_S = \frac{T_S \cdot r_S}{J_S} \tag{2.21}$$

$$\tau_S = \frac{2}{3} \frac{\left(R_{SO}^2 + R_{SO}R_{SI} + R_{SI}^2\right)}{\left(R_{SO} + R_{SI}\right)} \frac{T_S}{J_S} \tag{2.22}$$

$$\mu = \frac{\tau_S}{\sigma_S} \tag{2.23}$$

The remaining quantities: angular velocity of the adapter ($\dot{\phi}_A$), the axial strain rate ($\dot{\epsilon}$), the shear strain rate ($\dot{\gamma}$), and the sliding velocity (v_{ST}) depend upon the transmitted axial velocity (v_{AA}, Equation 2.24) and the transmitted transverse velocity (v_{AT}, Equation 2.25) as determined with the bar end velocity (v_{BE}) and the tangent direction (Equation 2.19). The angular velocity of the adapter (Equation 2.26), not only provides a means to track the opening angle of the adapter, but also allows for the other quantities to be determined using the correct tangent direction. These quantities are influenced by the specific opening angle, but the variation of the components is accounted for in the data reduction process through determination of the current opening angle (Figure 2.13).

$$v_{AA} = \frac{v_{BE} \cdot \cos\left(\frac{\phi_0}{2}\right) \cos(\theta)}{\sqrt{1 + \cos^2\left(\frac{\phi_0}{2}\right) \cos^2(\theta)}} \tag{2.24}$$

$$v_{AT} = \frac{v_{BE}}{\sqrt{1 + \cos^2\left(\frac{\phi_0}{2}\right) \cos^2(\theta)}} \tag{2.25}$$

$$\dot{\phi}_A = \frac{v_{AT}}{R_B} \tag{2.26}$$

(a) Tangential components.

(b) Variation with change of angle.
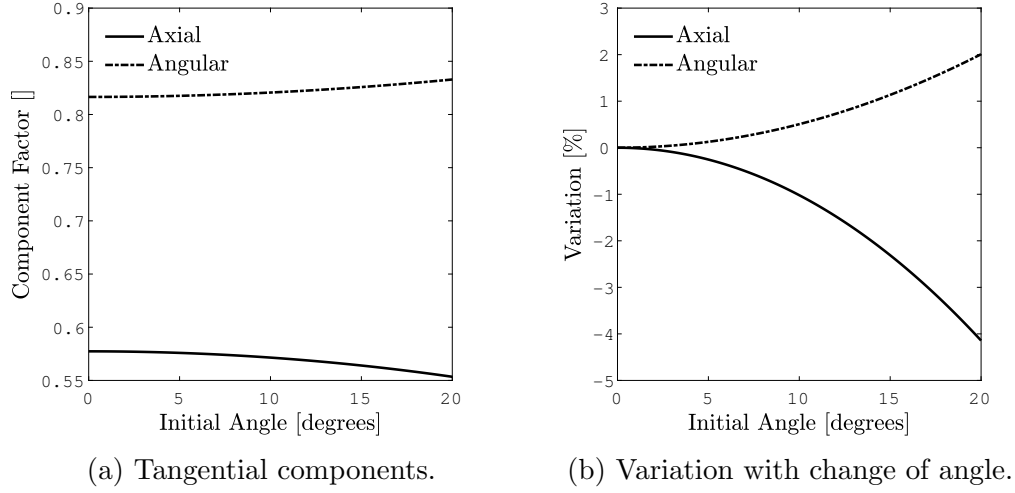
Figure 2.13. The components of the tangent vector change with opening angle for an inclination of 45 degrees. The variation of the components is small, even for moderate changes in angle. Reproduced with permission from [16]. Copyright (2017) Experimental Mechanics.

For shear stress-strain experiments, the axial strain rate is determined by the transmitted axial velocity (Equation 2.27), and the shear strain rate is determined by the transmitted transverse velocity (Equation 2.28). These provide two sets of stress-strain curves, one for axial and one for shear. Likewise for friction experiments, the axial strain rate is determined by the transmitted axial velocity (Equation 2.27), and the sliding velocity is determined by the transmitted transverse velocity (Equation 2.29). These provide and axial stress-strain curve and a friction coefficient-sliding velocity curve.

$$\dot{\epsilon} = \frac{v_{AA}}{L_S} \tag{2.27}$$

$$\dot{\gamma} = \frac{v_{AT}}{L_S} \tag{2.28}$$

$$v_{ST} = \frac{2}{3} \frac{\left(R_{SO}^2 + R_{SO} R_{SI} + R_{SI}^2\right)}{\left(R_{SO} + R_{SI}\right)} v_{AT} \tag{2.29}$$

2.2.3   Specimen Geometry

There are two limitations that affect the specimen's geometry for the combined compression-torsion Kolsky bar. The first is related to torsion and friction, where the specimen should be annular in shape. The second is that the impedance presented by the specimen must agree with the assumption that allows for the use of force transducers instead of a transmission bar. Both of these limitations result in the same geometry: the specimen must be annular in shape (Figure 2.3).

The restriction on geometry is also a benefit, particularly for experiments involving x-ray phase contrast imaging. Since an annular specimen has less material for the x-rays to penetrate, the images are less obfuscated and internal details are more clear.

Specific information on specimen geometry can be found in Section 2.3.

2.3   Specimen Preparation

Friction experiments on the side-impact torsion Kolsky bar were performed on three types of interfaces: metal on metal, metal on cast composite, and metal on machined composite. For the combined compression-torsion experiments, the composite was studied in shear and with friction against a metallic surface. The general sample preparation process involves creating a uniform surface on each specimen that is consistent across all of the experiments. For composites, the exact conditions of the surface is not directly under control, but the flatness and smoothness can be improved through mechanical means.

2.3.1   Metallic Materials

Two types of metal were used in the friction studies. The first pair was aluminum 6061 against aluminum 7075-T6, for which the friction between similar materials was studied to establish validity of the side-impact torsion Kolsky bar technique. The second is 1008 steel, used with the the particle composite. Regardless of material,

Table 2.1. Annular shim dimensions and tolerances.

	Aluminum	Steel
Outer Diameter	25.400 mm (1.000 in)	25.400 mm (1.000 in)
O.D. Tolerance	± 0.051 mm (± 0.002 in)	± 0.051 mm (± 0.002 in)
Inner Diameter	15.875 mm (0.625 in)	15.875 mm (0.625 in)
I.D. Tolerance	+ 0.279 mm (+ 0.011 in)	+ 0.279 mm (+ 0.011 in)
Thickness	3.175 mm (0.125 in)	3.175 mm (0.125 in)
Thickness Tolerance	± 0.178 mm (± 0.007 in)	± 0.076 mm (± 0.003 in)

each metallic specimen went through the same general preparation process to produce a desired surface finish.

The raw materials were acquired as thick annular shims, referred to as washers in the industry. These washers are precision ground as a plate before being punched into their annular shape. The washers are manufactured in standard sizes that are also used in the manufacture of the round bar used in the construction of the Kolsky bar apparatus (Table 2.1). These types of washers are meant to be used in applications where thickness and diameter are critical, and thus have tight tolerances.

The process of punching the washers does not leave a uniform surface, where lubricant and debris will leave indentations on the surface. Furthermore, bulk packaging leaves the surfaces exposed and the individual washers damage each other. While this may be an important factor for an application specific study, these conditions were deemed unsuitable, and more uniform and consistent surfaces where desired.

To create the necessary surface conditions, the washers were polished on one side. The washer punching process leaves one side flat, and the other with the typical rounded edges produced in a shear operation. Polishing the flat side of the washer not only decreases the amount of time required to produce the necessary surface conditions, but also ensures the specimen retains parallelism between the two surfaces. Each specimen, whether aluminum or steel, was polished to a near mirror finish using 3.8 micron grit (1200 grit). This process involved multiple steps, starting from the as-received surface, progressing step by step, grit by grit, until the surface was uniform and free of defects and indentations.

Combined Compression-Torsion Experiments

Friction experiments performed on the combined compression-torsion Kolsky bar made use of a platen that was affixed to the transducer assembly. Each platen was made from stainless steel and polished only to 10.6 micron grit (600 grit). The goal behind this reduction in polishing was to provide a uniform surface that induced enough material motion in the specimen to provide more interfacial motion during x-ray phase contrast imaging experiments.

Specimen Installation

These metallic materials, being non-porous, are relatively simple to install on the experimental apparatus. First, the surfaces to be adhered must be treated: by creating a rough surface using 10.6 micron grit (600 grit) abrasive, and by cleaning debris and oil from the surface. An appropriate adhesive should have a debonding strength greater than the shear strength of the entire specimen. That is, for friction experiments, cyanoacrylate adhesive is sufficient. However, the cyanoacrylate adhesive must be fully cured before the experiment is performed, as this type of adhesive typically does not self set on metallic surfaces. Using an accelerator mitigates this problem, but the adhesive requires a minimum time to produce a suitable bond (typically twenty minutes, but depends on the adhesive in use).

Alignment of the polished surface of the specimen is guaranteed through a small amount of axial pressure during the curing process. With one side of the specimen slightly rounded from the manufacturing process, the specimen will pivot to allow the flat, polished surface to be in full contact with the opposite surface. The adhesive then fills any gaps and cures into a solid, producing a strong bond and a specimen with proper surface alignment.

2.3.2 Soft Composite Material

The particle composite is a mixture of polydimethylsiloxane (PDMS, silicone rubber) and sugar crystal. This material is meant to be a safe alternative material to study in place of the real material which is extremely volatile and explosive. This type of material is referred to as a "simulant", as the material simulates the mechanical properties of the energetic material, except without the potential for a dangerous chemical reaction.

Modern simulant materials are often either proprietary or classified for reasons of national security. Access to these materials and their formulae is as restrictive as their energetic counterparts. There are some materials in literature that are are available to study without these restrictions, but their purpose as a simulated material is moot, as their energetic counterparts are not readily available for confirmation of the simulated properties. However, the application and utility of an experiment does not depend upon the validity of a material, especially if the experiment is designed to determine the properties of the material. So long as the each specimen is consistent, the utility of the experiment may be proven.

The simulant material used in the studies is a simulant of the energetic material PBXn-301 [70]. PBXn-301 is a polymer bonded explosive consisting primarily of pentaerythritol tetranitrate (PETN), which typically accounts for more than eighty percent of the total composite. Modern manufacturing processes are capable of producing these dangerous materials in virtually any shape, but laboratory scale experiments require more consideration. For safety reasons, the simulant form of PBXn-301 was preferred, where the PETN is substituted for another inert substance such as sugar. The appropriate size distribution of sugar particles was mixed with Sylgard and cast into two types of geometry (Figure 2.14) [70].

It is well known that the manufacturing process has an influence on the quality of a surface, regardless of material. For composite materials that must be cast, the composition at the surface may vary drastically from the composition of the bulk
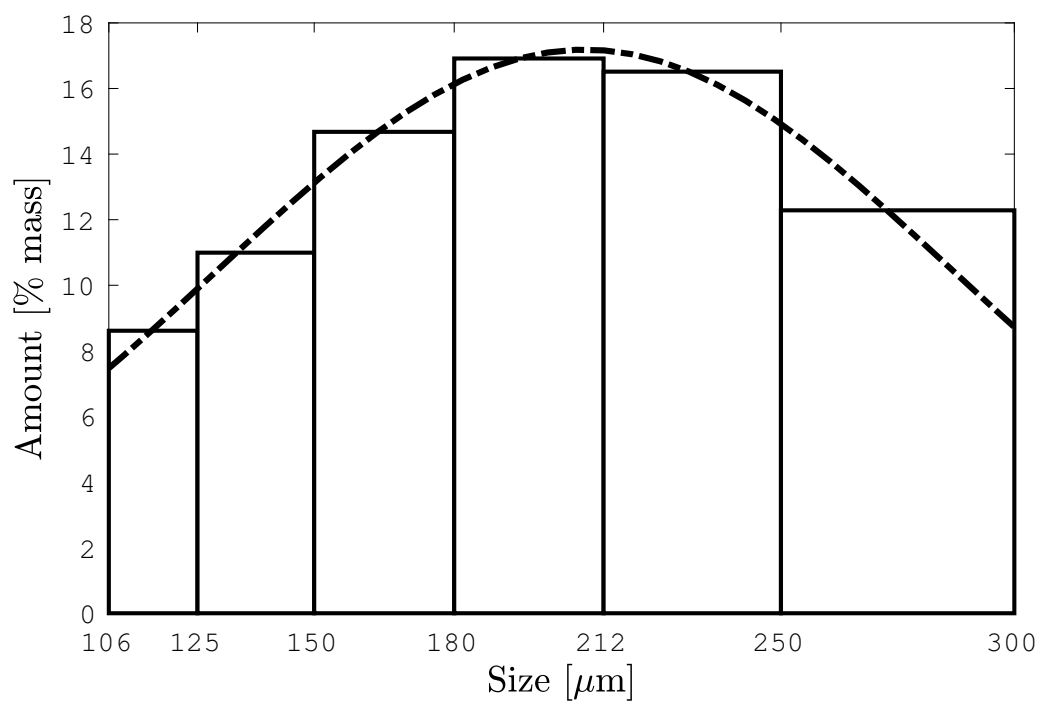
Figure 2.14. Size distribution of sugar particulate within the simulated PBXn-301 material.

(a) Machined specimen.   (b) Cast specimen.
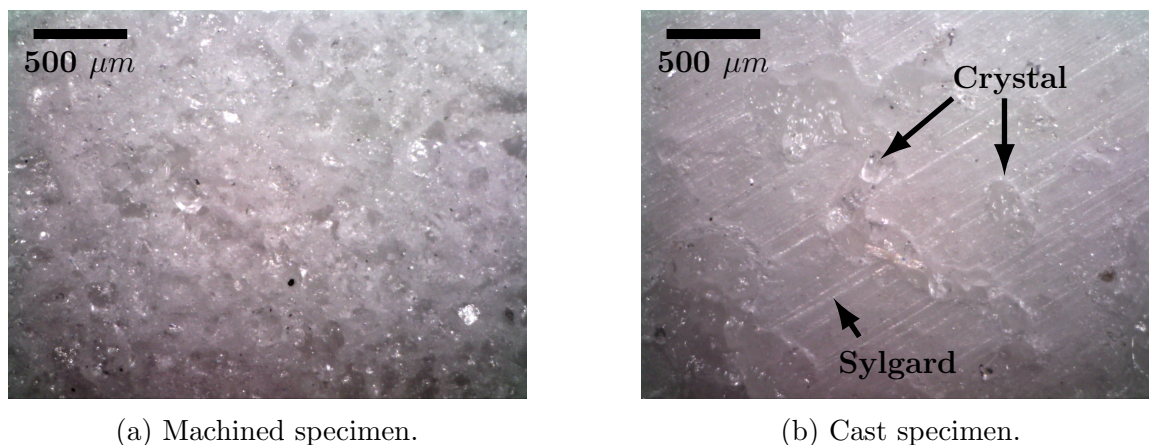
Figure 2.15. Surfaces of machined and cast specimen. The cast specimen has large regions of Sylgard, unlike the machined specimen that is mostly crystal.

material. The primary cause of this difference is capillary action, where the matrix material in liquid form prefers to pool toward the boundary between the walls of the mold and the particulate inside the composite mixture. The result is a casting that has surfaces that are composed mostly of the binder material (Figure 2.15b). In contrast, parts that are mechanically processed from this casting will then have surfaces with composition equivalent to the bulk composition (Figure 2.15a). This change in composition at the surface poses a potentially large problem for energetic materials, for which the composite is meant to improve stability of the volatile particles. The particular material state that may result in an accidental catastrophic chemical reaction is a topic of intense scrutiny. The important topic here is the different friction characteristics of the two surface conditions.

Mechanically Processed Specimen

The first type of specimen is one that has been mechanically processed. The composite mixture was first cast into a tube, which after curing, was then sectioned to form the individual annular specimens. The sectioning process is by no means perfect, and the parallelism between opposing sides of any given specimen will be far

from acceptable. However, the composite material is fairly compliant, and the particle aggregate provides sufficient stiffness for the annulus to be shaved and ground to a specified thickness and parallelism. A specimen produced using this process had surfaces with composition identical to the bulk composition, which is mostly the crystal particulate (Figure 2.15a).

Two sizes of the mold were produced: one for the side-impact torsion Kolsky bar, and one for the simultaneous compression-torsion Kolsky bar (Table 2.2). Both molds where produced from industry standard parts. The design of the mold is simplistic, and allows for extrusion of the cast part to be sectioned (Figure 2.16). Extruding the part incrementally allows for more uniform cuts and produces sections with more uniform thicknesses. The mold consists of three drill bushings and a dowel rod, components that are manufactured to tight tolerances. These components were sized and ground to form a tight seal and surface quality that minimizes adhesion of the Sylgard binder to the mold.

Table 2.2. Ideal mold and specimen dimensions.

	Side-Impact	Compression-Torsion
Outer Diameter	25.400 mm (1.000 in)	12.700 mm (0.500 in)
Inner Diameter	15.875 mm (0.625 in)	9.525 mm (0.375 in)
Tube Length	50.800 mm (2.000 in)	50.800 mm (2.000 in)
Specimen Thickness	3.175 mm (0.125 in)	1.588 mm (0.063 in)

Cast Specimen

An important part of the study was to characterize the friction response of a cast material. Thus, the composite material was cast directly into an annular shape, producing surfaces that were composed mostly of Sylgard (Figures 2.15b and 2.17). A specimen produced using this process required no further steps, as handling the surfaces would disrupt the thin Sylgard layer. The nature of this design requires that the specimen have a relatively large size. This mold was only used for the side-impact

Removable Bushing

Press Fit
Bushing
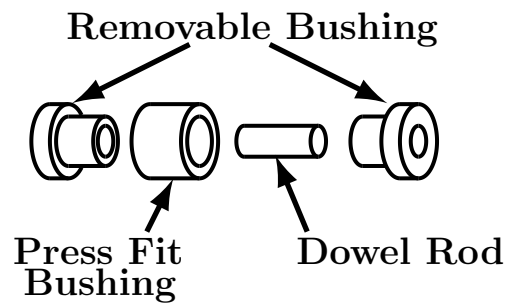
Dowel Rod

Figure 2.16. A four piece mold comprised of three drill bushings and a dowel rod. Internal surfaces were ground to prevent the casting material from adhering to the inside. The mold produces a tube which can later be cut into thin annular specimens. Reproduced with permission from [16]. Copyright (2017) Experimental Mechanics.

Mold Cavities

Relief Gates
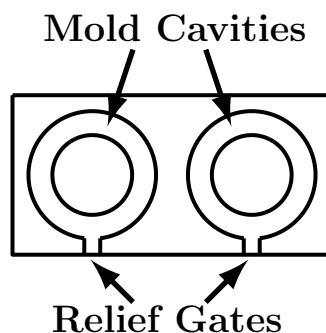
Figure 2.17. Two units of the washer mold. The physical mold consists of three pieces (two solid covers and the middle mold cavities), the middle piece simplifies the separation of each specimen from the mold.

torsion Kolsky bar, and not for the smaller combined compression-torsion Kolksy bar experiments.

X-Ray Phase Contrast Imaging

A specimen meant for an experiment using x-ray phase contrast imaging may need to be modified depending on the phenomena under study. In torsion, a specimen will appear to be motionless, as the two sides of the specimen will be moving in different directions. With the high density of interfaces, the specimen will appear to be a material with a dynamic morphology. To avoid this issue, an annular specimen may be cut to form a c-shaped specimen. This shape will allow the x-rays to pass through only one side of the specimen, allowing rotation and torsional deformation to be clearly observed. With the small size of the x-ray window (roughly 1 mm square), a small wedge spanning 20 degrees was removed from each annular specimen, producing a "window" that allowed the x-rays to penetrate only one side of the specimen.

Specimen Installation

The simulant material is relatively soft, and the sugar crystals provide an avenue for the material to absorb liquids. Thus, adhering this material with an adhesive

with low viscosity is not desirable. Cyanoacrylate adhesive is sufficiently strong for friction experiments, but may be absorbed by the materials. For a cast specimen, with surfaces of mostly binder, the adhesive will not be adsorbed. However, a mechanically processed specimen may absorb a cyanoacrylate adhesive to a depth of one millimeter or more. This may pose a problem for shear stress-strain experiments, but not for friction experiments where the shear strain is not measured or required.

The surface to which the simulant is being adhered must be treated to create a strong bond. First, a rough surface is required, with a minimum abrasive size of 10.6 micron grit (600 grit). Last, the surface must be cleaned of debris and oil in order for a strong bond to be created. The nature of the simulant material does not allow for the use of a cyanoacrylate accelerator, as the low viscosity fluid would be absorbed by the simulant material. Fortunately, the accelerator is not required, as cyanoacrylate adhesives tend to set relatively quickly in the presence of materials similar to sugar.

3. DEVELOPMENT

The development of two new and novel Kolsky bar techniques requires not only knowledge of the state of the art of Kolsky bar technology, but also of potential experiments that may be targeted for the apparatus. Many advancements developed for the compression Kolsky bar are also applicable to the other variants. Furthermore, although the individual pulse shaping techniques for each of the variants do not directly carry over, knowledge of the effects of pulse shaping materials on the generated waveforms helps to identify better means to control the shape of an incident wave.

3.1 Side-Impact Torsion Kolsky Bar

The side impact torsion Kolsky bar was originally developed as a table-top Kolsky bar for studying soft materials (Figure 2.1(a)) [27]. This design can be traced back to an older design that utilized small explosive charges to generate torsional waves with very short rise times [7]. The fundamental design concept is that the incident bar is forcibly rotated using one or more eccentric forces acting on a tab jutting out from the incident bar. However, these simplistic designs do not have the capacity to tailor the duration of the incident wave.

3.1.1 General Concept

Suppose the striker impacting the tab were to be made longer, then surely the incident torsion wave would also be longer. However, a longer period of motion, while linear for the striker, is angular for the incident bar. This means the interface between striker and the tab on the incident bar is constantly changing (Figures 3.1a and 3.1b). With this in mind, the end of the striker cannot be a right circular cylinder, but must

have a cylindrical profile. This allows for a full line contact between the striker and tab regardless of the relative angle between the two (Figures 3.1c and 3.1d). Placing a pulse shaper in between the striker and the tab allows for full pulse shaping of the torsional wave.

Now, with a full set of strikers, and duration of torsional incident wave is possible. However, only one striker is necessary, and there is no guarantee the striker will maintain a favorable alignment to provide for a line contact with the tab. By adding another section, termed the loading bar, the striker may retain the right circular cylinder shape. Here the loading bar remains nearly fixed relative to the tab, and the line contact is all but guaranteed (Figure 2.1). Furthermore, the new interface between the striker and the loading bar provides another opportunity for pulse shaping the torsional wave.

In this configuration, the duration is still dependent on the length of the striker. For simplicity, it is sufficient to change the striker length depending on the desired duration of the torsion wave. Although, the eccentric nature of the tab does not provide enough impedance to stop the loading bar. Since the amplitude of the torsion wave is directly proportional to the length of the tab, small to moderate forces are sufficient to generate large torsional stresses. This poses a problem where the primary portion of the torsion wave will have the appropriate amplitude and duration, but will continue with decaying amplitude until the loading bar is no longer capable of applying a force. At this point the torsion wave will begin to unload and decay in an exponential style as a result of the inertia of the tab.

Borrowing concepts from dynamic sample recovery, a single loading device may be added to the loading bar (Figure 3.2) [4]. Here, the striker may be as long as is desired, as the loading bar may be "turned off' by the single loading device. Mechanically, the wave within the loading bar is reversed by the single loading device, causing the loading bar to separate from the tab and cease generating a torsional wave. The effectiveness of the single loading device is determined by two factors, the impedance ratio with the loading bar, and the degree to which the single loading device is fixed.
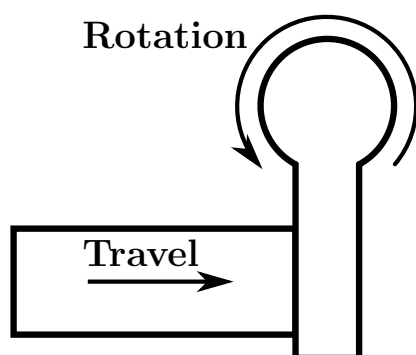
(a) Face contact.
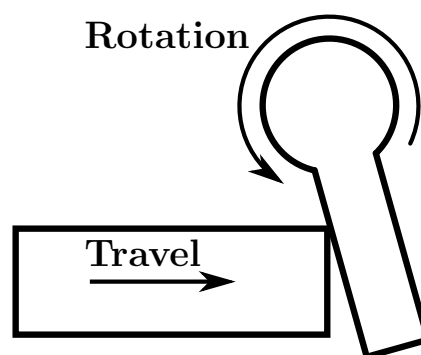
(b) Point contact.
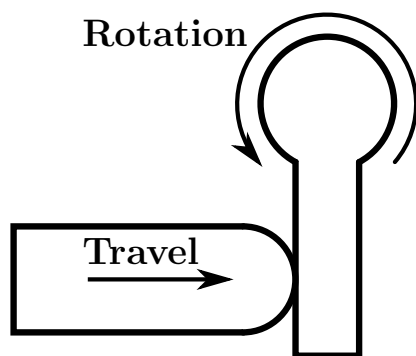
(c) Line contact.
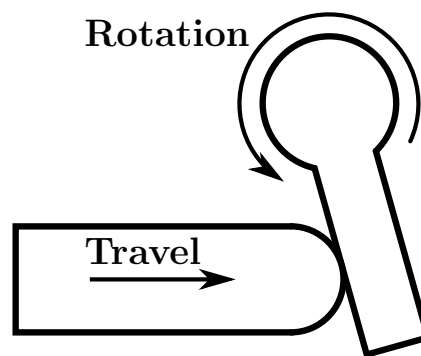
(d) Line contact.

Figure 3.1. Loading bar contact with the tab. A rounded end provides consistent contact regardless of the angle of the tab.
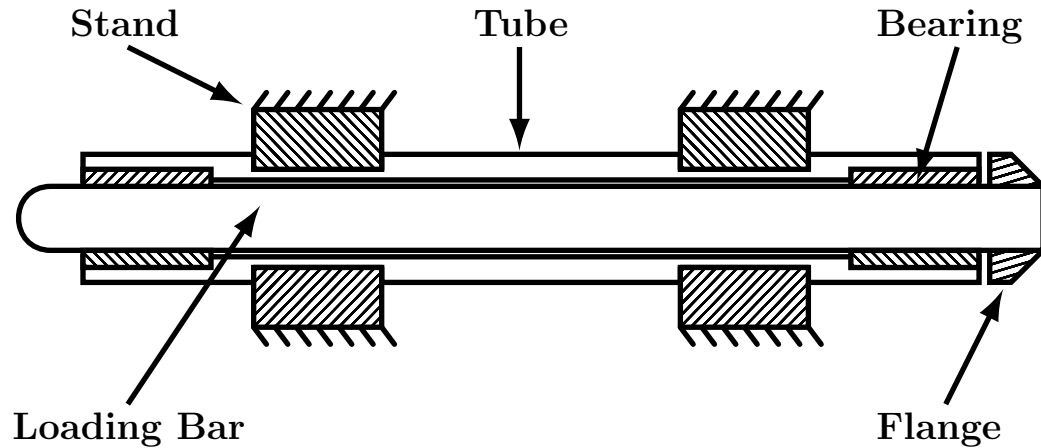
Figure 3.2. Loading bar with single loading device. Contact of the flange with the tube will reverse the particle velocity of a wave within the loading bar.

Having a larger cross sectional area than the loading bar is sufficient, but the effectiveness of the single loading device may be increased by increasing the density and stiffness as well. If the single loading device is able to move, only a portion of the wave within the loading bar will be reversed. However, fixing the device may prove to be difficult if larger forces are involved, as the total force within the single loading device will be twice that expected from the wave (see Equations 1.5 and 1.6 with a large impedance ratio).

With this apparatus, a torsional wave may be generated with any desired shape, duration, and amplitude: an improvement over past torsion Kolsky bar designs. However, deeper analysis of this system is necessary, as physical mechanisms must be manufactured and assembled using real parts and real materials.

The first hurdle to overcome is how to attach a tab to a bar in a manner that does not adversely affect the waveform (Figure 2.1(a)). There are many possible solutions, but the intended function of the apparatus must be considered first. For shear experiments, the shear strain rate is determined by the length of the specimen. Thus a shorter specimen will experience a higher strain rate. For friction experiments,

the variable of interest is the sliding velocity. Thus, a larger diameter specimen will experience a higher sliding velocity. In order to target a specific range of sliding velocities and shear strain rates, the diameter of the bars must be appropriate such that both are easily achievable. In addition, the length of the incident bar must also be chosen such that there is no overlap between the incident and reflected waves during an experiment with the nominal duration. Keeping in mind that the shear wave speed is lower than the bar wave speed, torsion bars inherently require shorter incident and transmission bars than the compression and tension variants.

Supposing the targeted sliding velocities are between one and ten meters per second, and the minimum duration of the incident torsion wave is one millisecond, a moderate choice of bar size is 25.4 mm in diameter and 3.66 meters in length (equivalent to a 1 inch diameter, 12 foot long bar). A bar of this size cannot easily be machined with a tab from a solid piece of material. Instead the tab must be affixed to the bar in another manner using an interface that is conducive to transmitting torsional waves. Furthermore, many questions should be answered before constructing a physical mechanism, many of which may be answered by analyzing the dynamics of the system without physically constructing the system.

3.1.2   Torsional Interface Studies

Transmitting torsional waves is non-trivial. One may consult a local hardware store to observe possible torque transmitting geometries. Two ideal shapes considered for transmitting torsional waves where the hexagon (Figure 3.3a), and the key-slot (Figure 3.3b). Another shape was defined which led to the development of the simultaneous compression-torsion Kolsky bar. This shape is based upon the screw, with two opposing inclined planes on the end of a cylindrical bar. This particular interface has four surfaces, two of which are the inclined planes, and the other two are parallel with the bar axis. It is these planes parallel with the bar axis that are ideal for transmitting torque (Figure 3.3c). The hardware equivalent of this shape is the

(a) Hexagon. (b) Key-slot.

(c) Parallel planes. (d) Parallel planes (reversed).
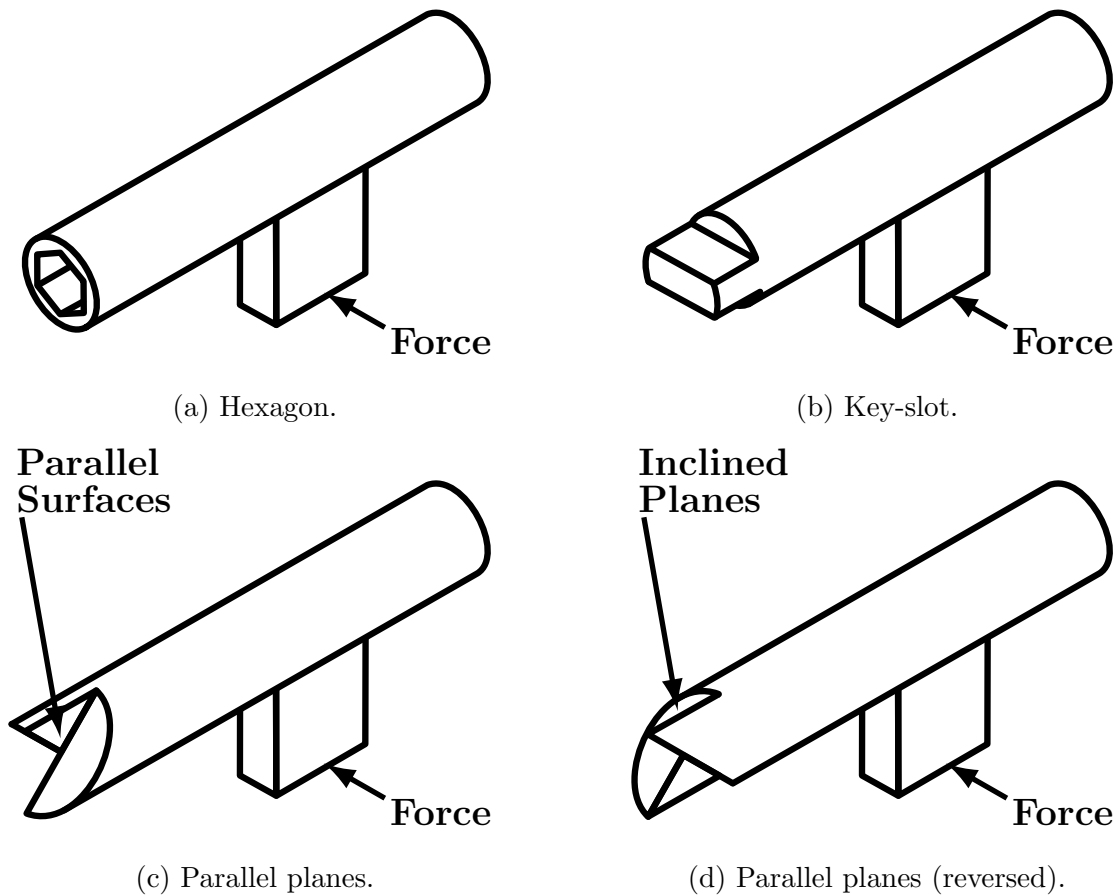
Figure 3.3. Four interfaces that transmit torque. The effectiveness depends on machining tolerance and the impedance presented by the interface. Adapted with permission from [28]. Copyright (2015) Experimental Mechanics.

tamper-proof screw, which permits the application of torque in only one direction. In reverse, the tamper-proof screw transforms the applied torque into a force which then ejects the screw driver from the head of the screw. This principle was identified for possible application of combined compression-torsion (Figure 3.3d).

When waves are involved, fewer faces means less wave interaction and fewer reflections. Thus, when a less than ideal interface is involved, an incoming wave may be partially reflected, resulting in a wave that may later return and influence future motion. Furthermore, the transmitted portion of the wave will have a different amplitude than expected. Thus, an interface near a specimen may mean the specimen

(a) Compression and tension.   (b) Torsion.
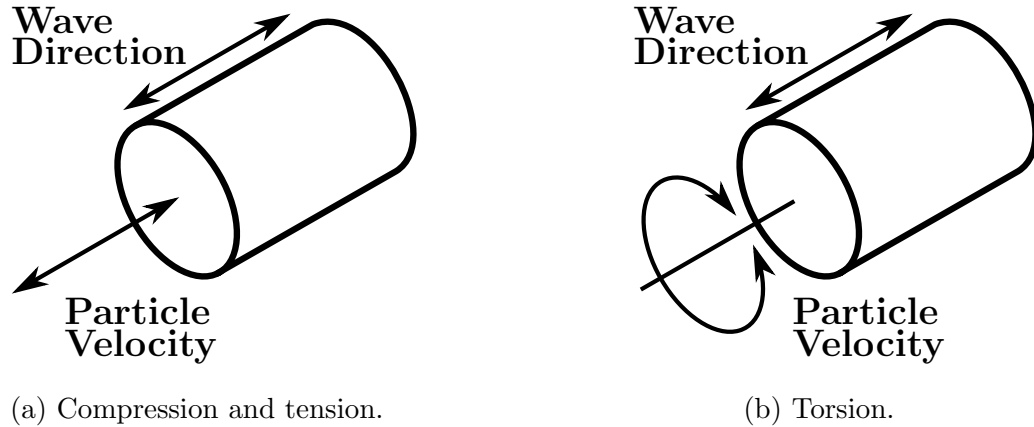
Figure 3.4. Wave directions and particle velocity directions for compression, tension, and torsion.

does not experience the stress state that was expected from a measurement taken at a point away from the specimen.

Unfortunately, the particle motion in torsion is significantly different from that of tension and compression. In tension or compression, the particle velocity is aligned with the axis of the bar (Figure 3.4a), meaning an ideal interface is one with surfaces perpendicular to the bar axis. In torsion, the particle velocity is around the bar axis (Figure 3.4b), meaning the ideal interface has surfaces that are in plane with the bar axis (Figure 3.3c). This type of geometry is non-trivial to produce with tight tolerances using either additive or subtractive manufacturing processes.

Ultimately, the best possible interface for torsional wave propagation is that which may be produced with the tightest possible tolerances. With tighter tolerances, there is less displacement before parts come into contact, meaning any incoming wave will be able to immediately transmit through the interface. The key-slot interface was found to be the most ideal, as the simplified geometry does not require complex machining practices, resulting in the potential for tighter tolerances.

3.1.3   Governing Equations

Before analysis of a system may begin, there must be design details in place, particularly when wave propagation is involved, as interfaces disrupt the waveform and direction. Analysis of the mechanics of the torsion bar did not begin until after a simple prototype was constructed, but was instrumental in resolving problems related to the loading bar, pulse shaping, and single loading device. Furthermore, deeper analysis on various waveform components was not possible until waveforms in the real system were generated, as the phenomena found in the real waveforms were not known to exist.

The governing equations of the side-impact torsion Kolsky bar were originally derived with the intention of studying the duration of the wave and the effects of tab inertia and angle on the shape of the torsional wave. However, experimenting with parameters as well as the real apparatus uncovered many other variables that influence the torsion wave. These include striker length, loading bar length, torsion interface geometry, and non-inertia related tab geometry. Each of these have a direct impact on either how the torsion wave is generated or how the torsion wave propagates.

The governing equations are based on simple dynamic theory and represent a system that undergoes rigid body motion (Figure 3.5). Wave propagation is considered outside of the loading bar-tab interface, but still within the loading bar and torsion bar. Solutions to the governing equations are determined numerically, where wave propagation may be accounted for with relative ease. The most fundamental assumptions are that the entire system is linearly elastic and the contact between the loading bar and tab is a line contact (as opposed to a face contact or point contact). The governing equations themselves assume the loading bar is in contact with tab, but this fact may be supplemented with a contact law that allows the tab to be represented as a separate entity from the loading bar. The contact law is a necessary addition when analyzing wave propagation within the tab, as the contact condition in the real system exhibits this behavior.
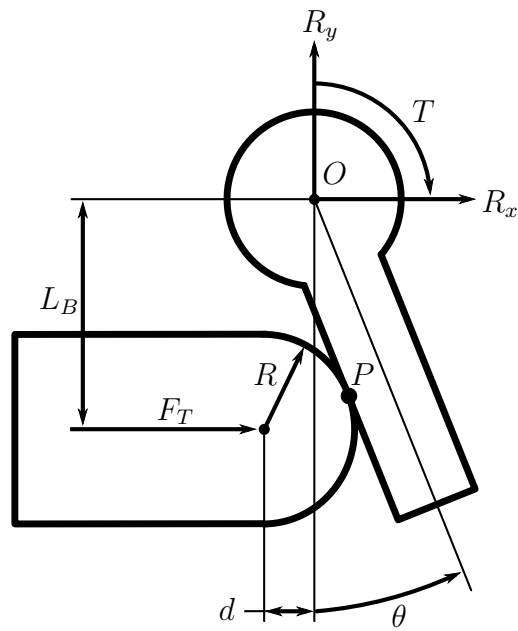
Figure 3.5. Free body diagram of the loading bar contacting the tab and incident bar. The contact is assumed to be a line contact. Adapted with permission from [28]. Copyright (2015) Experimental Mechanics.

The governing equations boil down to conservation of angular momentum of the tab and a relation for the displacement of the loading bar (Equations 3.1 and 3.2). The force in the loading bar (F_T) is determined by a numerical wave propagation algorithm and transmitted to the tab across the interface. The resultant torque (T) on the tab is also supplemented with a wave propagation algorithm within the short segment in which the tab exists (consult Equation 2.1 and Figure 3.10). Thus, the total torque on the tab is a sum of the force-moment from the loading bar and the shear stress in the incident bar. The displacement (d) of the loading bar and the angle of the tab (θ) are then used to determine the line of contact (P) between the loading bar and tab to determine if the two bodies are in contact (Equation 3.2). The offset of the loading bar to the torsion incident bar (L_B) contributes directly to the amplitude of the torsion wave, but is augmented by the loading bar radius (R) and the line of contact (P). The primary equation is influenced by the mass moment of inertia of the tab (I_{ww}^0), meaning the torsion wave will have a decay at the end of the waveform (Equation 3.1). The reaction forces on the torsion incident bar $(R_x$ and $R_y)$ describe the transverse forces applied to the torsion incident bar and are indicators of how much flexure there could possibly be without sufficient support of the system.

$$\ddot{\theta} = \frac{F_T(L_B - R sin\theta)}{I_{ww}^0} - \frac{2G\dot{\theta}J}{C_s I_{ww}^0} \tag{3.1}$$

$$d = d_0 + \int_0^t v_{end} dt \tag{3.2}$$

3.1.4   Numerical Solutions & Frequency Domain

Wave propagation may also be studied using the finite element method. This approach however does not yield a fully formed solution, as the solution is entirely dependent upon the input to the numerical system. This is a result of how the finite element matrix is formulated for wave propagation, which is based upon the particular wave guide model that is desired.

The basis for the one dimensional finite element method of this type, also referred to as the spectral finite element method, is based on the solution for waves in a one dimensional wave guide which may be described using a Fourier series (Equation 3.3). The spectral coefficients are then a function of space (Equation 3.4), and are all that are important, as all of the quantities are defined on the same discrete frequencies (ω_n) determined by the Fourier transform.

$$u(x,t) = \sum_n \hat{u}_n(x) e^{i\omega_n t} \tag{3.3}$$

$$\hat{u}_n(x) = c_n e^{-ikx} \tag{3.4}$$

The simplicity of this method in studying wave propagation can be illustrated using a rod as a simple wave guide. The finite element method makes use of the rod model equated to the applied forces (Equation 3.5). For wave propagation, the rod model is equated to the acceleration of the material (forces may be applied for an inhomogeneous solution, Equation 3.6). Applying the spectral representation of the solution shows how a majority of the form is eliminated from the governing equation (Equations 3.7, 3.8, 3.9, and 3.10).

$$EA\frac{\partial^2 u}{\partial x^2} = \sum F \tag{3.5}$$

$$EA\frac{\partial^2 u}{\partial x^2} = \rho A\frac{\partial^2 u}{\partial t^2} \tag{3.6}$$

$$\frac{\partial^2 u}{\partial t^2} = -\sum_n \omega_n^2 c_n e^{-ikx} e^{i\omega_n t} = -\sum_n \omega_n^2 \hat{u}_n(x) e^{i\omega_n t} \tag{3.7}$$

$$\frac{\partial^2 u}{\partial x^2} = -\sum_n k^2 c_n e^{-ikx} e^{i\omega_n t} = -\sum_n k^2 \hat{u}_n(x) e^{i\omega_n t} \tag{3.8}$$

$$EA\frac{\partial^2 u}{\partial x^2} = -EA\sum_n k^2 \hat{u}_n(x)e^{i\omega_n t} =$$
$$\rho A\frac{\partial^2 u}{\partial t^2} = -\rho A\sum_n \omega_n^2 \hat{u}_n(x)e^{i\omega_n t}$$

(3.9)

$$\sum_n (\rho A\omega_n^2 - EAk^2)\hat{u}_n(x)e^{i\omega_n t} = 0 \rightarrow (\rho A\omega_n^2 - EAk^2)\hat{u}_n(x) = 0 \qquad (3.10)$$

The finite element problem is now an Eigen-value problem, with the Eigen-value being the spectrum relation that describes how the waves propagate in space (Equation 3.10). For a one-dimensional rod, the spectrum relation is simple (Equation 3.11), providing a constant wave speed (phase speed, Equation 3.12) that is coincidentally identical to the group speed (Equation 3.13). Furthermore, the speeds are equivalent for all frequencies, meaning the wave is non-dispersive, and will retain its shape indefinitely in an infinite wave guide.

$$k = \sqrt{\frac{\rho A}{EA}}\omega_n \qquad (3.11)$$

$$C = \frac{\omega}{k} = \sqrt{\frac{E}{\rho}} \qquad (3.12)$$

$$C_g = \frac{\partial\omega}{\partial k} = \sqrt{\frac{E}{\rho}} \qquad (3.13)$$

The same process holds in angular form for torsion using a one dimensional wave guide (Equation 3.14 for the finite element method and Equation 3.15 for the spectral method). The Fourier representation of the solution (Equations 3.16 and 3.17) lead to a similar Eigen-value problem (Equation 3.18). The phase speed (Equation 3.19) and group speed (Equation 3.20) for this one-dimensional torsion wave guide are also

identical and independent of the frequency, meaning these torsional waves are also non-dispersive.

$$GJ\frac{\partial^2\theta}{\partial x^2} = \sum M \tag{3.14}$$

$$GJ\frac{\partial^2\theta}{\partial x^2} = \rho J\frac{\partial^2\theta}{\partial t^2} \tag{3.15}$$

$$\theta(x,t) = \sum_n \hat{\theta}_n(x)e^{i\omega_n t} \tag{3.16}$$

$$\hat{\theta}_n(x) = c_n e^{-ikx} \tag{3.17}$$

$$\sum_n (\rho J\omega_n^2 - GJk^2)\hat{\theta}_n(x)e^{i\omega_n t} = 0 \rightarrow (\rho J\omega_n^2 - GJk^2)\hat{\theta}_n(x) = 0 \tag{3.18}$$

$$C = \frac{\omega}{k} = \sqrt{\frac{G}{\rho}} \tag{3.19}$$

$$C_g = \frac{\partial\omega}{\partial k} = \sqrt{\frac{G}{\rho}} \tag{3.20}$$

However, the solution to the Eigen-value problem is not fully formed, as illustrated by the fact that the Eigen-values may be determined without knowledge of the individual frequency components of a signal (i.e. the Fourier series). Although, for the one-dimensional cases, the elastic deformation is known to be equivalent to the applied load (Equations 3.21 and 3.22). Thus, the relationship between displacement (or angle) and the applied load may be determined, and a full solution formed with the Eigen-values (Equations 3.23 and 3.24). It is worth noting that the complexity of this operation increases with the order of the wave guide model, and may result in an indeterminate system as more variables are introduced.

$$EA\frac{\partial^2 \hat{u}}{\partial x^2} = -\hat{P} = EA \cdot (-ikc_n) \rightarrow c_n = \frac{\hat{P}}{ikEA} \tag{3.21}$$

$$GJ\frac{\partial^2 \hat{\theta}}{\partial x^2} = -\hat{T}L = GJ \cdot (-ikc_n) \rightarrow c_n = \frac{\hat{T}L}{ikGJ} \tag{3.22}$$

$$\hat{u} = \frac{\hat{P}}{ikEA}e^{-ikx} \tag{3.23}$$

$$\hat{\theta} = \frac{\hat{T}L}{ikGJ}e^{-ikx} \tag{3.24}$$

If the applied torque on an incident torsion bar is known, the resultant wave and field quantities may be determined as a function of time using the spectral finite element method. There are three possible sources for the loading information: the physical experiment, which provides a torque; the governing equations, which also provide a torque; and the loading bar, which may be idealized as a rectangular axial wave and provides a force. Furthermore, the flexibility of the finite element method allows for additional degrees of freedom to be added to the model. Thus, longitudinal, shear, torsion, and flexural behaviors may be captured with a singled model.

The system as a finite element model was studied in two forms: one with a tab (Figure 3.6), and one without a tab (Figure 3.7). The model without the tab had the moment of inertia superimposed upon the elements where the tab would have been. The purpose of using these two models was to understand the effects of wave propagation within the tab, which experiences both shear waves and flexural waves. Furthermore, the model with the tab made use of an eccentric force, whereas the model without the tab made use of a torque. Thus, there are four solutions to the side-impact torsion Kolsky bar problem, each of which provides different insight into how the apparatus functions. Material properties and geometric dimensions were maintained from experiment to numerical analysis (Table 3.1).
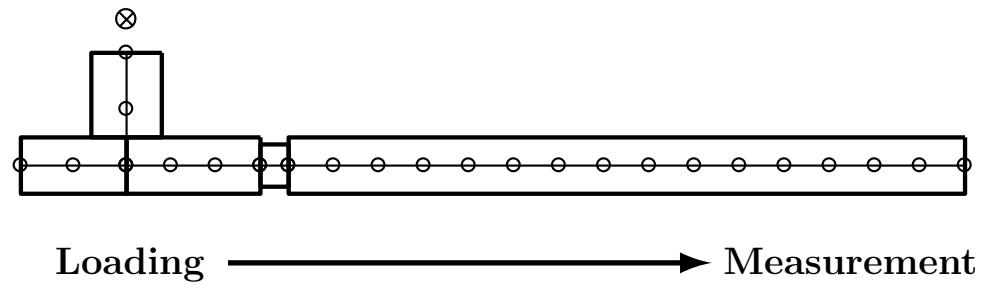
Figure 3.6. Representative mesh of the finite element model with a tab. The system is loaded with an eccentric force.
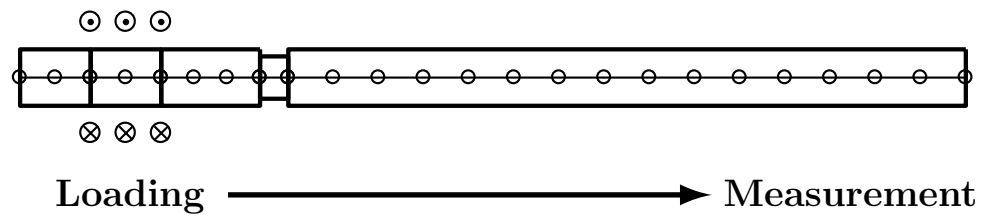
Figure 3.7. Representative mesh of the finite element model without a tab. The system is loaded with a torque rather than a force.

Table 3.1. Values common to experiment and analysis. The impedance ratios are only varied in the numerical methods.

Description	Value	Units
Density	2700	kg/m^3
Young's Modulus	70	GPa
Shear Modulus	27	GPa
Bar Wave Speed	5092	m/s
Shear Wave Speed	3162	m/s
Striking Velocity	6.3	m/s
Low Impedance Ratio	0.32	
Unity Impedance Ratio	1.0	
High Impedance Ratio	5.0	
Bar Diameter	25.4	mm
Loading Bar Length	596.9	mm
Incident Bar Length	7315.2	mm
Striker Length	698.5	mm
Loading Bar Offset	31.75	mm
Impact Mechanism Length	114.3	mm
Tab Distance to Bar	73.025	mm
Tab Distance to End	47.625	mm
Tab Width	31.75	mm
Tab Length	31.75	mm
Tab Thickness	12.7	mm
Single Loading Gap	3.28	mm

3.1.5 Loading Bar & Striker

The loading bar and striker are not two independent entities that are involved in the production of a torsional wave. In fact, the length of the loading bar is closely coupled to the length of the striker. With a loading bar that is too short compared to the striker, the torsion wave will have a series of steps; too long, and the torsion wave will have a series of valleys. An initial hypothesis may be that the contact between the loading bar and the impact mechanism is intermittent, but this hypothesis is only partially correct.

Ideally, the loading bar would be in a state of rigid body motion. As the impact mechanism does not highly influence the state of the loading bar, the waveform within the loading bar remains mostly constant throughout time. In the real system, the waveform within the loading bar is not perfectly rectangular and has a finite, non-zero rise time and release time. Thus, for a loading bar that is shorter than the striker, there will be a period where the wave is overlapped with the end of itself, producing a step in the torsional waveform (Figure 3.8c). For a loading bar that is longer than the striker, there will be a period between the reflections of the wave where the stress is zero, and thus the force applied to the impact mechanism is zero, producing a valley in the torsion waveform (Figure 3.8a). The length of the loading bar must then be perfectly matched (Figure 3.8b) to the length of the striker, otherwise the torsional waveform will suffer.

Determining the appropriate length of the loading bar is quite a simple matter. First, the loading bar must contain a non-dispersive wave, otherwise the waveform will evolve over time and produce unpredictable (although consistent) steps and valleys in the torsion wave. This is accomplished with the use of a large diameter pulse shaper, roughly half the diameter of the bar. For a pulse shaper of annealed copper, the thickness should be less than one milli-meter. This pulse shaper will produce a rectangular waveform with a moderate rise time. The rise time may then be related to linear distance through the longitudinal wave speed of the loading bar. Removing this

(a) Striker too short.   (b) Acceptable striker.   (c) Striker too long.
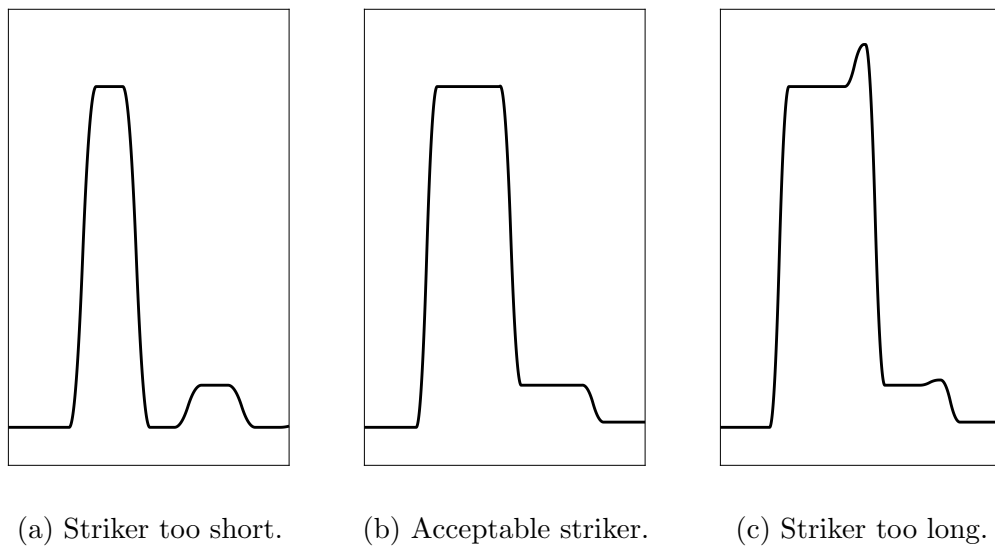
Figure 3.8. Effect of striker and loading bar length on the particle velocity of the loading bar.

distance from the length of the loading bar allows the rising portion of the waveform to overlap with the releasing portion, helping to produce a near state of rigid body motion.

3.1.6 Calibration of Torsion Interface

The incident bar and the impact tab are connected across an interface in the real apparatus. For complex geometries, determining the impedance ratio created by the interface is not a trivial matter. For cases such as the hexagonal interface and key-slot interface, the impedance ratio may be determined empirically. Accomplishing this task is easiest when using a striker that is shorter than the loading bar, which results in a noticeable period of nearly zero stress followed by a secondary peak. The section discussing the effect of ratio between loading bar and striker length (Section 3.1.5) mentioned that the valley is partially influenced by the impedance ratio of the torsion interface. It is true that the secondary peak is caused by a mismatch of length between the striker and loading bar. However, the amplitude of the secondary peak is augmented by the amount of energy transmitted into the tab and torsion bar. The impedance ratio may only be determined without the use of the single loading device, otherwise the device may adversely influence the secondary peak.

Iteratively solving the governing equations with parameters equivalent to the real apparatus allows for the impedance ratio to be found when compared to experimentally obtained data (Figure 3.9). This value is useful when comparing analytical and numerical solutions to experimental results. However, when attempting to reduce the number of variables, it is more suitable to set the impedance ratio to unity, which removes many wave reflection terms from the solution. However, the physical apparatus may benefit from a torsion interface impedance ratio of non-unity, which will inherently inhibit the transmission of flexural waves produced by eccentric loading of the tab.
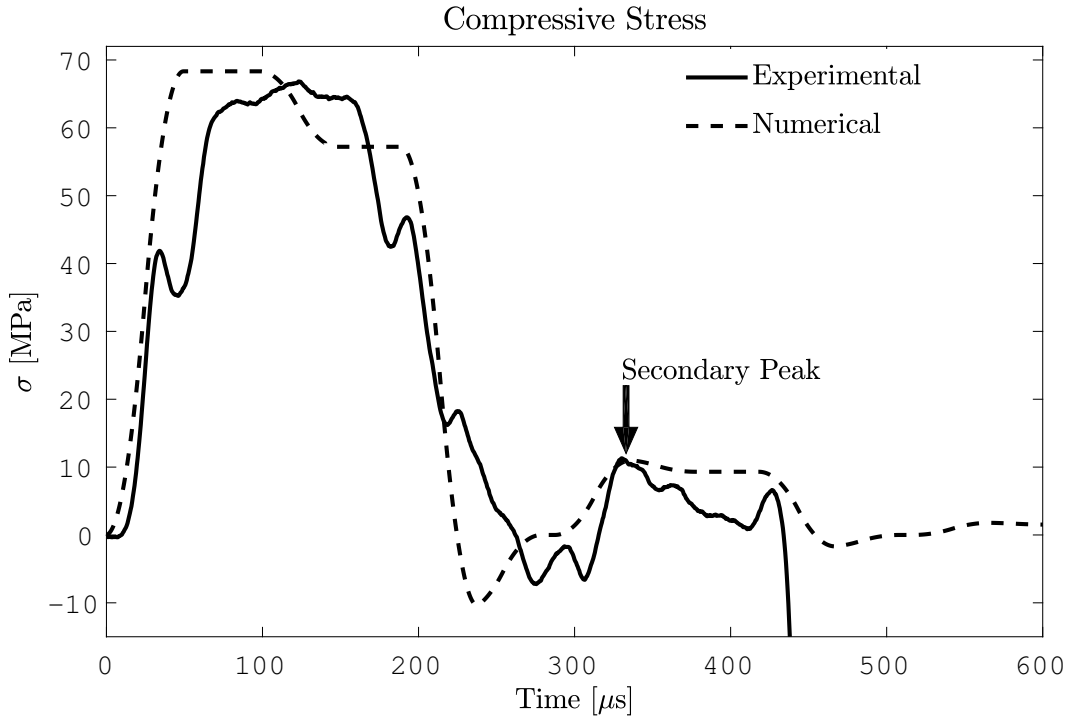
Figure 3.9. Numerical calibration of the torsion interface impedance ratio.

As a side note, the experimental signal as measured from the loading bar (Figure 3.9) shows two large peaks at 50 and 200 micro-seconds. These are a result of threads which allow the attachment of a flange. Using a pulse shaper that allows more deformation will smooth out these peaks. However, the loading bar does not need such a high quality signal, as these portion of the wave will ultimately be masked with a tuned striker length.

3.1.7 Reverberation

An impedance ratio other than unity at the torsional interface results in reverberation of the initial torsion wave within the short segment containing the tab (Figure 3.10). Subsequent reflections of this wave alter the contact between the tab and loading bar, adversely affecting the shape of the resultant torsion wave (Figure 3.11). Even in an ideal situation, where the interface between the incident bar and the im-
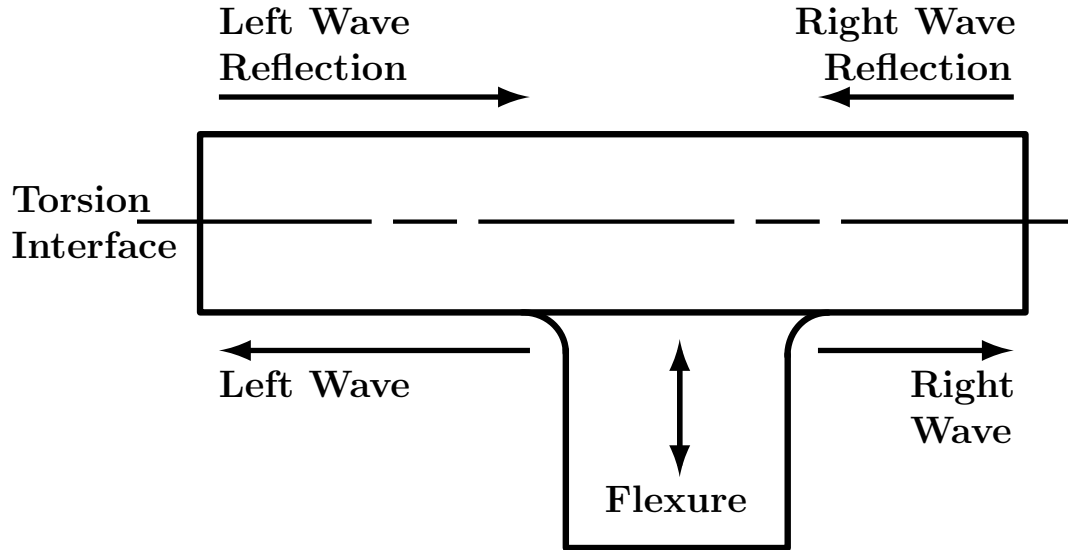
Figure 3.10. Wave reflection within the impact mechanism. The waves interact with the tab to alter the contact with the loading bar.

pact mechanism has an impedance ratio of unity, the design of the tab results in a minimum of one wave reflection, which may produce this same result.

Experimentally, there are two solutions to this problem: use a pulse shaper, or change the design of the tab. Neither of the solutions are restrictive, but the latter may generate more shear (transverse to the bar axis) as opposed to torsion (around the bar axis) and flexure within the real apparatus if the tab is not centered in the impact mechanism. Furthermore, using a more ideal torsion interface mitigates this problem by reducing the number and amplitude of wave reflections within the tab.

The solution to the governing equations revealed that the primary cause for the periodic peaks and valleys was contact between the tab and loading bar. This observation is possible when using a contact law between the tab and loading bar. A simple binary law is sufficient, where the line of contact (P) is determined through both Equation 3.1 and Equation 3.2. For this law, the force is either transmitted or not, and the deformation of the components is not accounted for. If the point is not identical from both calculations, the load is effectively removed from the tab.
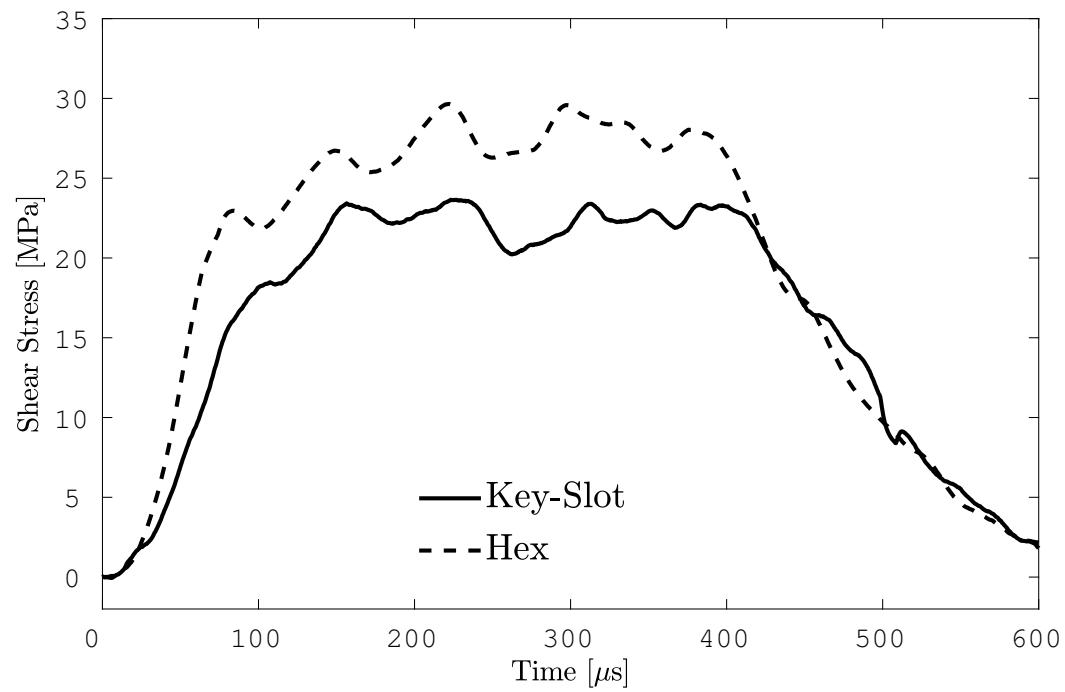
Figure 3.11. Oscillations on the incident torsion wave as a result of the contact between the tab and loading bar. Adapted with permission from [28]. Copyright (2015) Experimental Mechanics.
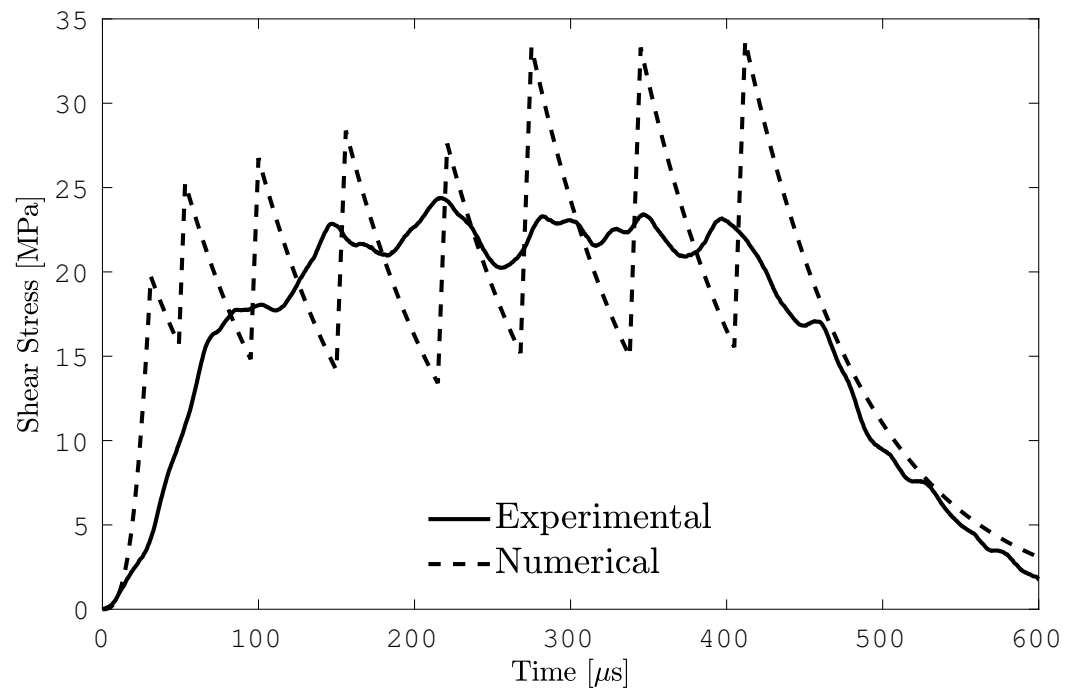
Figure 3.12. Effect of reverberation within the impact mechanism on contact with the loading bar. The contact law is binary and does not account for elastic deformation.

Without accounting for wave propagation, the coupling of Equations 3.1 and 3.2 would not produce this result (Figure 3.12). However, the interaction of the waves augments the torque within the impact mechanism, thus altering the angular acceleration, angular velocity, and angle, producing an inconsistency with the displacement of the loading bar. Close observation of Figure 3.12 shows that the experimental and numerical peaks and valleys do not precisely line up. This discrepancy is a result of the torsion interface which is of finite, non-zero length; something that is not easily captured in a set of equations.

Reverberation of torsional waves within the mechanism has been identified as the source of the oscillations on the torsion incident wave. An easy solution to implement to remove the oscillations is to use a pulse shaper at this interface, which is already required when attempting to form a specific waveform. However, stiff pulse shapers do not filter out this noise, and the root cause is much more fundamental. Also, a simple calculation will show that the period of the oscillations is nearly proportional to the length of the impact mechanism. However, the quantity is not within acceptable tolerance for any conclusion to be made. Rather, the two finite element models were employed to illustrate the effect of geometry on the reverberations within the tab.

To uncover the root cause of the oscillations, analysis of the waveform must occur in the frequency domain. Using fundamental models for the modes of wave propagation (shear, torsion, longitudinal), the relationship between the geometry of the impact mechanism and the resultant torsional waveform may be found in a quantitative manner. The important values determined from the impact mechanism are the total length of the mechanism, the length forward of the tab, the length behind the tab, the width of the tab, the thickness of the tab, and the length of the tab. These geometric quantities are related to specific frequency components in the waveform through one or more wave speed relations. The most relevant here is the shear wave speed.

A simple analysis shows that the oscillations occur at the same times as a pair of waves reflecting across the entire length of the impact mechanism. This is a result of
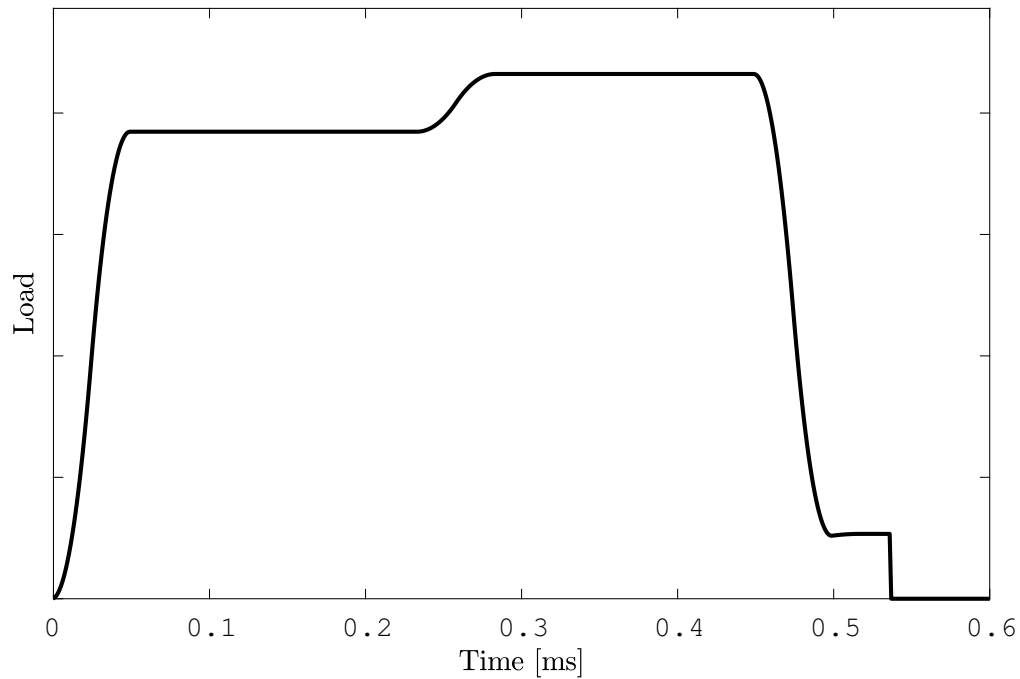
Figure 3.13. Idealized loading profile captured from the end of the loading bar using the analytical approach. The single loading device comes into effect just after 0.5 milli-seconds.

deformation traveling down through the tab, and then propagating in both directions in the impact mechanism. These waves also interact with the tab during transit, thus altering the contact with the loading bar.

The finite element models require an input load in order to predict the torsion incident wave. An idealized force profile was determined using the simple wave propagation algorithm from the analytical approach to determine the force at the end of the loading bar, including the influence of the single loading device (Figure 3.13). This force was then scaled appropriately to provide an idealized torque for the model without a tab.

The predicted torsion incident waveforms from the two finite element models illustrate one key factor in the source of the reverberations: the tab. For the model without the tab, the oscillations are present for only the interface with a high impedance

Figure 3.14. Predicted torsion incident wave for the model without a tab. The oscillations are present for only the highest impedance ratio.

ratio (Figure 3.14). Where as the model with a tab shows oscillations for all impedance ratios (Figure 3.15). This observation shows that the prior conclusion of wave reflection within the impact mechanism alone is not sufficient to produce the oscillations, and that the tab is in fact the culprit.

Analysis of the resultant torsional waveform in the frequency domain illustrates the dependence of the waveform on the various geometric quantities (Figures 3.16 and 3.17). The overall effect of any given component may not be directly observable, whereas others may have a drastic effect, resulting in spectral peaks or valleys. Thus, when comparing the geometric quantities to the frequency response, peaks and valleys that correspond to the geometric quantity or to a multiple of the quantity are indications that the geometry is influencing the waveform in a strong manner.

These key frequencies (f) are identified through an inverse relation between the geometric distance (D) and the wave speed (C_S), any coefficients specific to the
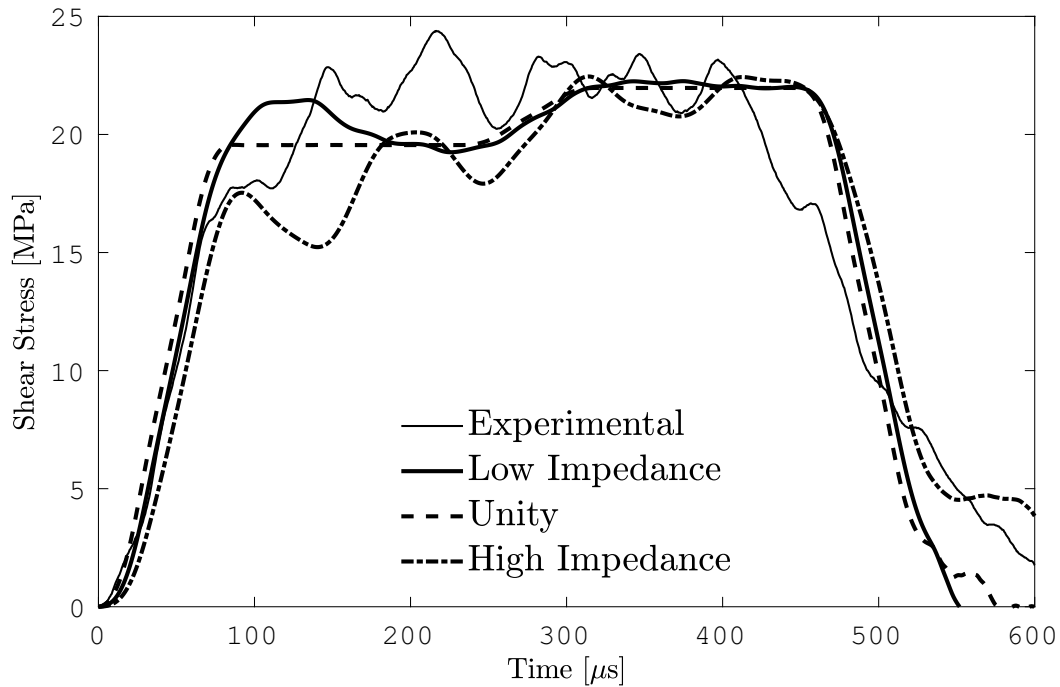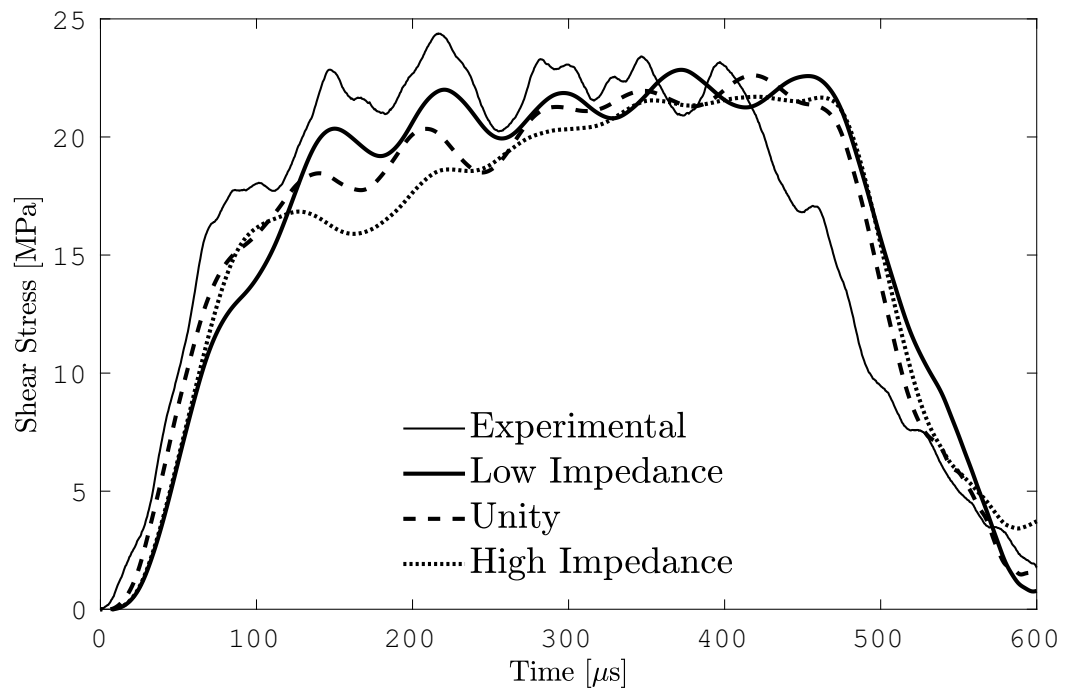
Figure 3.15. Predicted torsion incident wave for the model with a tab. The oscillations are present for each impedance ratio.

Table 3.2. Key frequencies associated with transit distance for various possible wave paths.

Description	Size $[mm]$	Frequency $[kHz]$
Tab Width	63.5	49.8
Tab Length	88.9	35.6
Toward End	95.3	33.2
Toward Bar	114.3	27.7
Total Length	228.6	13.8

Fourier transform must also be applied, though these depend on the form of transform used (Equation 3.25). Some example frequencies based on distances that a wave may encounter within the impact mechanism are provided (Table 3.2). Since the simplified finite element model does not have a tab, many spectral peaks are not present where expected (Figure 3.16). Whereas the tabbed finite element exhibits peaks that the simplified model does not (Figure 3.17).

$$f \propto \frac{C_S}{D} \tag{3.25}$$

To further probe if a frequency component is influenced by the geometry (i.e. the system) and not by the input, a signal may be augmented with one or more band gaps. To generate this signal, the Fourier transform of the time domain signal is required. With the signal in the frequency domain, key components may be removed. In this example, a band of nearly twenty kilo-Hertz centered on a frequency of thirteen kilo-Hertz was removed (Figure 3.18). The frequency of thirteen kilo-Hertz corresponds to the amount of time a torsion wave requires to transit twice the length of the impact mechanism (Table 3.2). With this frequency component and neighboring components removed, the response should have no components within this range unless the system creates them (Figure 3.18). In this case, the tabbed finite element model does in fact have a wave that reverberates within the impact mechanism, and a small spectral peak appears in the response.
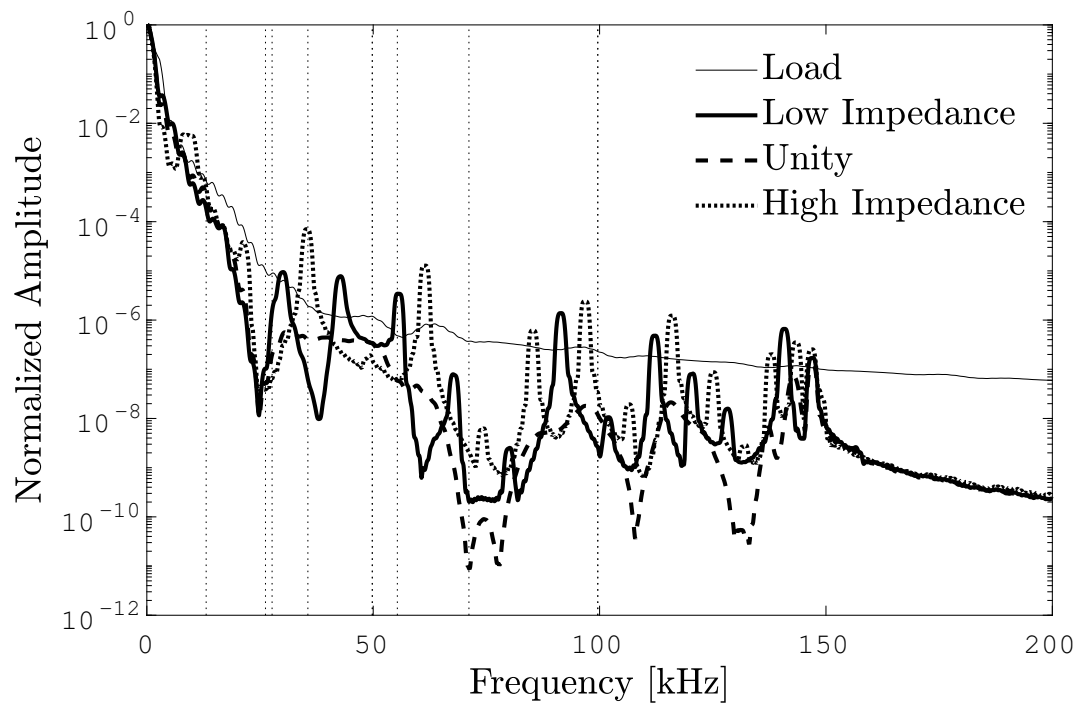
Figure 3.16. Frequency response of the simplified finite element model. Many spectral peaks are not present at the key frequencies associated with the tab.
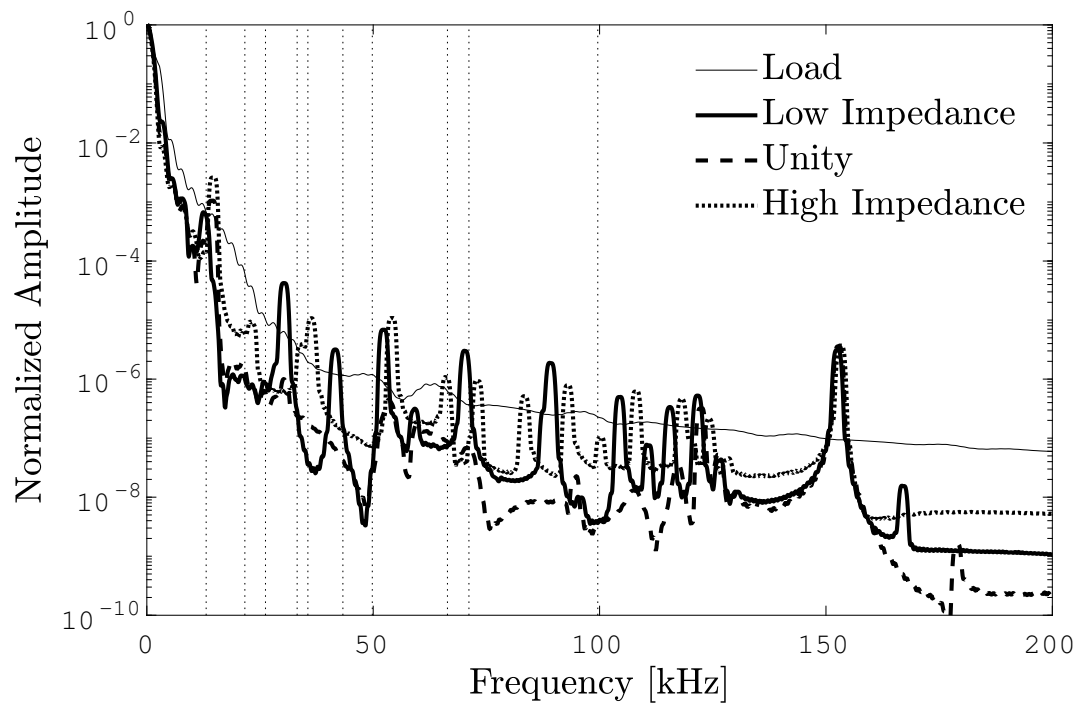
Figure 3.17. Frequency response of the tabbed finite element model. Many more spectral peaks are present due to the presence of the tab.
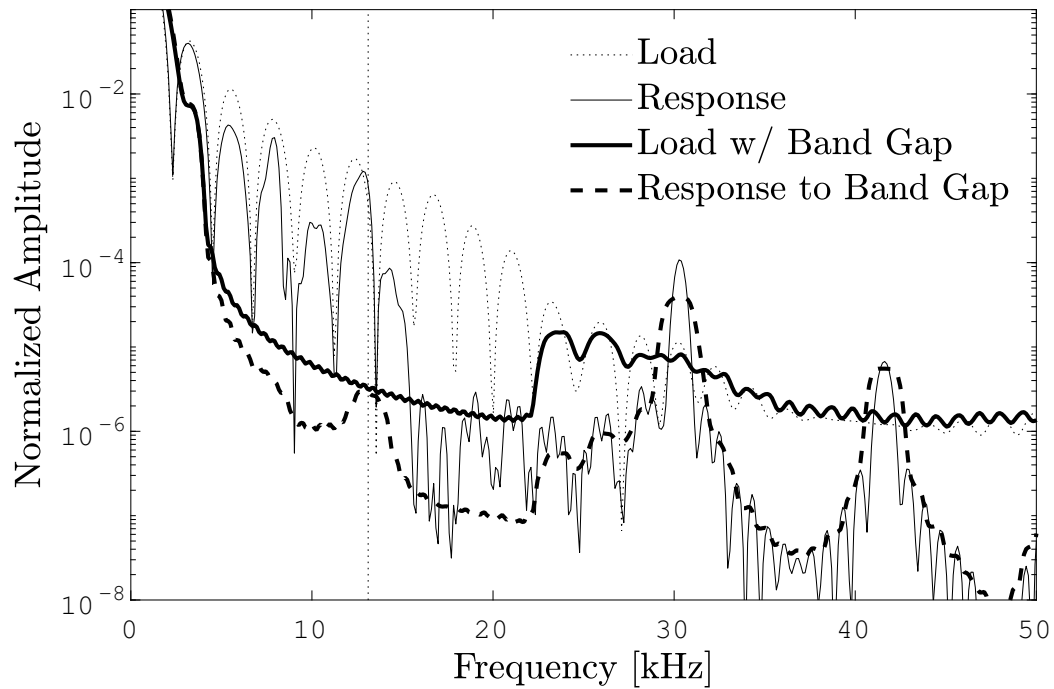
Figure 3.18. Frequency response of the tabbed finite element model to the idealized load and a load with a band gap. A spectral peak is formed at a key frequency associated with the length of the impact mechanism.
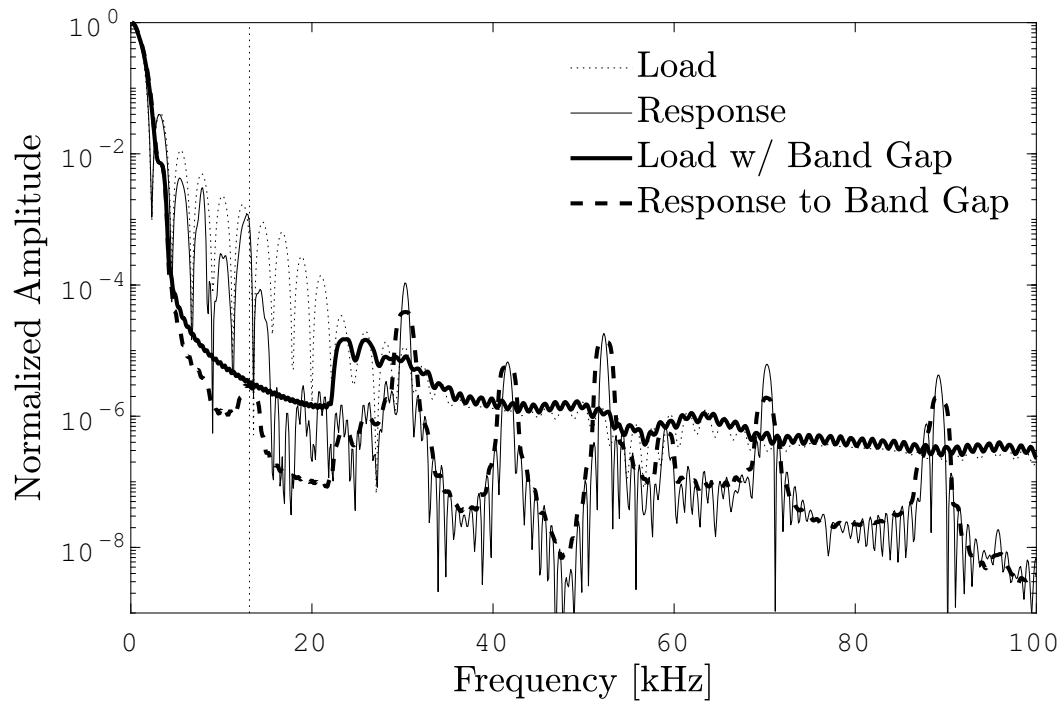
Figure 3.19. Frequency response of the tabbed finite element model to the idealized load and a load with a band gap, illustrating how the impact mechanism augments the waveform.

The response of the finite element model with a tab also shows spectral peaks and valleys beyond the band gap that are also present in the response to the idealized load (Figure 3.19). While many of these peaks and valleys correspond to the geometry, analysis of their sources was not necessary. With the source of the oscillations identified, work to eliminate the oscillations could proceed. The solution to removing the oscillations is of course to use a pulse shaper that is sufficiently compliant to absorb the related frequency components. Permanent deformation of the pulse shaper is also useful, as certain components may be reintroduced to the waveform when the pulse shaper is relaxed. Ultimately, the selection of pulse shaper geometry and material depends on the waveform required, and the process of selection involves trial and error.

3.1.8 Inertia

Unlike conventional torsion Kolsky bar experiments, the side-impact torsion Kolsky bar exhibits a tail off, or decay of the incident torsion wave. This tail off is a result of large rotational inertia presented by the tab. The inertia of the tab also influences the oscillations in the torsion incident wave, as the primary frequency is determine by flexure of the tab, which is in turn influenced by the thickness of the tab. Both of these observations are illustrated quite well with the governing equations when using a simple binary contact law (Figure 3.20).

An ideal experiment would have a fast decay, meaning the tab should be thin. Yet, a thinner tab increases the frequency of the oscillations and will also be subject to large forces and possible permanent deformation, meaning the tab should be somewhat thick. The best solution is somewhere in the middle, and the remaining issues should be smoothed out with a pulse shaper. Furthermore, the unloading portion of a Kolsky bar experiment is rarely important, as the specimen is being relaxed at this point during an experiment.
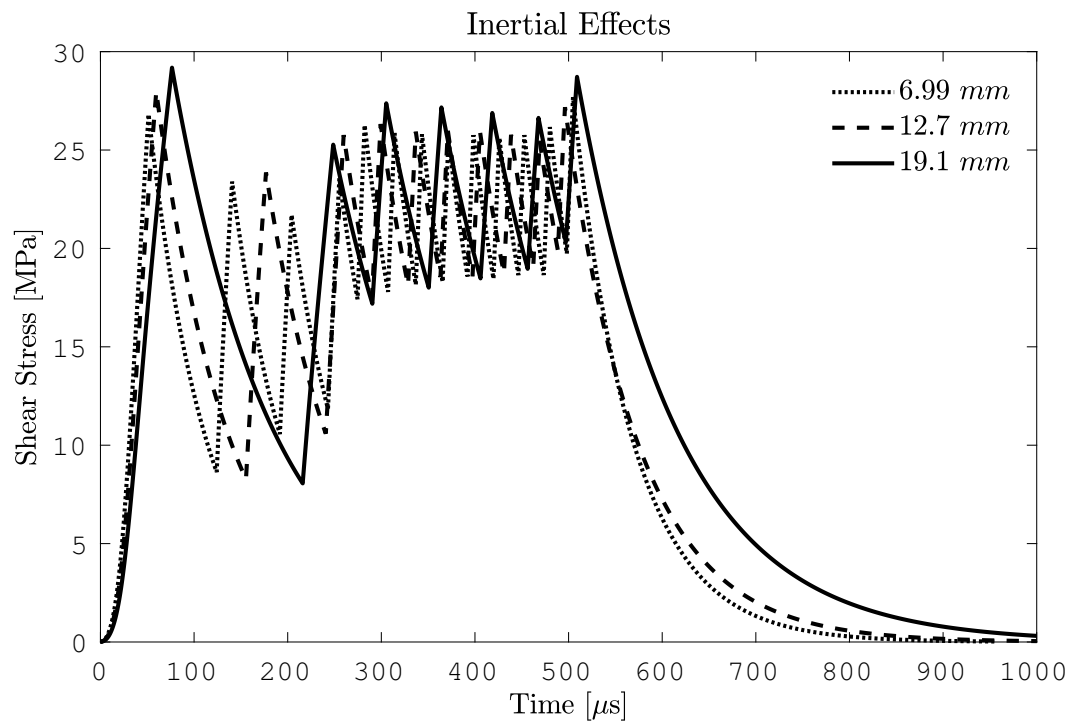
Figure 3.20. The effect of tab inertia on the incident torsion wave. A thicker tab induces a longer decay and a longer period between oscillation as a result of higher flexural stiffness.

3.1.9 Flexural Deformation

A large concern with the torsion Kolsky bar experiment is flexing of the bar. If the bar is bent during an experiment, the specimen may be exposed to inadvertent compression or tension, or an interface may experience uneven pressure. In the side-impact torsion Kolsky bar experiment, there are two sources for flexural deformation. The first, and most obvious source is the fact that the torsion bar is loaded with an eccentric force. A lesser known source, which is present in the compression and tension variants is geometric.

The eccentric force that generates the incident torsion wave is not fully utilized by the impact mechanism. The moment arm (i.e. the tab) does not absorb the force, this is why the loading bar requires the single loading device. However, in order for there to be only rotation of the impact mechanism, there must be a resistive force on the impact mechanism to prevent transverse motion. If this resistive force is not sufficient to resist the eccentric force, a flexural wave will be generated within the incident bar. To ensure this is not possible, the impact mechanism should be supported by tight fitting bearings that are of the same material as the impact mechanism. This ensures that the mechanical impedance is the same, and that the force will be transmitted to the foundation of the apparatus.

The second source of flexure is geometric in origin, and pertains to the linearity of the incident and transmission bars. Suppose the bar is slightly bent in one orientation. After rotation about the central axis, the bar would prefer another orientation. However, being supported by fixed bearings, the bar is now being forced into the original shape, introducing flexure into the bar. From an experimental standpoint, the use of a half Wheatstone bridge configured for axial strains will cancel out the effects of bending on the measurement. However, flexure still exists within the apparatus, dispersion of the waves is inevitable, and the response specimen will be influenced by these changing boundary conditions.

This geometric misalignment of the bars is possible during installation of the bars and is also induced by motion of the foundation. Unlike other Kolsky bar experiments, the side-impact torsion Kolsky bar requires a foundation that is both flexurally stiff and torsionally stiff. This rules out the typical h-beam and optical tables, as the transverse forces required to resist the eccentric force are too great, and these common foundations will deform during an experiment, resulting in erroneous measurements. Unfortunately, this plagued much of the early development of the side-impact torsion Kolsky bar, prompting deeper analysis of the system and its components.

The requirement that the foundation be both flexurally stiff and torsionally stiff determines the possible shapes: mainly that the cross section must be a closed shape. To contrast the types of foundations: an h-beam is capable of resisting deformation due to gravity when the topology of the floor is less than ideal, h-beams do no resist torsion or lateral forces effectively (Figure 3.21a). An optical table is typically a sandwich structure consisting of precision ground plates mounted to a stiff core. The optical table also resists deformation due to gravity on uneven floors. However, the optical table does not resist large lateral forces, as the sandwich structure will fail and become separate. A closed section, such as a box beam or a tube, is capable of resisting flexural deformation in all directions (Figure 3.21b). This shape is also capable of resisting torsion, making the shape ideal for the foundation of the side-impact torsion Kolsky bar.

In other words, proper mounting surfaces for the apparatus eliminate the need to worry about sources of flexural deformation other than general misalignment of the apparatus. Using a half Wheatstone bridge configured for bending, the flexural strain within the bar will be nearly immeasurable, with an amplitude close to the amplitude of the ambient noise (Figures 3.22a and 3.22b). This is not to say that the flexing could not be further improved, but that the flexure is quite small compared to what is electrically measurable.
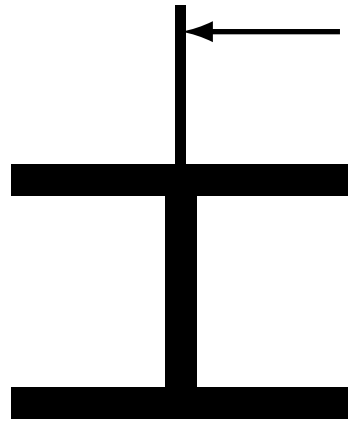
(a) Open cross-section.
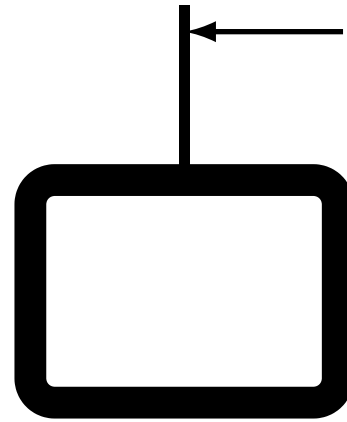
(b) Closed cross-section.

Figure 3.21. The closed cross-section offers multi-directional bending stiffness as well as torsional stiffness.
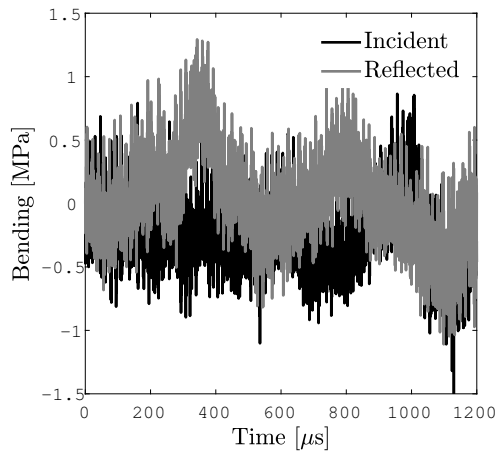
(a) Incident & reflected.
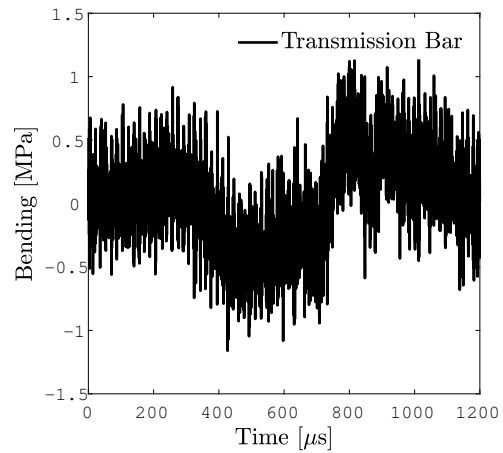
(b) Transmitted.

Figure 3.22. Flexural stresses measured during an experiment. The amplitude is nearly the same as the ambient electrical noise.

(a) Torque only.   (b) Torque and force.
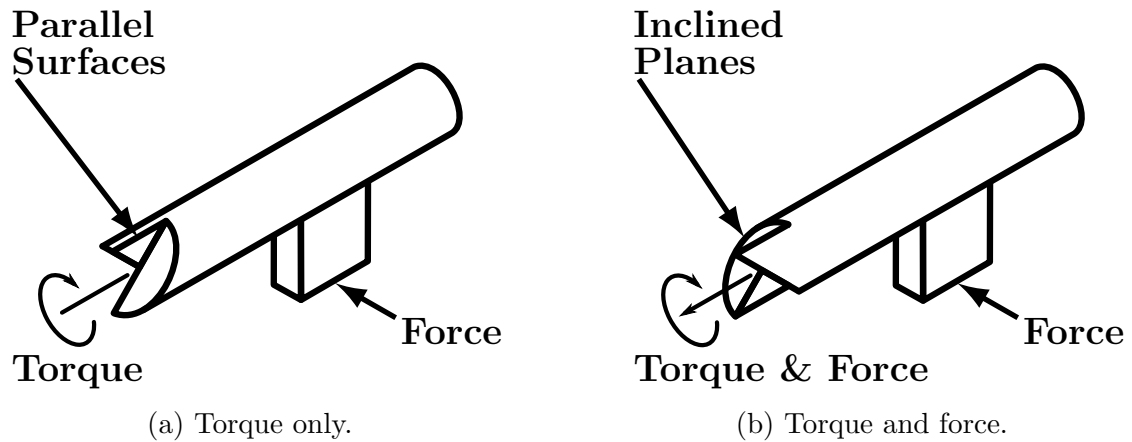
Figure 3.23. The impact mechanism with inclined planes. Rotation in one direction produces only a torque, the other a torque and a force.

3.2 Combined Compression-Torsion Kolsky Bar

Development of the side-impact torsion Kolsky bar produced an ideal torsion interface for transmitting torque (Figure 3.23a). Reversing the direction of the inclined planes produces an interface that is capable of producing force from an applied torque (Figure 3.23b). However, the difference in wave speeds between longitudinal and shear waves means that any set of waves produced far from the specimen will diverge and arrive at the specimen at different times. Therefore, the side-impact torsion Kolsky bar with this torsion interface would not be suitable for combined dynamic compression and torsion without modification.

3.2.1 Different Wave Speeds

To circumvent the issue regarding different wave speeds, the interface may be placed close to the specimen. In this configuration, a single incident wave, whether compression or torsion, will be converted to simultaneously load the specimen with compression and torsion. While this configuration is entirely possible to implement on the side-impact torsion Kolsky bar, there was a strong desire to observe materials under dually dynamic compression and torsion. This is possible with the help of x-ray

phase contrast imaging, for which a remote apparatus already exists. With limited space, the apparatus was designed around a compression Kolsky bar, which is far more compact than the L-shaped side-impact torsion Kolsky bar.

In this setup, an incident compression wave encounters a torque adapter, which in turn transmits both compression and torsion (Figure 2.4). Since the specimen is mounted directly to the torque adapter, there is very little time for the two waves to diverge. For aluminum, a compression wave will reach a distance of 25.4 mm three micro-seconds faster than a torsion wave. With the torque adapter less than 25.4 mm long, the delay between the onset of loading is less than three micro-seconds.

3.2.2 Verifying Functionality

The torque adapter, being a set of contacting inclined planes, does not maintain a uniform contact for all opening angles. For an opening angle of zero, the planes are fully in contact, and the adapter will fully transmit a compression wave without generating any torque. When the opening angle is non-zero, the two halves of the adapter are in contact at only two points that lie on the edge of an ellipse created by the intersection of the cylindrical component with the inclined plane (Figure 2.12). Since the two halves of the adapter are symmetric, the ordinate on the ellipse is actually half of the opening angle, requiring the half angle relation in Equation 2.19. One major issue however, is that the contact is dependent on the specimen.

A fundamental assumption of the data reduction process is that the two halves of the torque adapter are always in contact. Reflection of a compressive wave within the specimen adapter (Figure 2.4) will easily result in a higher particle velocity and cause separation of the torque adapter, thus invalidating the experiment. Furthermore, insufficient resistance to the generated torque may produce the same effect, causing the opening angle to rapidly close.

For shear experiments, these conditions will only be present if the impedance presented by the specimen is sufficiently small that the response of the specimen cannot

Incident Bar

Inclined Planes

Sleeve Bearing

Bar Adapter

Specimen Adapter
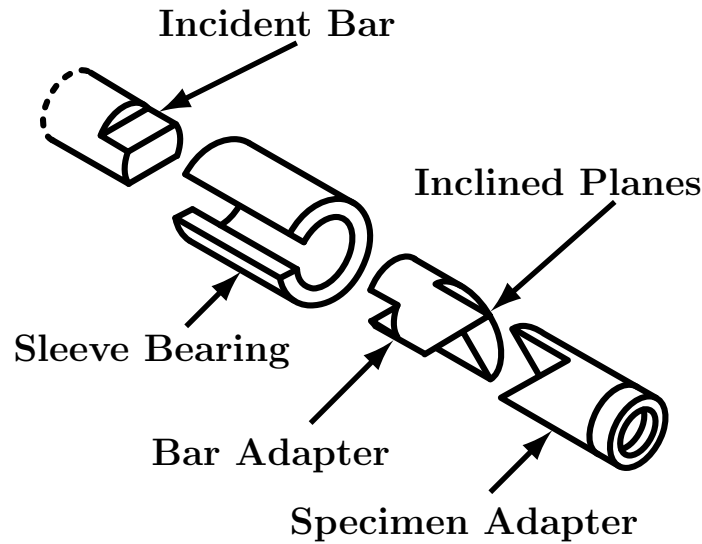
Figure 3.24. The torque adapter with a support bearing. The bearing has a slot that allows the opening angle to be set and monitored.

counteract the motion of the torque adapter. Fortunately, only the most compliant of materials will suffer from this condition. For friction experiments, the specimen adapter is essentially free floating. Thus, without sufficient pre-compression, the interface will present no torsional resistance to the torque adapter, and the experiment will fail. These failures are easy to identify, as no load is measured from the transducers due to the torque adapter closing prematurely.

To resolve the problem with the torque adapter closing prematurely, a small amount of resistance must be applied to the torque adapter prior to the experiment. One approach is to contain the torque adapter within a sleeve bearing (Figure 3.24). Sleeve bearings are manufactured to have low friction on their bearing surfaces, meaning the torque adapter is somewhat free to move longitudinally and rotationally. For the friction experiment, the sleeve bearing maintains alignment of the torque adapter throughout the experiment. Furthermore, the small amount of friction with the sleeve bearing helps to maintain the initial opening angle.

3.2.3   Resolving Uncertainty

However, there is still an uncertainty regarding the rate at which the adapter closes, particularly for friction experiments. Since the scale of the apparatus and specimen are small, there is no measurable torque within the incident bar, even during shear experiments. Without this quantity, one must assume that the torque adapter is not being presented with any torque to resist closing prematurely. Due to the time scale at which this experiment occurs, the only recourse is to observe the event using high speed imagery (Figures 3.25 and 3.26). Observing the motion shows that the torque adapter follows the elliptical path until the adapter is nearly closed. When the opening angle is small, the adapter transistions from a point contact to a full surface contact, an event which is evident in the imagery beginning at 191.1 μs (Figure 3.26g). For the striker with length of 204.8 mm, the duration of the incident compression wave is just shy of 120 micro-seconds, meaning the adapter functions as intended throughout the duration of the experiment.

(a) t = 0.0 μs　　　(b) t = 9.1 μs　　　(c) t = 18.2 μs

(d) t = 27.3 μs　　　(e) t = 36.4 μs　　　(f) t = 45.5 μs

(g) t = 54.6 μs　　　(h) t = 63.7 μs　　　(i) t = 72.8 μs

(j) t = 81.9 μs　　　(k) t = 91.0 μs　　　(l) t = 100.1 μs

(m) t = 109.2 μs　　　(n) t = 118.3 μs　　　(o) t = 127.4 μs
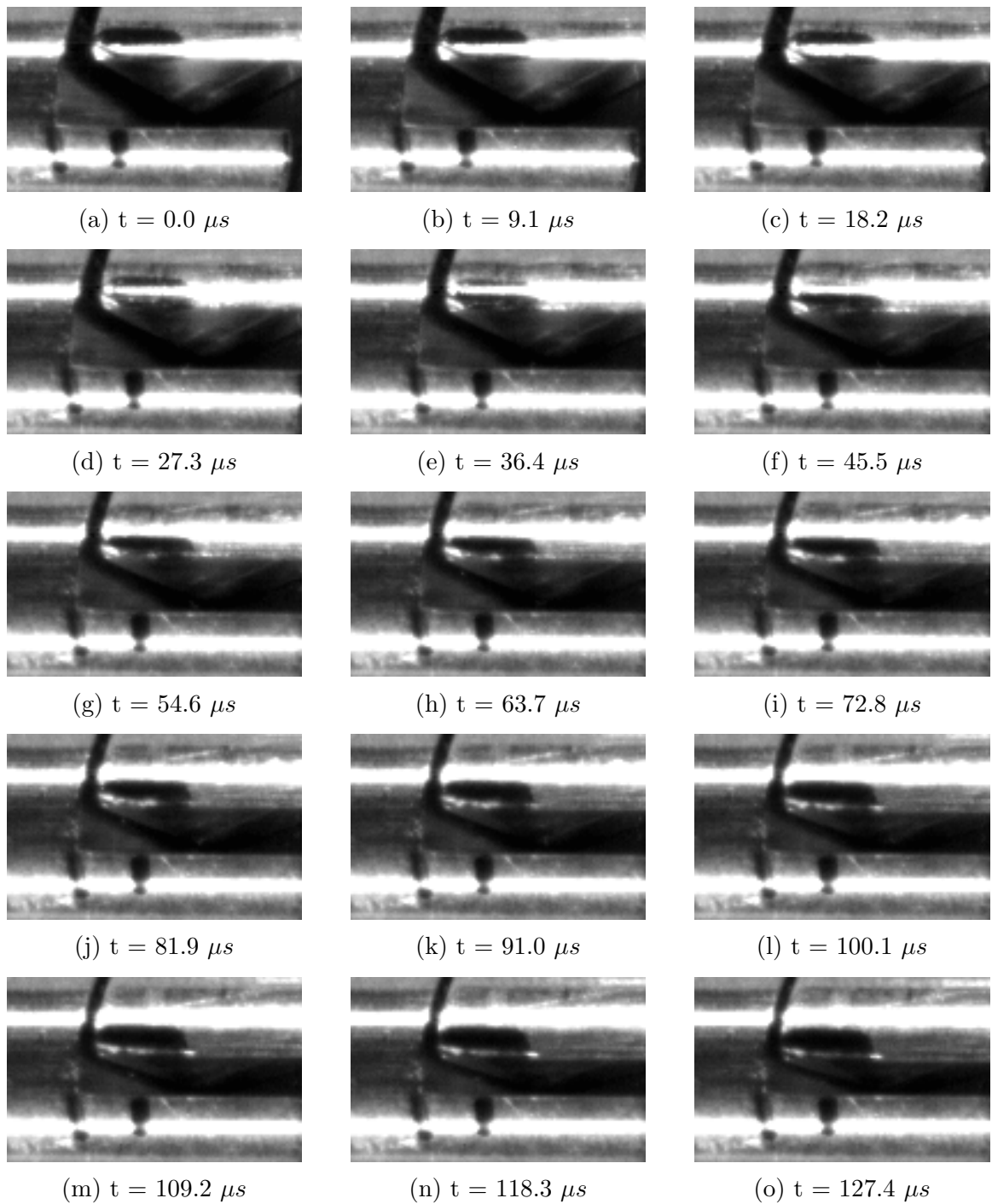
Figure 3.25. High speed images show the torque adapter follows the elliptical path for the duration of the incident wave. Adapted with permission from [16]. Copyright (2017) Experimental Mechanics.

(a) t = 136.5 μs (b) t = 145.6 μs (c) t = 154.7 μs

(d) t = 163.8 μs (e) t = 172.9 μs (f) t = 182.0 μs

(g) t = 191.1 μs (h) t = 200.2 μs (i) t = 209.3 μs

(j) t = 218.4 μs (k) t = 227.5 μs (l) t = 236.6 μs

Figure 3.26. High speed images show the torque adapter jumps to the closed position at 191.1 μs, when the opening angle is nearly zero. Adapted with permission from [16]. Copyright (2017) Experimental Mechanics.

4. STUDIES

New experimental techniques require validation and proof that the results are accurate and consistent with previous techniques. This however, is not to say that the studies should prove the function of the apparatus as hypothesized, but instead that the results of an experiment represent the behavior of the materials. An example of this contrast is the torque adapter for the combined compression-torsion Kolsky bar. While it is important that the function of the torque adapter is verified, that issue is a rather small point, as the experiment would be useless if it were unable to be used to characterize materials (see Section 3.2.3 for details regarding the torque adapter).

4.1 Side-Impact Torsion Kolsky Bar

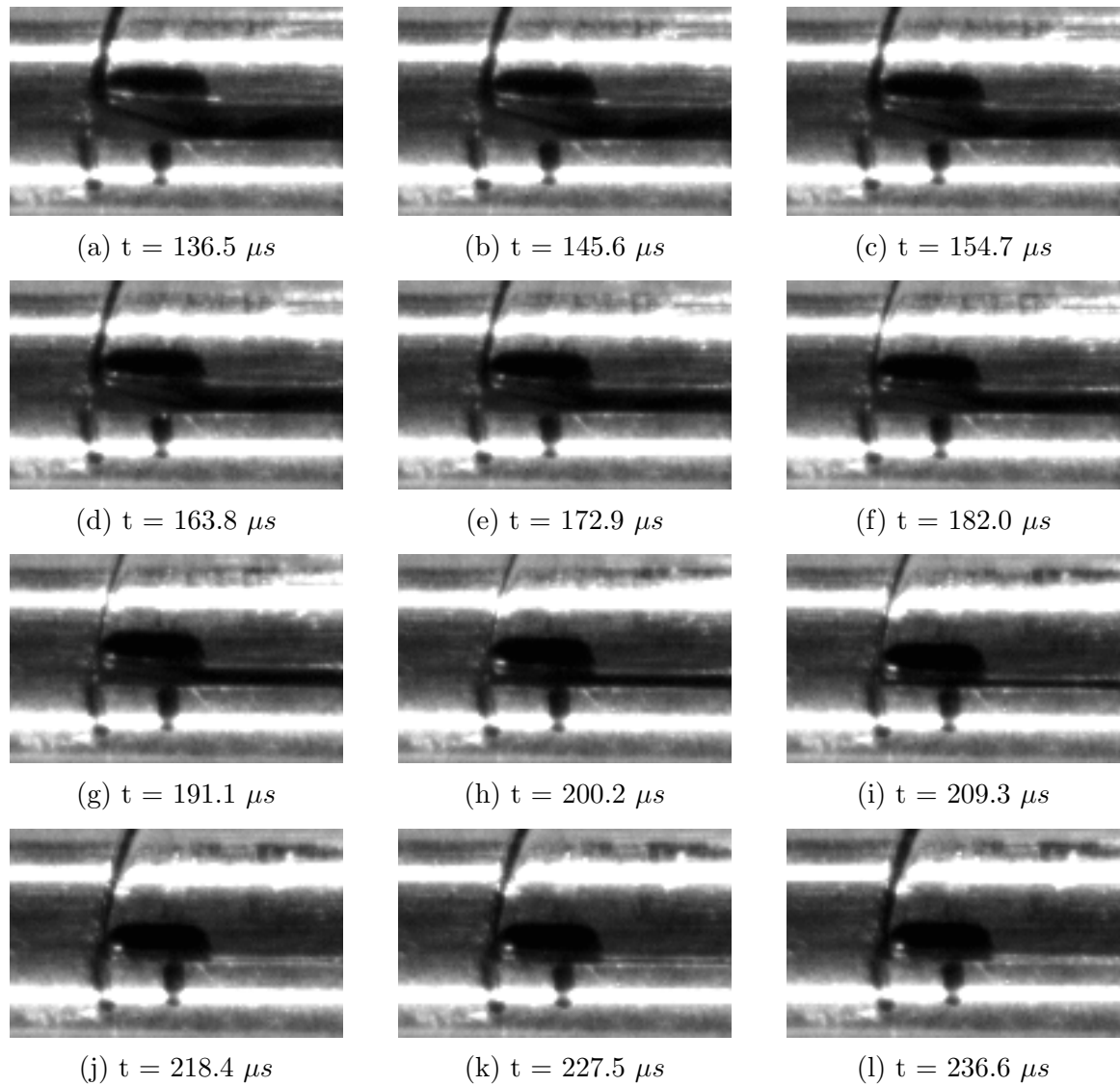New techniques also need to be explored to reach their full potential. For Kolsky bar experiments, this may mean exploring pulse shaping techniques in addition to studying materials. It is well known that a Kolsky bar experiment must exhibit dynamic equilibrium to be considered valid. The method of achieving dynamic equilibrium is not unique. This concept applies to the side-impact torsion Kolsky bar, where there are no known pulse shaping techniques. Although friction experiments do not readily display the characteristic of dynamic equilibrium, the use of a pulse shaper is required to produce a desirable incident waveform.

4.1.1 Pulse Shaping

Developing an understanding of pulse shaping for the side-impact torsion Kolsky bar is crucial, as the technique has no past use. Other torsion Kolsky bar techniques

at best make use of attenuators to smooth out an incident waveform. However, the raw waveform generated by the side-impact technique requires pulse shaping due to interactions with the tab and loading bar. While this raw signal could certainly be used, it would be very difficult to discern material behavior from mechanical noise on the measured waveforms.

The use of a pulse shaper serves two purposes: to smooth out mechanical noise, and to tailor the shape of the wave. The same principles for pulse shaping that apply to the compression Kolsky bar also apply to the side-impact torsion Kolsky bar. The difference however, is in the relative stiffness of the pulse shaper. For the compression Kolsky bar, the pulse shaper is typically annealed copper. For some materials, it is suitable to use a pulse shaper that is slightly larger than and of the same material as the specimen.

For the side-impact torsion Kolsky bar, the pulse shaper must be very soft compared to the apparatus (Section 3.1.7). These materials include the softest of metals (tin, lead, etc), and more preferably, rubber. Rubber is widely available in as many, and possible more, configurations as metallic alloys. For natural rubbers, the composition and stiffness may not be under control. However, synthetic rubbers may be fine tuned depending on the type of polymer and the amount of plasticizer in use. Synthetic rubbers can be tuned to be perfectly linearly elastic or have a stress-strain curve that is either concave up or concave down.

The strength of the pulse shaper also plays an important role by controlling how much stress may be transmitted through before being augmented. In conjunction with the size of the pulse shaper, the strength allows for bilinear waveforms that range from nearly rectangular to nearly triangular shapes.

Through experimentation, the ideal material for generating a rectangular wave with moderate rise time should be nearly linearly elastic, with low material strength. Unfortunately, most metals do not satisfy this condition. Being linearly elastic, most metals produce a fast rise time, but do not remove the oscillations introduced by the

tab, as the material does not compress enough to mitigate the factor that results in the oscillations.

If rise time is not an important factor, as the duration of the torsional wave is often more important, a more compliant material may be suitable. Along with the compliance comes lower strength, resulting in a pulse shaper that is more effective at removing the oscillations. An ideal material for a pulse shaper to generate a rectangular waveform is vulcanized rubber. This type of rubber is sufficiently stiff to produce a modest rise time, but also sufficiently compliant that the reverberations that lead to the oscillations are mitigated by the pulse shaper. Thus, using rubber that is softer than vulcanized rubber will allow bilinear waveforms and even softer will allow triangular waveforms. However, the lower bound of the stiffness of the pulse shaper is not known. Although, foam rubbers are in fact too soft, producing an incident torsion waveform that appears just as the stress-strain curve for foam rubber, with a period of cell collapse followed by a rapid increase in stress (Figure 4.1).

4.1.2 Metallic Friction

The friction behavior of metals is dependent upon many variables, including surface quality. One may hypothesize that there should be a period of no sliding (i.e. static friction), then a period of sliding (i.e. dynamic friction). However, this outcome is highly dependent upon the surface quality at the interface. For a polished surface (3.8 micron grit or 1200 grit), there will be little, if any evidence of a static friction peak (Figure 4.2). For a rougher surface (10.6 micron grit or 600 grit), there will be a static friction peak (Figure 4.3). The study of this peak requires more consideration, as the appearance of the peak is dependent upon many other experimental factors.

One hypothesis for the lack of a static friction peak in Figure 4.2 is that the rise time of the incident torsion wave is too long. This is an limitation of the side-impact
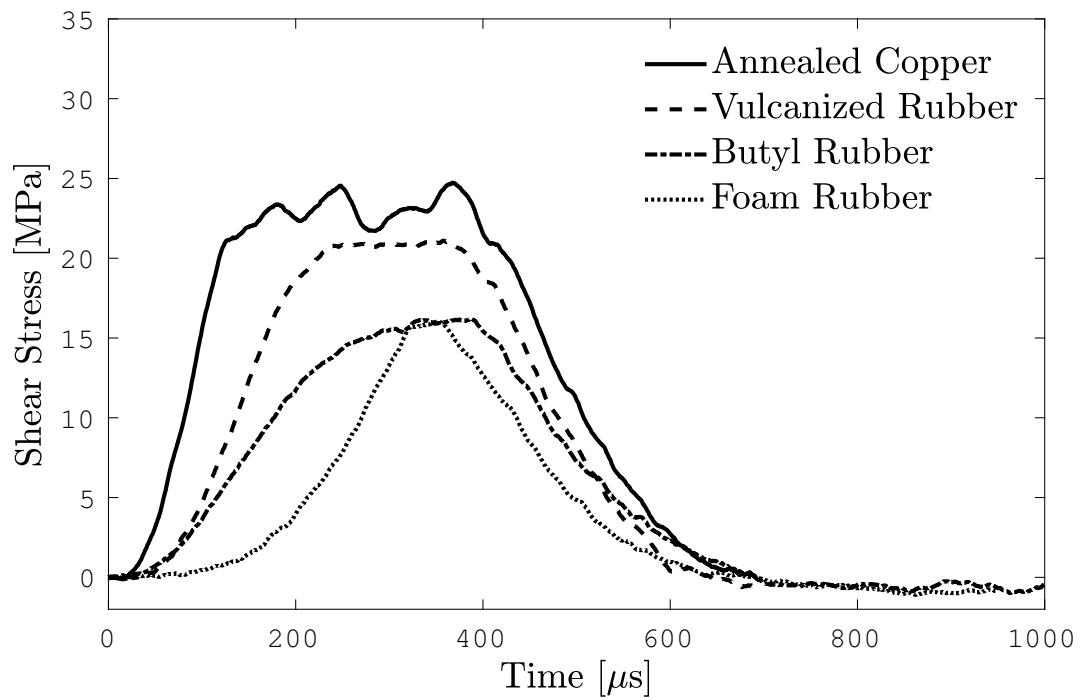
Figure 4.1. Example pulse shapers and the corresponding incident torsion wave. Adapted with permission from [28]. Copyright (2015) Experimental Mechanics.
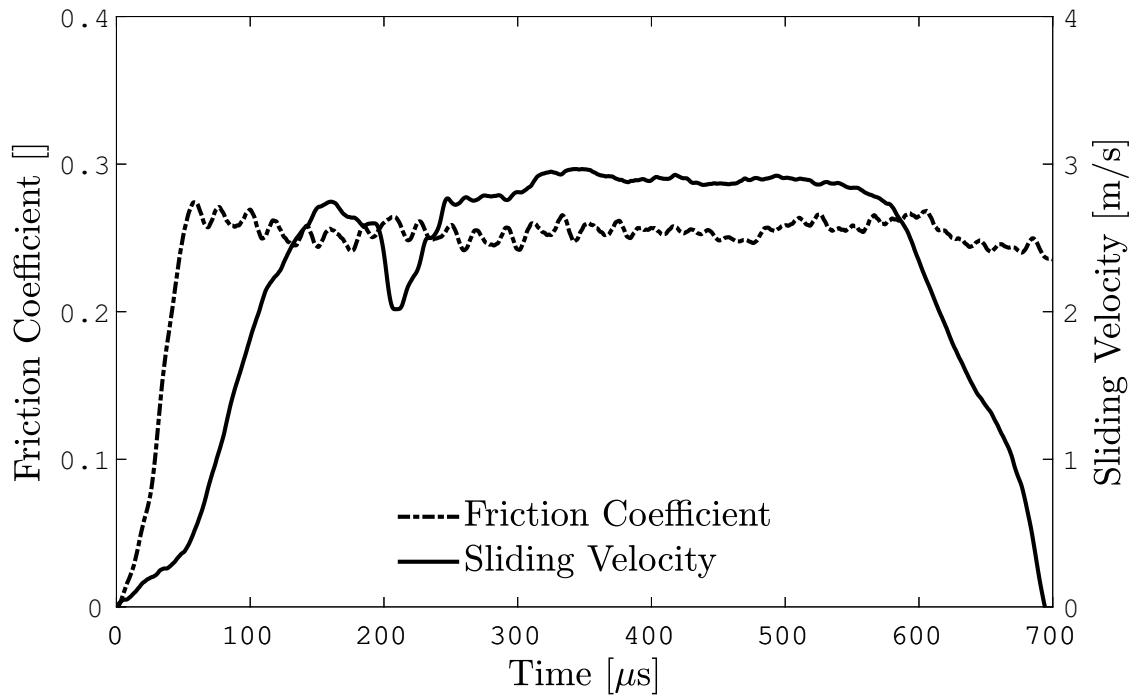
Figure 4.2. Friction behavior for aluminum 6061 against aluminum 7075-T6 with 12.9 MPa of axial compression. Note the lack of a static friction peak. Adapted with permission from [28]. Copyright (2015) Experimental Mechanics.

(a) Friction coefficient.

(b) Sliding velocity.
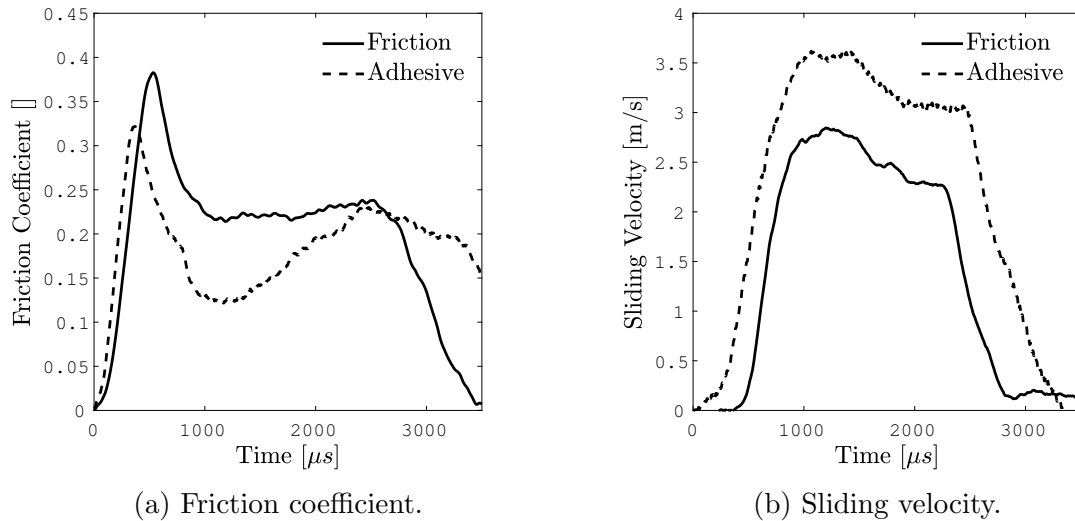
Figure 4.3. Example of failing adhesive influencing the measurement of the friction coefficient and sliding velocity. The appearance of a static friction peak is no accompanied by a corresponding lack of sliding velocity.

torsion Kolsky bar. However, the presence of the static friction peak is not prevalent in literature pertaining to the study of friction using a torsion Kolsky bar [23, 24].

There is another consideration when studying metallic materials on a torsion Kolsky bar. Since there is no simple way of affixing the specimen onto the apparatus, the joint must be well understood, particularly when using adhesives. Failure of the adhesive may result in erroneous conclusions of the friction behavior by producing an artifact that appears to be a static friction peak (Figure 4.3). This peak typically occurs at the beginning of the transmitted wave, producing the illusion that a certain stress level must be overcome before sliding occurs. However, it is imperative that the adhesive be observed after the experiment, as the adhesive may have failed, thus altering the measurement.

4.1.3 Particle Composite Friction

The particle composite under study was a stable, non-reactive mechanical mock for volatile material. The composite was composed mostly of inert sugar crystal and a small amount of polymer binder (by mass). When mixed, the composite is a slurry, and must be cast or formed into shape. The casting process introduces different surface conditions than if the material where machined. The friction behavior of the material was studied at two sliding velocities (1.0 m/s and 3.0 m/s) and three different compression levels (0.75 MPa, 1.0 MPa, and 1.25 MPa). The behavior is clearly influenced by the manufacturing process, an important factor to consider for the volatile version of this material (Table 4.1).

Regardless of the manufacturing method, a general trend has been observed within the calculated friction coefficient (Figure 4.4). There are six regimes for this fairly compliant material: loading, shear deformation, beginning of sliding, steady sliding, interface evolution, and unloading. Some of these regimes may be condensed or expanded depending on the surface conditions, but the shear deformation before sliding is always present. The shear deformation is evident in that sliding velocity is
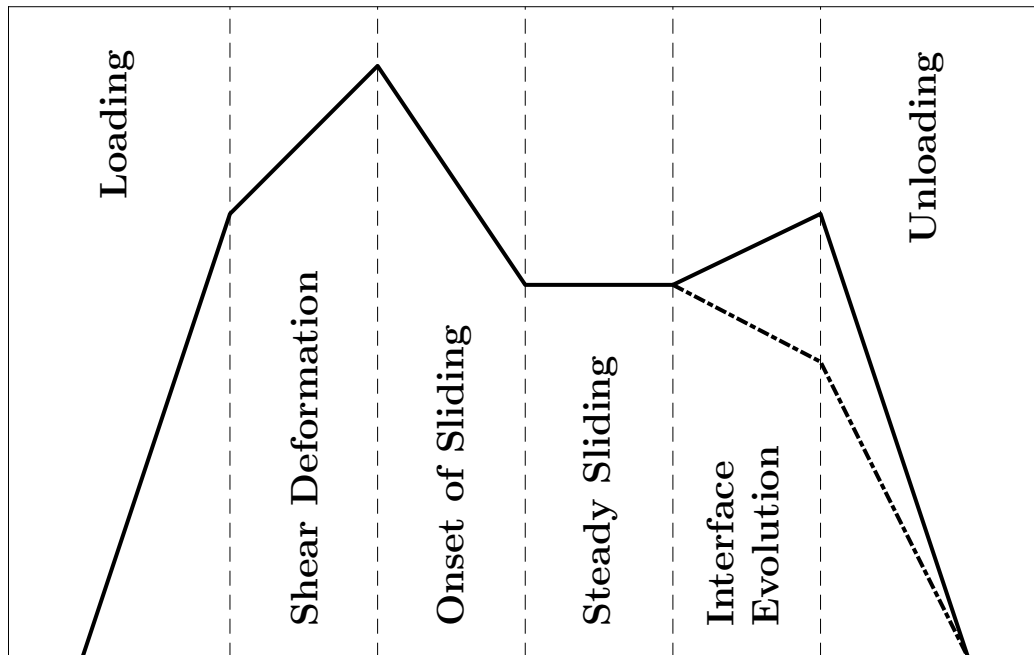
Figure 4.4. Different regimes within a typical friction coefficient response. Not all regimes are present or discernible depending on specific material behavior.

non-zero where this "peak" appears, indicating that there is relative motion between the incident and transmission bars. This could also mean there is sliding, but the general friction behavior is that a critical stress must be overcome before sliding begins. Ultimately, whether sliding begins very early depends upon the material, and could be verified using high speed imagery. As a side note, the specimen count from each batch was limited. While each condition could have been performed using a single batch, each specimen was taken from a different batch. While this increases the irregularity between individual experiments, the overall results are more indicative of the material rather than of a single batch of material.

An interesting observation, particularly for the machined material, is that the friction coefficient is nearly the same for all compression levels. For a larger amount of compression, the amount of shear supported by the interface increases according to Coulomb's law of friction (Equation 2.14), a quantity that is directly proportional to

Table 4.1. Overall average friction coefficient of the plateau region for the simulant material.

|	Low Velocity	High Velocity
Machined	0.274 at 1.3 m/s	0.249 at 3.0 m/s
Cast	0.385 at 1.0 m/s	0.338 at 2.7 m/s

the amount of transmitted torque. This means that for a given incident torsion wave, the reflected torsion wave is decreased, resulting in a lower sliding velocity. One may expect to observe a different friction coefficient with the different conditions. This prospect opens several avenues for potential future studies related to modeling of friction behavior.

The friction behavior of the mechanically processed material is relatively simple (Figures 4.5, 4.6, 4.7 for the lower sliding velocity and Figure 4.8, 4.9, and 4.10 for the higher sliding velocity). With a sliding velocity of 1 m/s, the friction reaches a plateau for a majority of the experiment. At 3 m/s the friction shows signs of surface evolution as the friction coefficient displays a net decrease over the duration of the experiment. This decrease can be explained by the interface being lubricated by the broken sugar crystals.

In contrast to the mechanically processed material, the cast material has more rubber at the interface (Figures 4.11, 4.12, and 4.13 for the lower sliding velocity and Figures 4.14, 4.15, and 4.16 for the higher sliding velocity). At a sliding velocity of 1 m/s, the cast material behaves similarly to the mechanically processed material, showing a plateau in the friction coefficient, except with an overall higher friction coefficient. However, at the higher sliding velocity of 3 m/s, the behavior changes drastically. The beginning of the experiment shows a large peak, approaching a friction coefficient up to 0.5. This peak is followed by a rapid drop and then a gradual decrease in friction coefficient. The quick onset of sliding as marked by the rapid decrease in friction coefficient is due to the nature of the surface of the material. Being rubber-like, the surface "sticks" to the metallic surface until a critical stress is reached, at which point, the material releases. It is hypothesized that had this material been entirely rubber, that this slip event would be followed by a stick event [50]. However, having only a thin layer of rubber bound to aggregate just below the surface, the specimen experiences significant surface evolution due to separation of crystals from this thin layer.
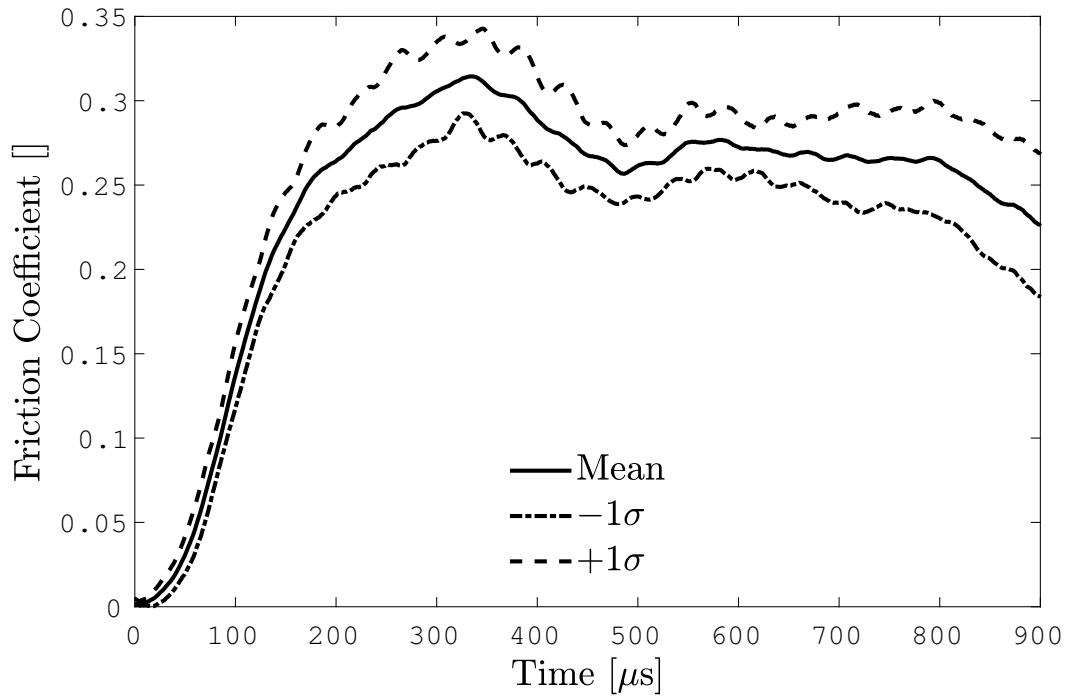
(a) Friction coefficient.
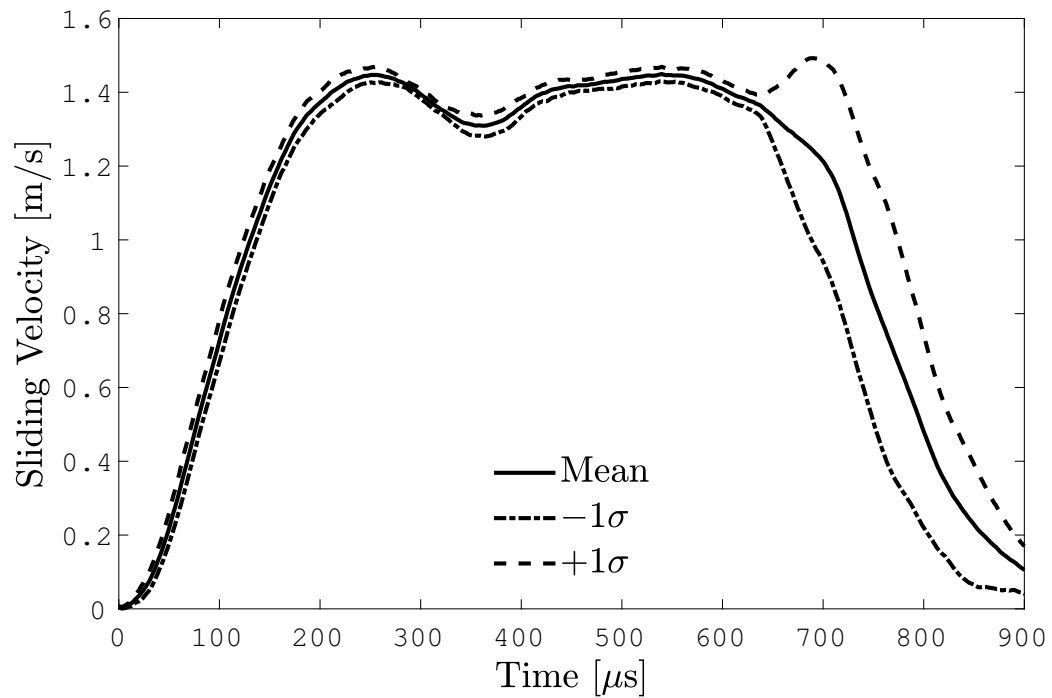
(b) Sliding velocity.

Figure 4.5. Machined PBXn-301 simulant against 1008 steel at the lower sliding velocity of 1 m/s and axial compression of 0.71 MPa. Data shows the average and the first positive and negative standard deviation.

(a) Friction coefficient.

(b) Sliding velocity.

Figure 4.6. Machined PBXn-301 simulant against 1008 steel at the lower sliding velocity of 1 m/s and axial compression of 1.04 MPa. Data shows the average and the first positive and negative standard deviation.
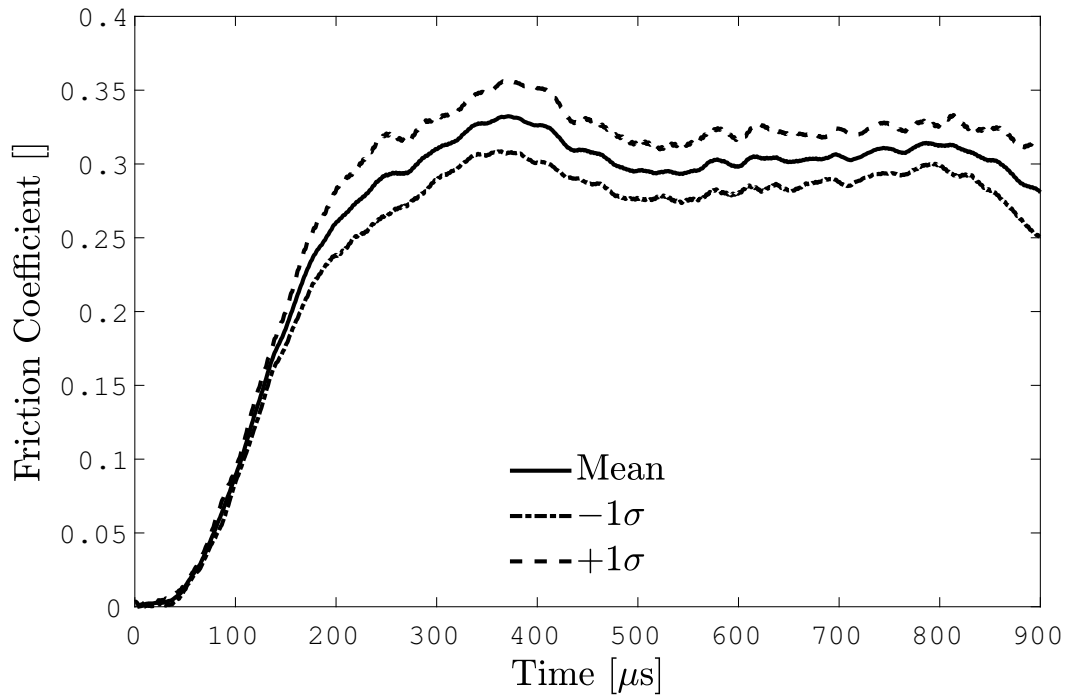
(a) Friction coefficient.

(b) Sliding velocity.

Figure 4.7. Machined PBXn-301 simulant against 1008 steel at the lower sliding velocity of 1 m/s and axial compression of 1.32 MPa. Data shows the average and the first positive and negative standard deviation.
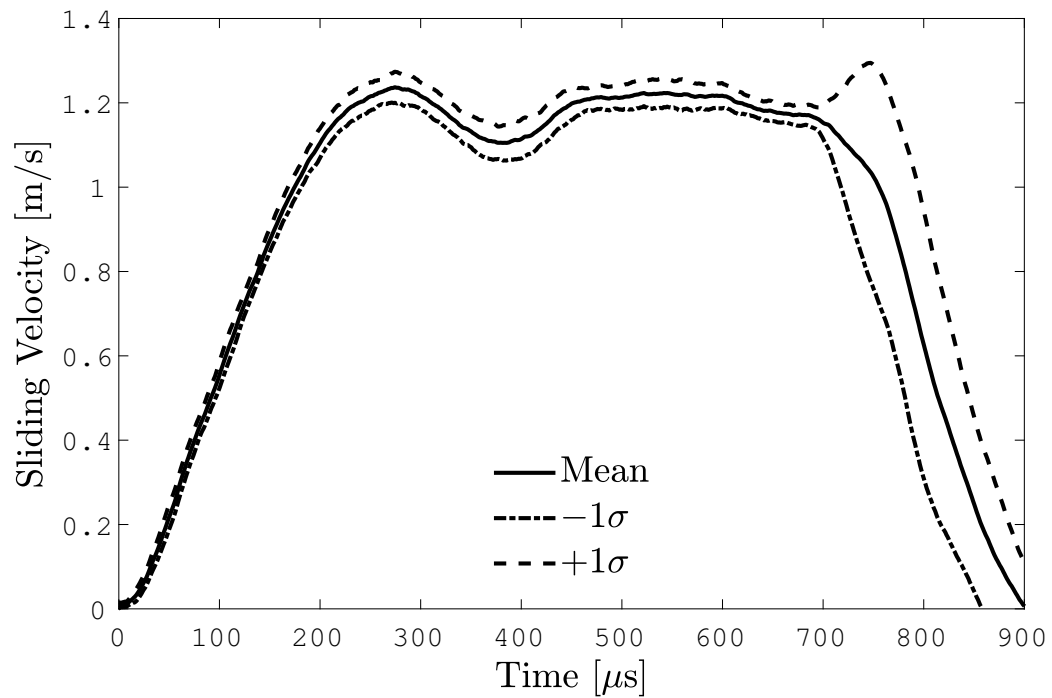
(a) Friction coefficient.

(b) Sliding velocity.

Figure 4.8. Machined PBXn-301 simulant against 1008 steel at the lower sliding velocity of 3 m/s and axial compression of 0.69 MPa. Data shows the average and the first positive and negative standard deviation.
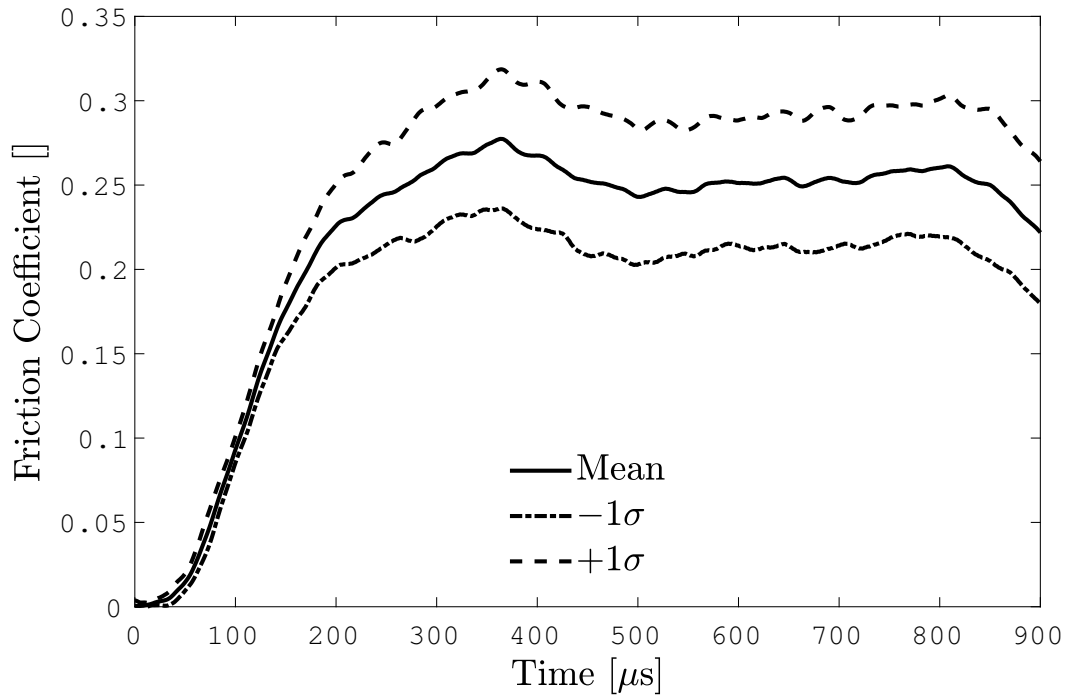
(a) Friction coefficient.

(b) Sliding velocity.

Figure 4.9. Machined PBXn-301 simulant against 1008 steel at the lower sliding velocity of 3 m/s and axial compression of 1.10 MPa. Data shows the average and the first positive and negative standard deviation.
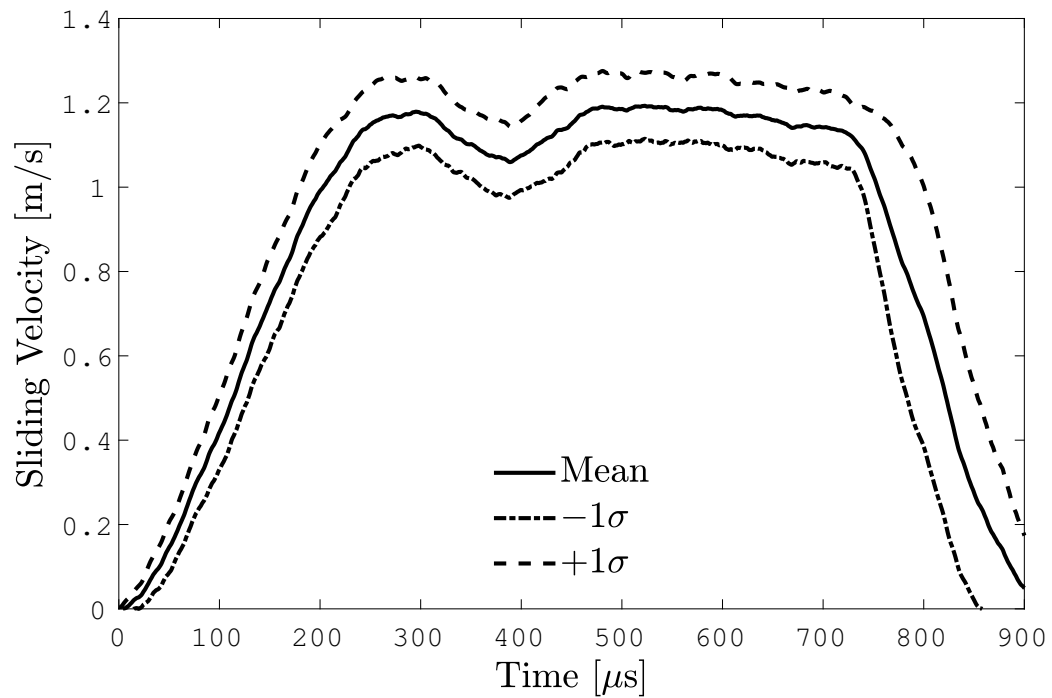
(a) Friction coefficient.

(b) Sliding velocity.

Figure 4.10. Machined PBXn-301 simulant against 1008 steel at the lower sliding velocity of 3 m/s and axial compression of 1.30 MPa. Data shows the average and the first positive and negative standard deviation.
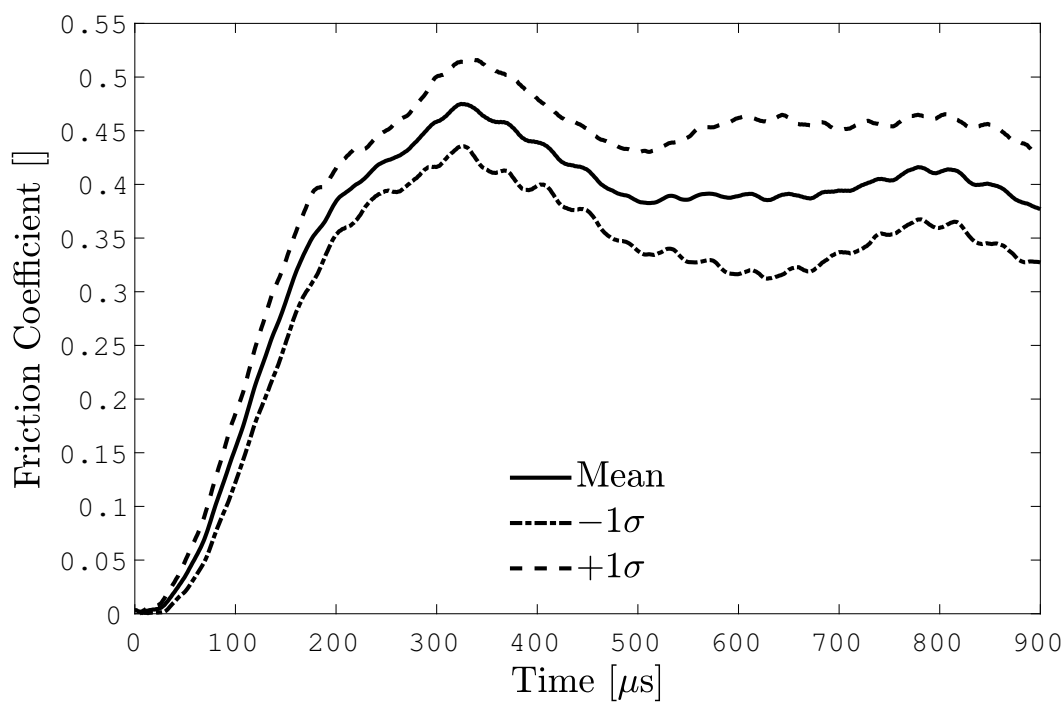
(a) Friction coefficient.
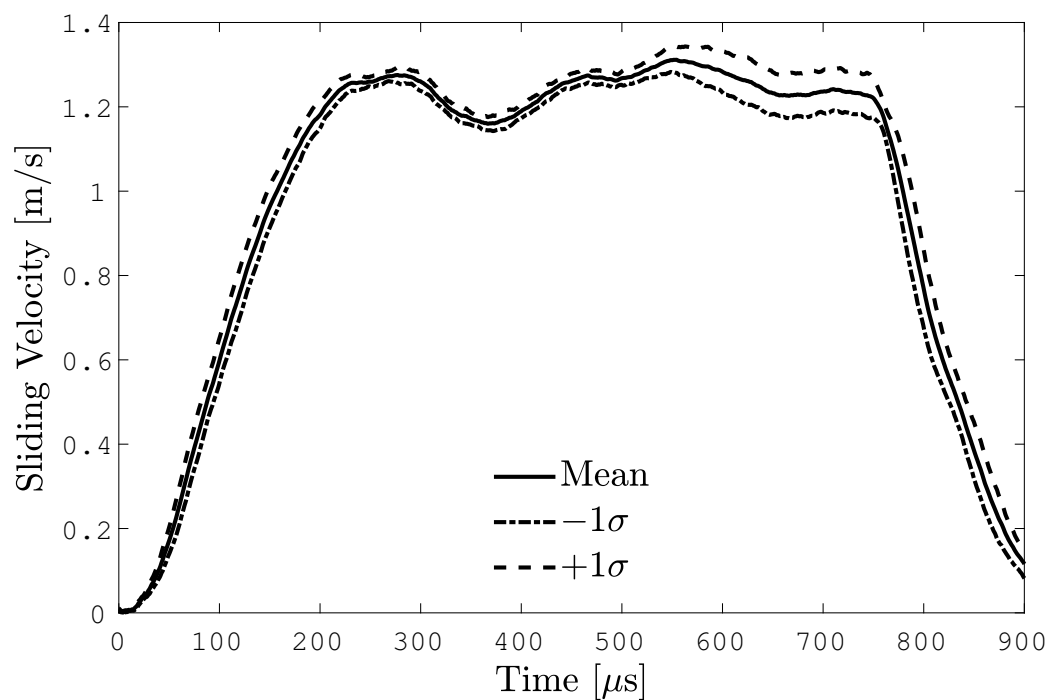
(b) Sliding velocity.

Figure 4.11. Cast PBXn-301 simulant against 1008 steel at the lower sliding velocity of 1 m/s and axial compression of 0.70 MPa. Data shows the average and the first positive and negative standard deviation.
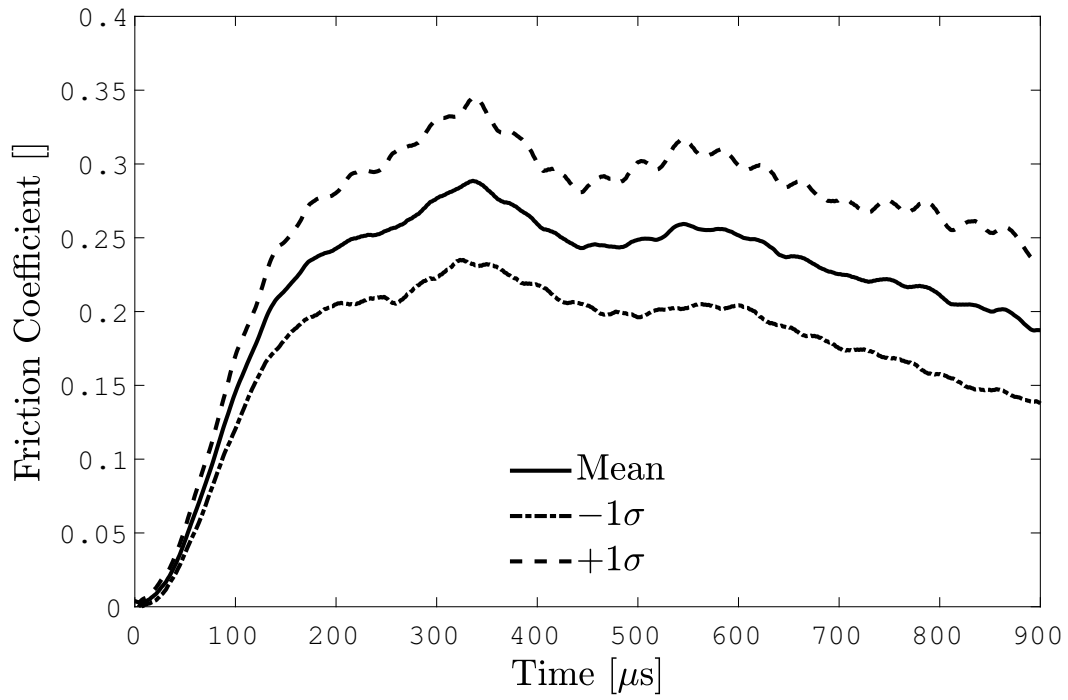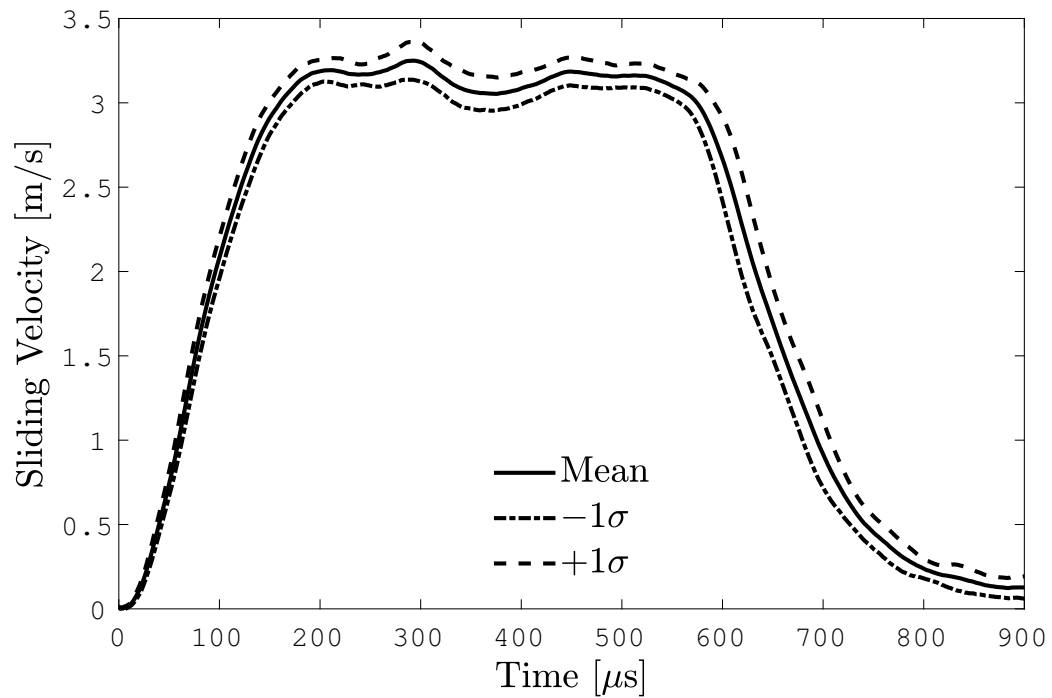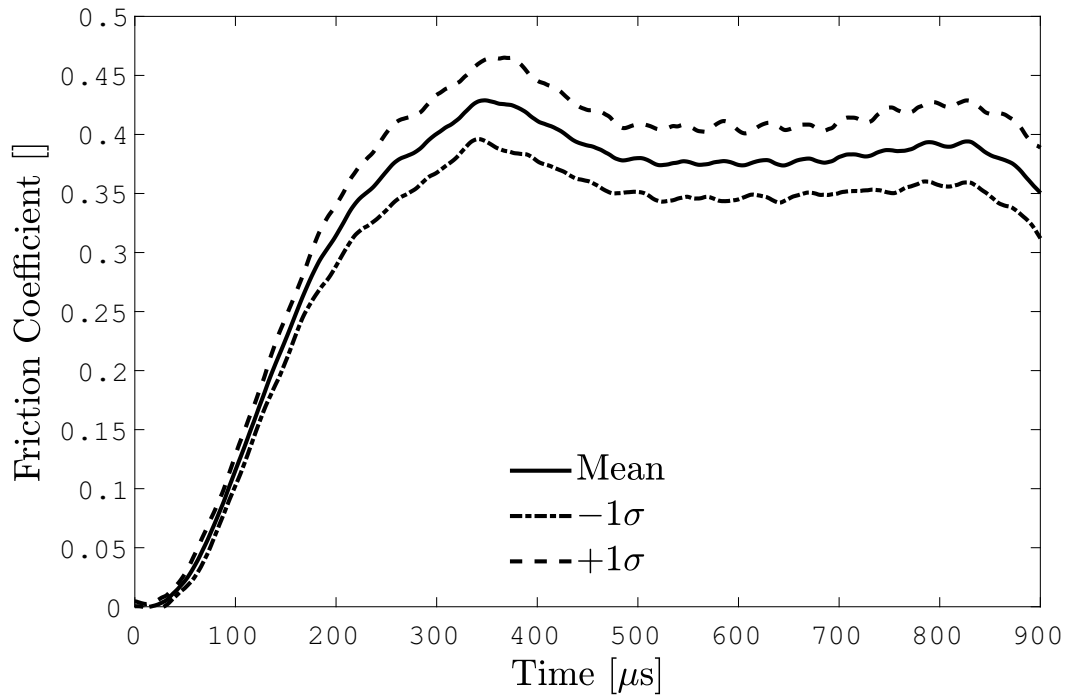
(a) Friction coefficient.
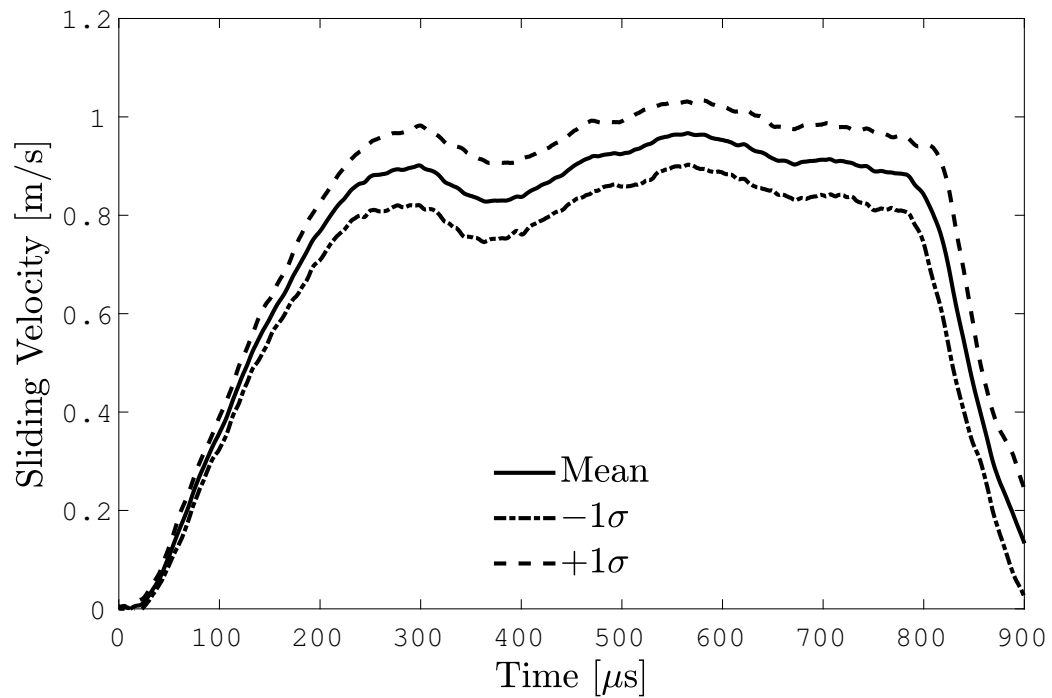
(b) Sliding velocity.

Figure 4.12. Cast PBXn-301 simulant against 1008 steel at the lower sliding velocity of 1 m/s and axial compression of 1.11 MPa. Data shows the average and the first positive and negative standard deviation.
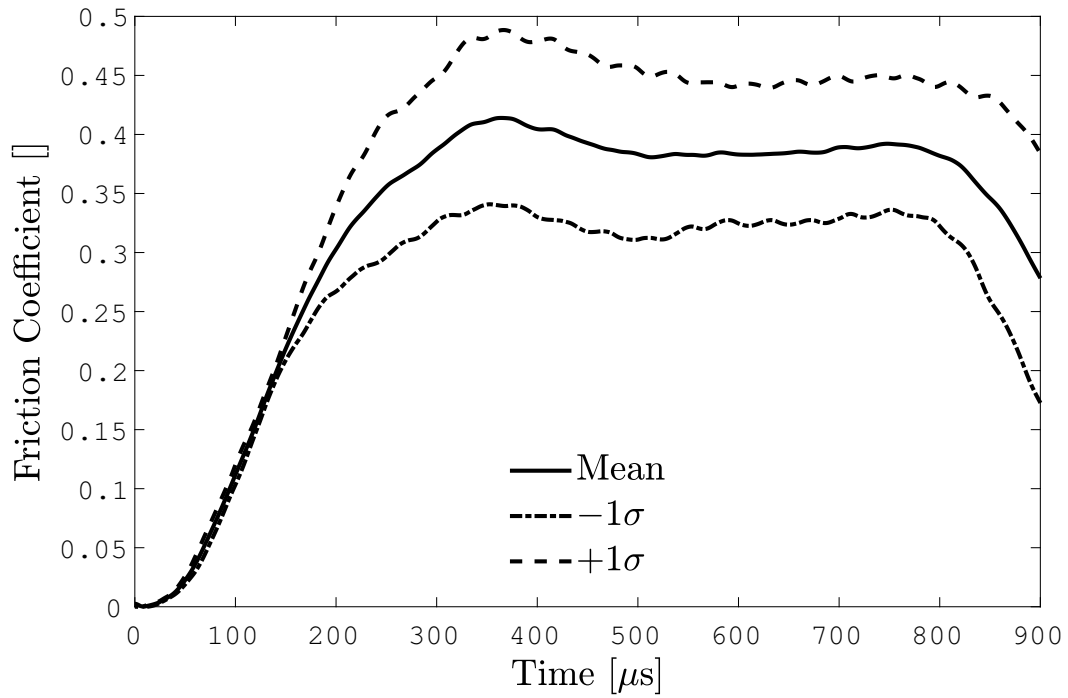
(a) Friction coefficient.
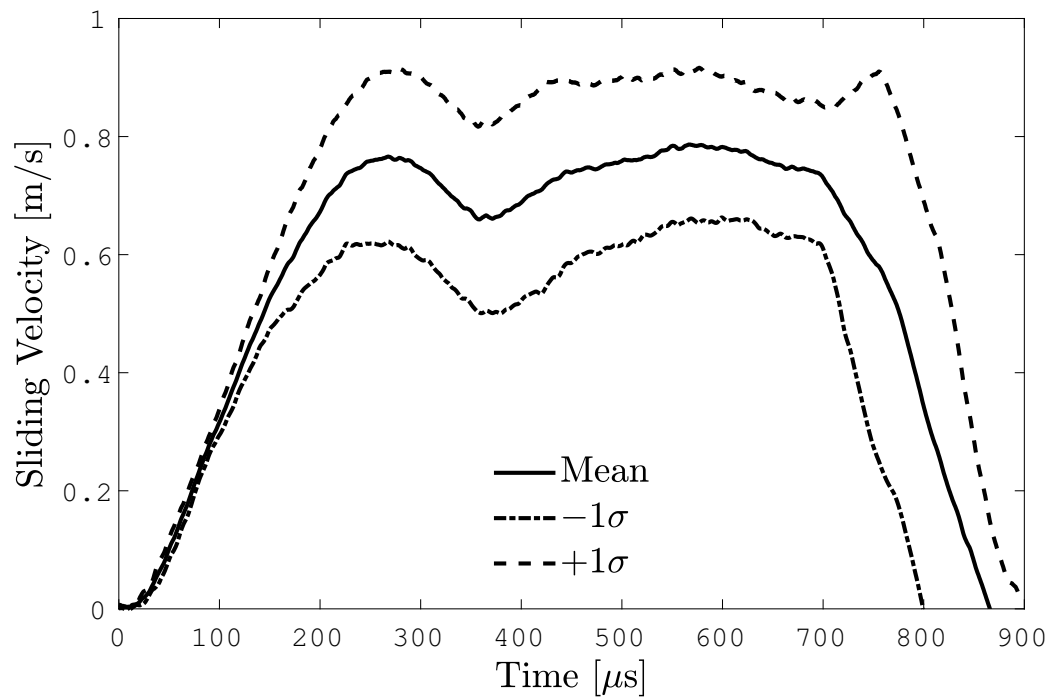
(b) Sliding velocity.

Figure 4.13. Cast PBXn-301 simulant against 1008 steel at the lower sliding velocity of 1 m/s and axial compression of 1.36 MPa. Data shows the average and the first positive and negative standard deviation.
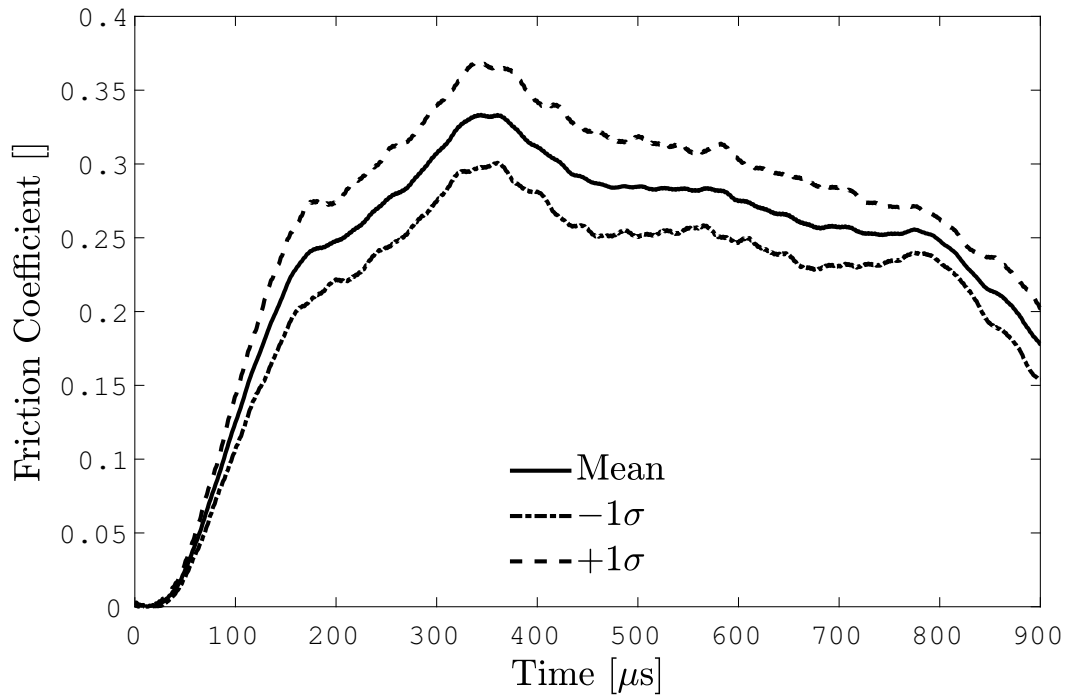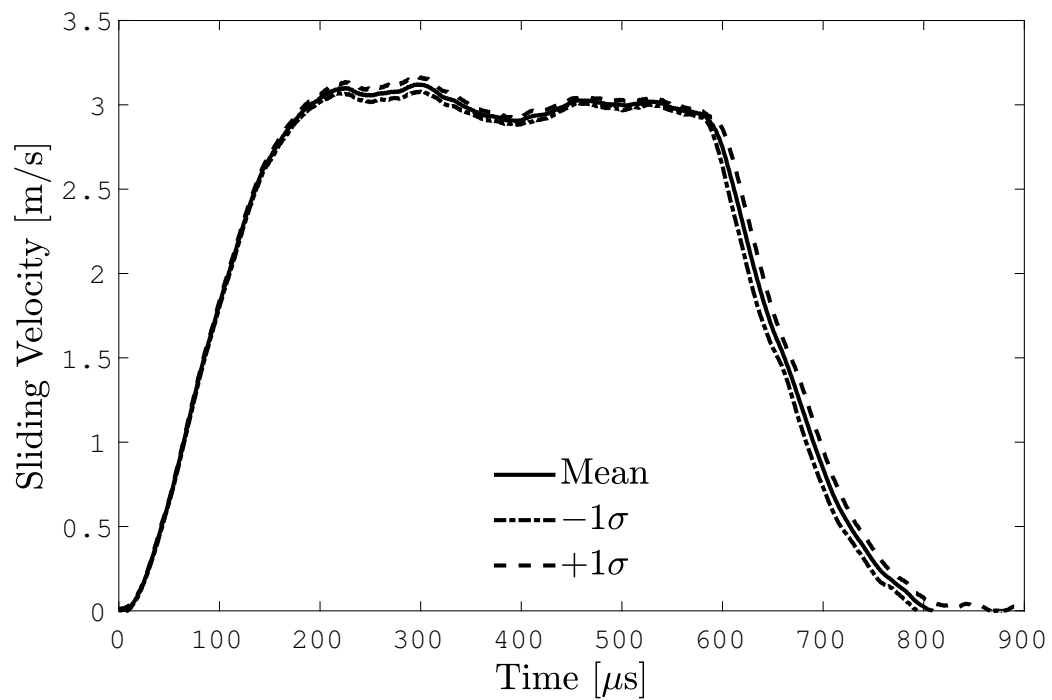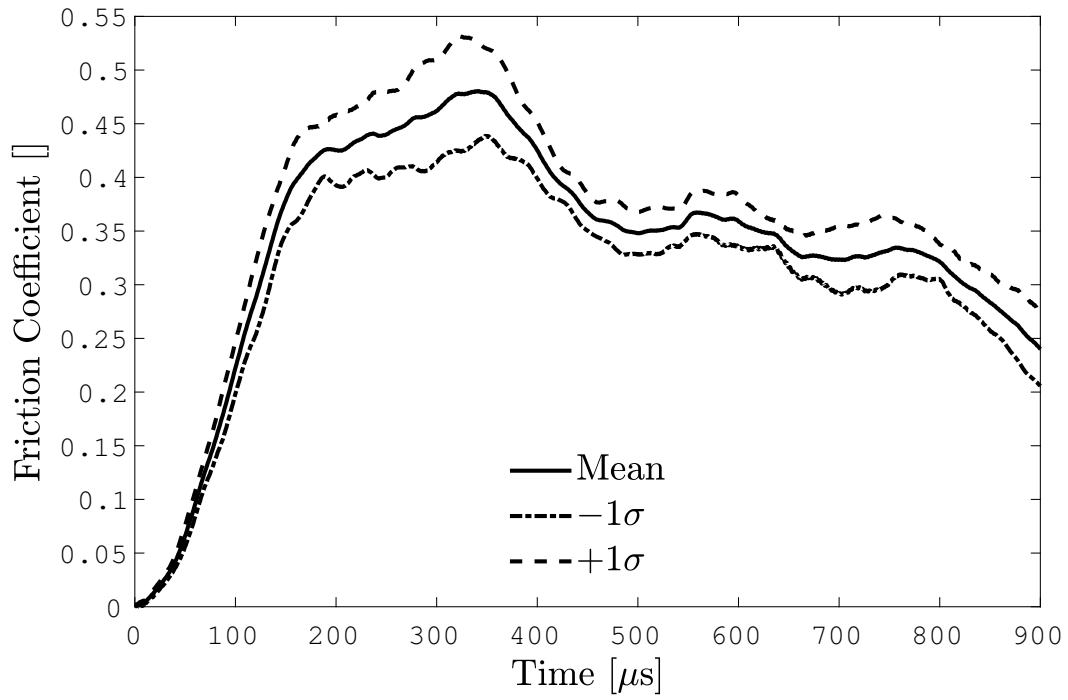
(a) Friction coefficient.
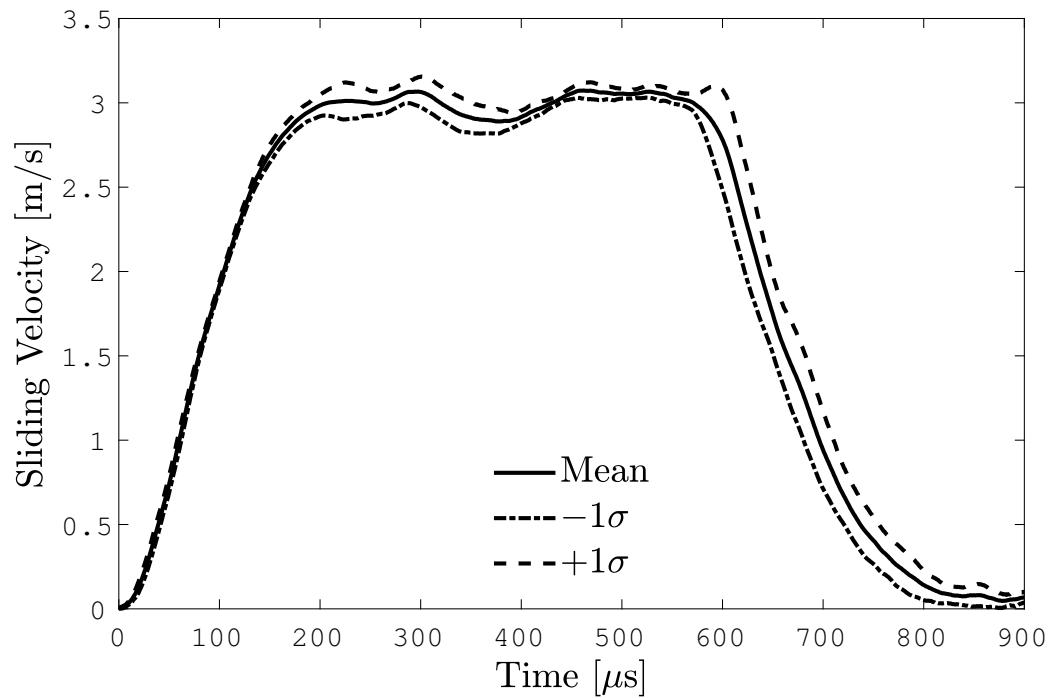
(b) Sliding velocity.

Figure 4.14. Cast PBXn-301 simulant against 1008 steel at the lower sliding velocity of 3 m/s and axial compression of 0.68 MPa. Data shows the average and the first positive and negative standard deviation.
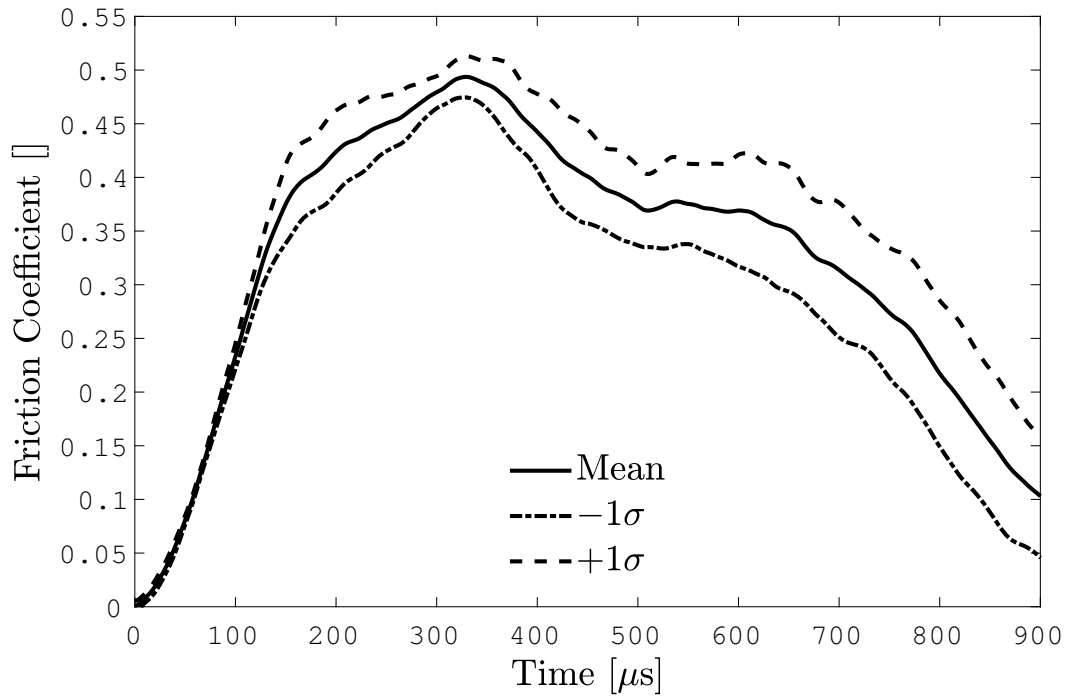
(a) Friction coefficient.
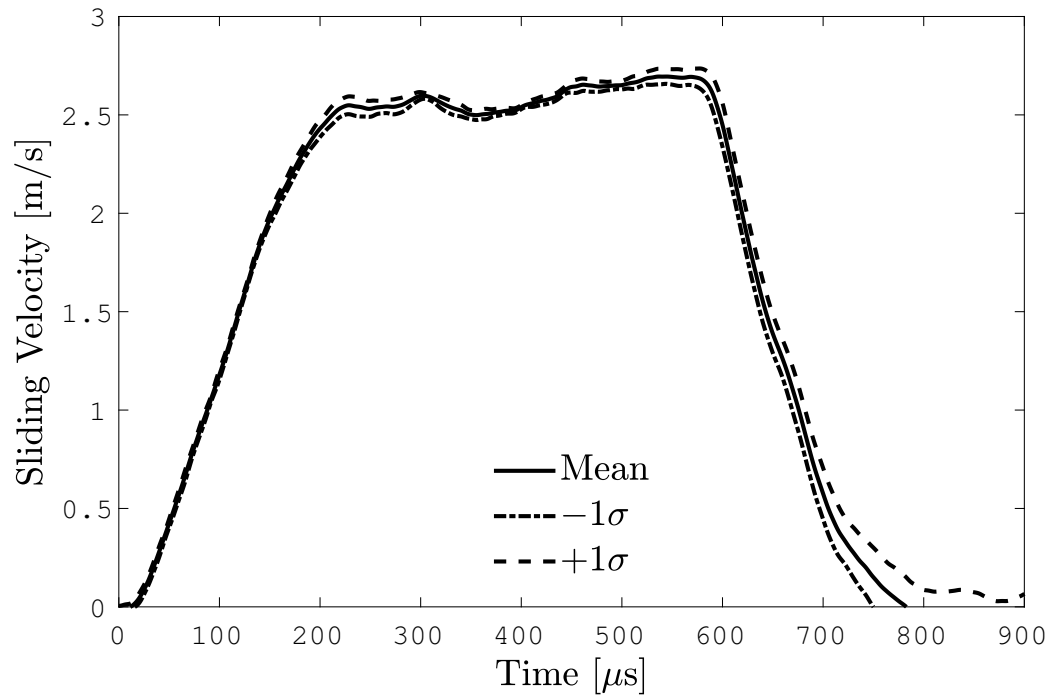
(b) Sliding velocity.

Figure 4.15. Cast PBXn-301 simulant against 1008 steel at the lower sliding velocity of 3 m/s and axial compression of 1.10 MPa. Data shows the average and the first positive and negative standard deviation.
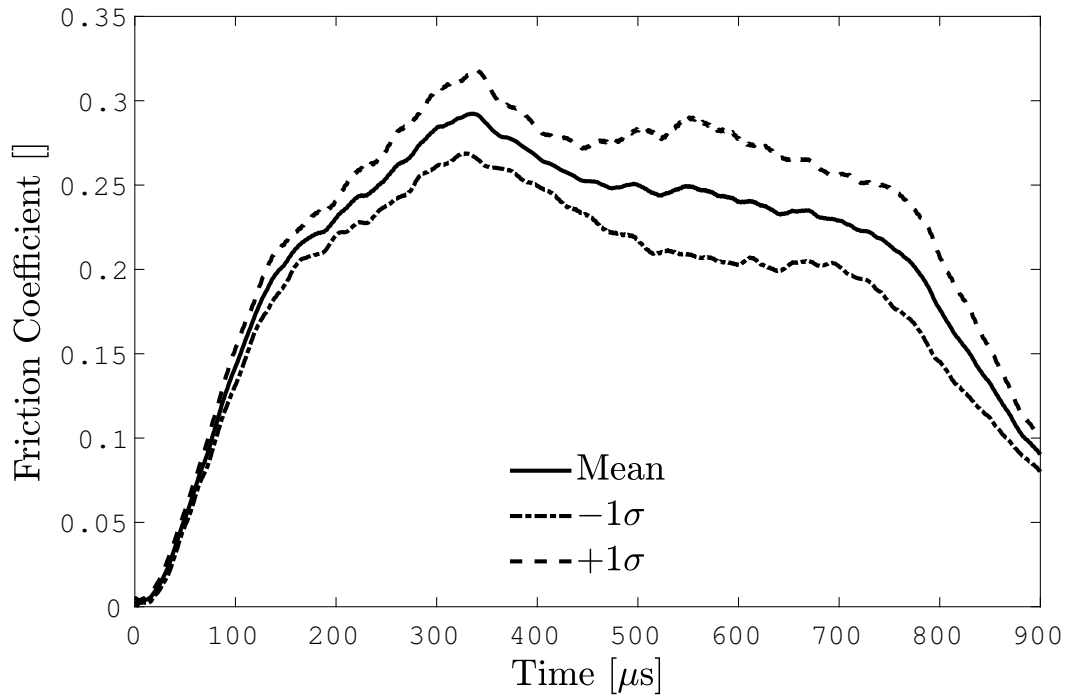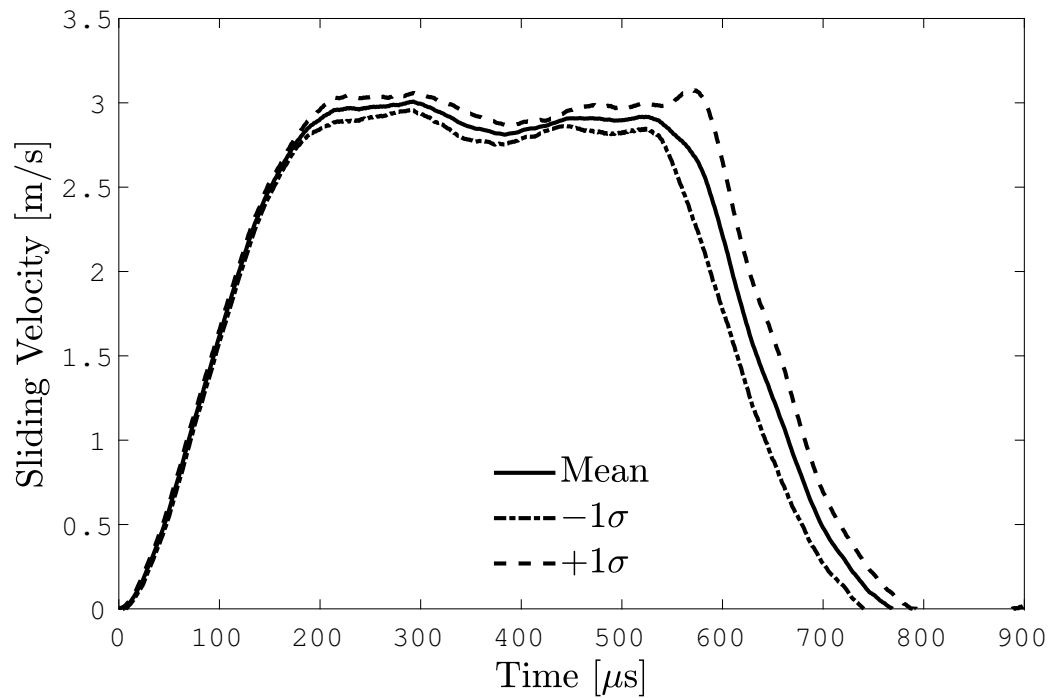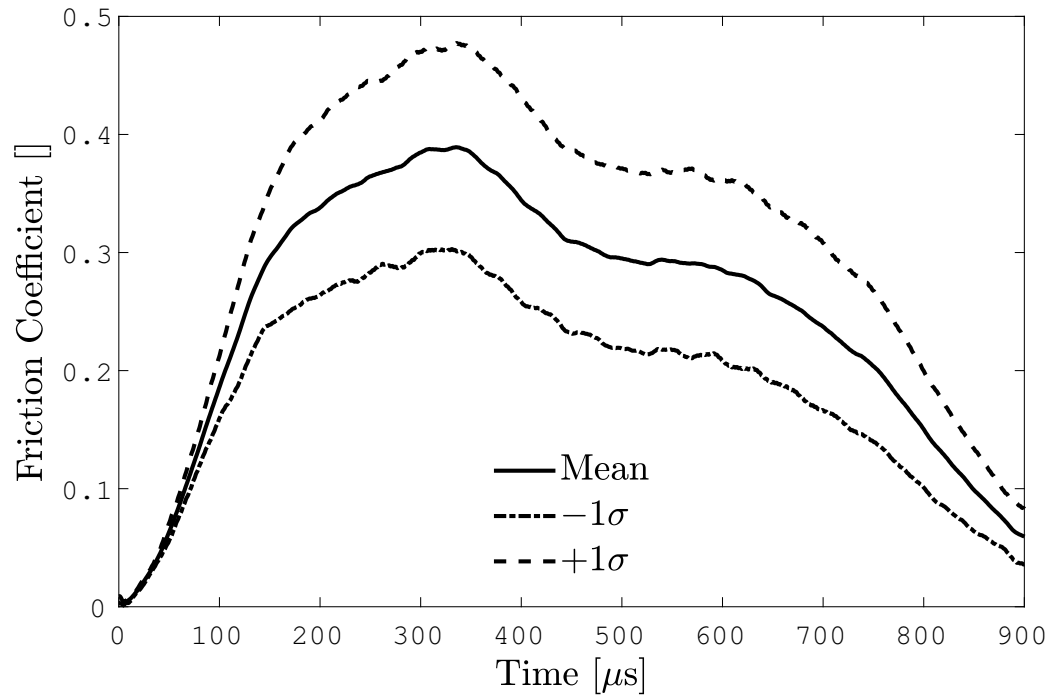
(a) Friction coefficient.
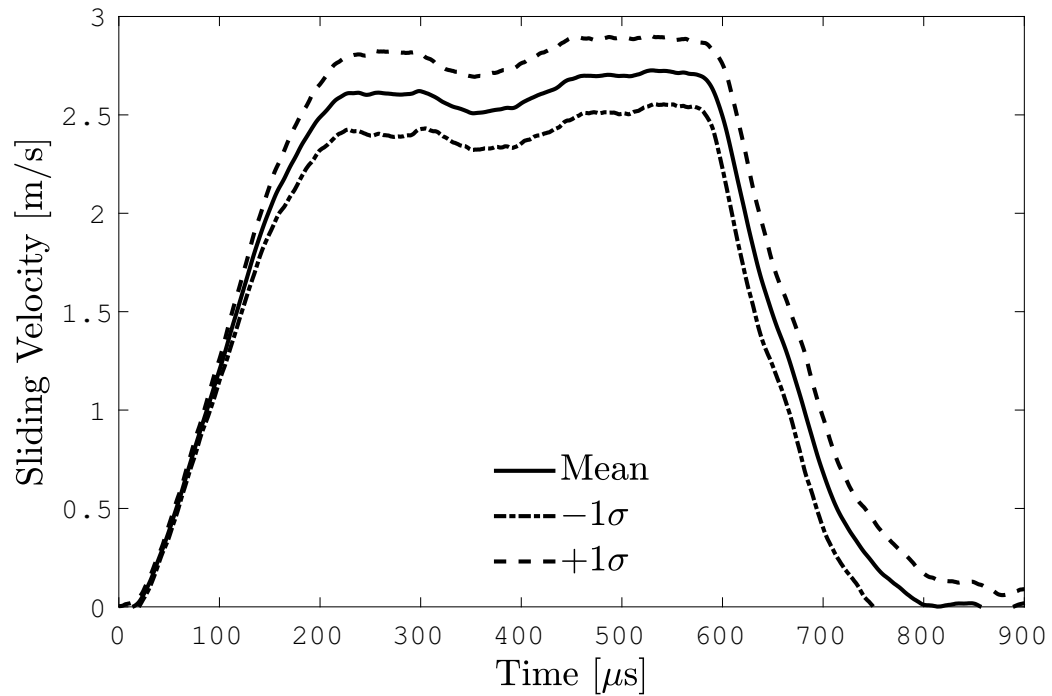
(b) Sliding velocity.

Figure 4.16. Cast PBXn-301 simulant against 1008 steel at the lower sliding velocity of 3 m/s and axial compression of 1.34 MPa. Data shows the average and the first positive and negative standard deviation.

4.2   Combined Compression-Torsion Kolsky Bar

The compression Kolsky bar experiment is mature and is capable of providing repeatable incident waveforms. The apparatus itself can be made compact to fit in the smallest of places. Assuming the mechanical impedance of the specimen is small compared to the incident bar, the transmission bar may be removed entirely, effectively halving the length of the apparatus. The condition that the specimen has a relatively low mechanical impedance must be verified.

Verifying that a specimen satisfies the assumptions of an experiment is relatively simple, even when comparing the mechanical impedance of a material with unknown properties. The assumption can be verified by comparing the measured incident and reflected waveforms (Figure 4.17). The fact that these two waveforms are so similar also means that any torque generated within the incident bar would be immeasurable without a specialized transducer.

4.2.1   Friction Experiments

Compression-torsion experiments involving friction were conducted with a striking velocity of 4.5 meters per second and a copper pulse shaper 6 *mm* in diameter and 1.1 *mm* thick (Figure 4.18). To prevent damage to the transducers, the overall travel of the incident bar was limited to 0.5 *mm* through the use of a single loading device. In this configuration, the single loading device reverses the wave in the incident bar after the first passage of the wave, preventing a second wave from moving the bar into the transducers.

Friction experiments are conducted in an unstable configuration for the compression-torsion Kolsky bar. This is due to the fact that the specimen is attached to the apparatus on only one side, leaving half of the torque adapter free floating. With little resistance from the specimen, the torque adapter is free to close with little influence. These experiments benefited greatly from a sleeve bearing that not only contains the
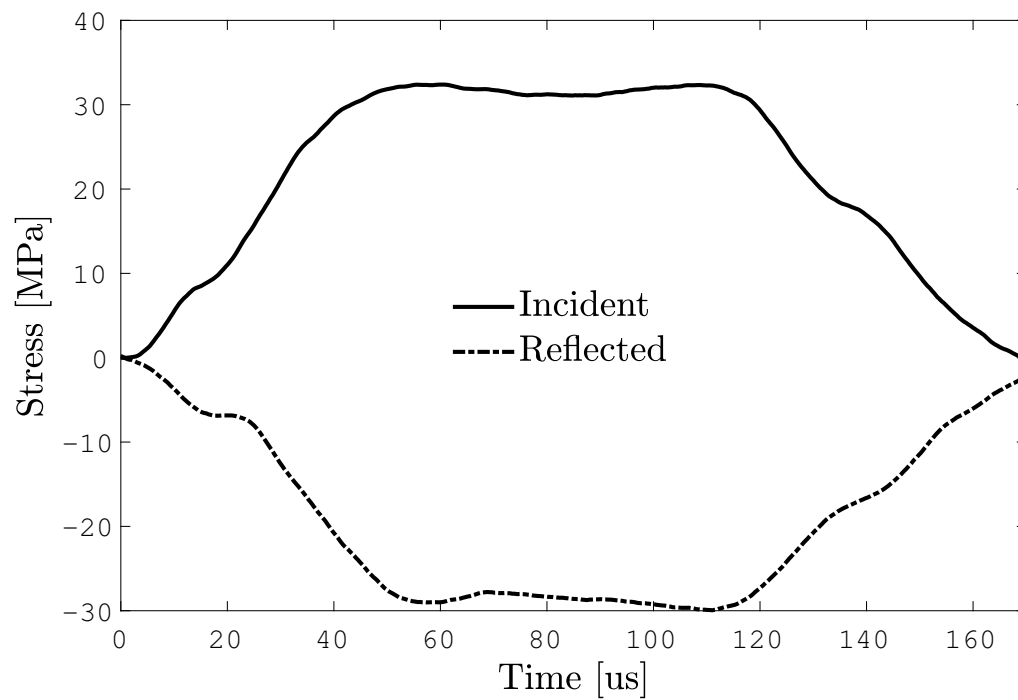
Figure 4.17. Example incident and reflected waveforms. The similarity implies that the experiment does not violate the assumption regarding mechanical impedance of the specimen. Adapted with permission from [16]. Copyright (2017) Experimental Mechanics.

components of the torque adapter, but also provides enough friction that the adapter functions as intended.

The dynamic nature of the compression and torsion stresses requires consideration when analyzing data. Since both stress states begin and end with zero stress, the inverse relationship that the compressive stress has with friction results in singularities both at the beginning and end of the experiment (Figure 4.18a). It could be argued that there is a small static compressive stress present, otherwise the torque adapter would fall apart. However, the principle behind the friction measurements is to extract data during constant sliding velocity.

The dynamics of the torque adapter results in peculiar behavior of the axial quantities. Based on the angle of inclination of the planes, one may expect that the amount of transmitted compressive stress would increase as the angle increases due to the fact that the planes are becoming more parallel (Figure 4.18c). The higher angle of inclination requires the torque adapter to spin faster, a higher angular velocity results in a higher sliding velocity (Figure 4.18b). Considering conservation of momentum, this requires that the forward velocity of the torque adapter be decreased relatively. The result is that for a higher angle of inclination, the axial strain rate is decreased (Figure 4.18d), and the sliding velocity is increased (Figure 4.18b). One implication is that the total strain applied to the specimen is proportionally less than for a smaller angle of inclination. The validity of each experiment relies on the torque adapter following the elliptical pathway. Analyzing the opening angle is possible (Figure 4.18e, but not sufficient to guarantee that a friction experiment using this apparatus is valid (See Section 3.2.3).
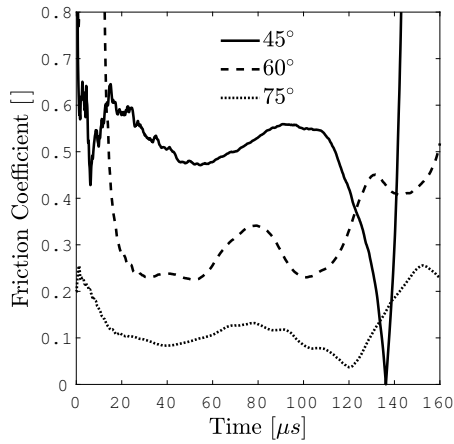
(a) Friction coefficient.
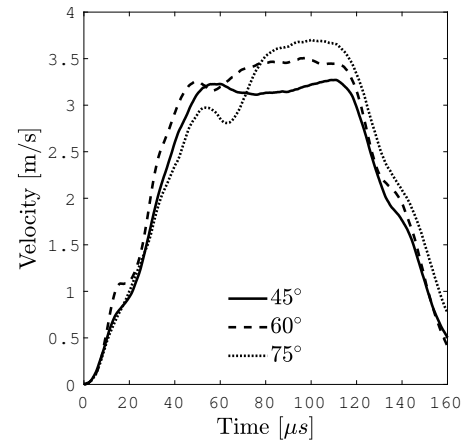
(b) Sliding velocity.
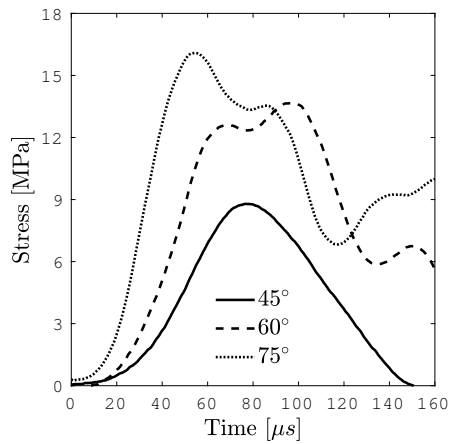
(c) Compressive stress.
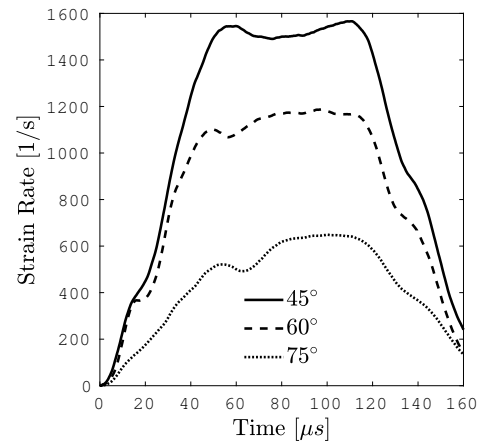
(d) Axial strain rate.
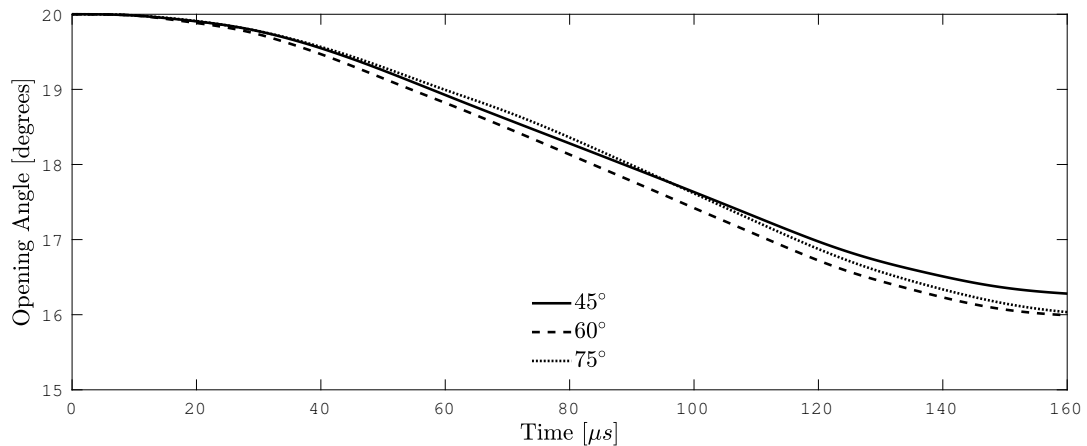
(e) Opening angle.

Figure 4.18. Friction experiments using three angles of inclination. Adapted with permission from [16]. Copyright (2017) Experimental Mechanics.

4.2.2   Shear Stress-Strain Experiments

Compression-torsion experiments involving shear stress and shear strain were conducted with similar conditions as the friction experiments: a striking velocity of 4.5 meters per second and a copper pulse shaper y.1 mm in diameter and 0.5 mm thick (Figure 4.19). Since the specimen is adhered to both the transducers and the torque adapter, there is little cause for the torque adapter to become misaligned or to fall apart during an experiment. However, the sleeve bearing helps to ensure that the specimen is installed correctly by providing a means to align and retain the specimen while the adhesive is curing.

The strain rates of the shear stress-strain experiment follow a similar trend as the friction experiment. When the angle of inclination is increased, the shear strain rate increases and the axial strain rate decreases. However, since the specimen is adhered to the transducers, the torque adapter is not free to rotate, and the gain in angular velocity and shear strain rate is not as high as with the friction experiments, as the specimen now has a higher capability to influence the system (Figure 4.19b). With little change in shear strain rate, the total shear strain of the specimen is nearly identical for each angle of inclination (Figure 4.19a). In contrast, the total axial strain is significantly reduced for higher angles of inclination (Figure 4.19c). Verifying that the torque adapter has not closed (Figure 4.19e) is not as important for shear stress-strain experiments, as the specimen prevents the torque adapter from closing.

(a) Shear stress-strain.

(b) Shear strain rate.
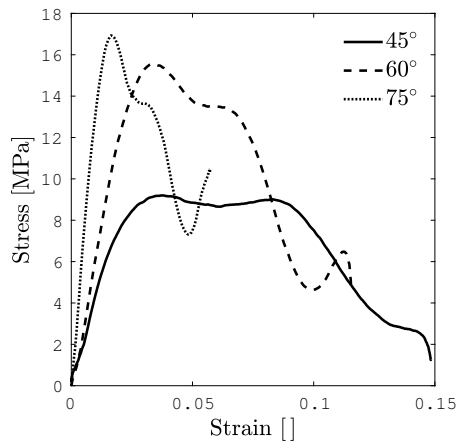
(c) Axial stress-strain.
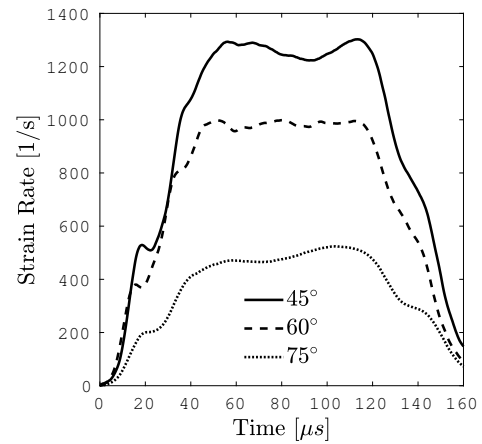
(d) Axial strain rate.
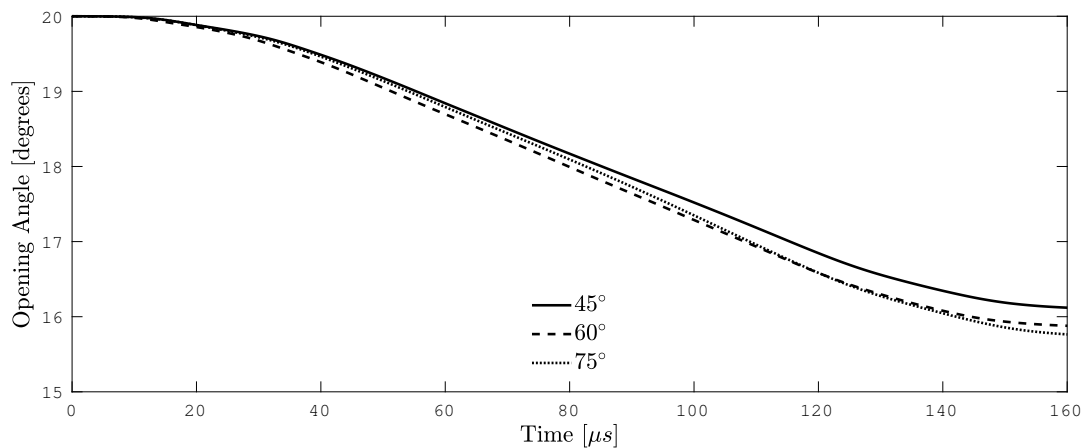
(e) Opening angle.

Figure 4.19.   Shear stress-strain experiments using three angles of inclination. Adapted with permission from [16]. Copyright (2017) Experimental Mechanics.

4.2.3 X-Ray Phase Contrast Imaging

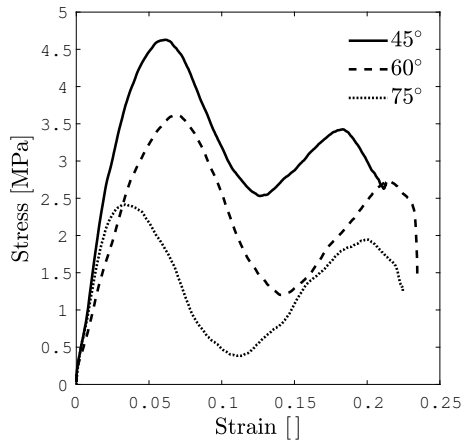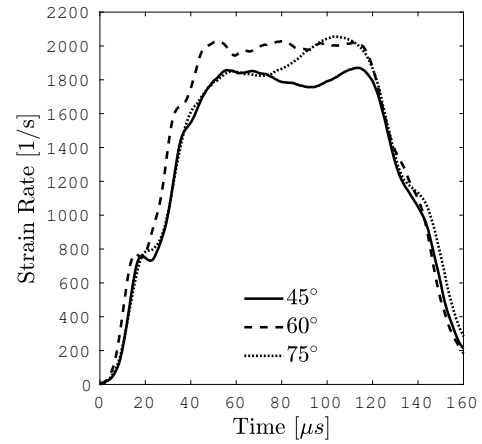The experiments at Argonne National Laboratory provide more insight into material behavior than the Kolsky bar experiments or experiments with high speed imaging alone. Since the x-rays are able to penetrate through the specimen and phase contrast imaging was employed, each and every interface between crystal and binder is highlighted. In addition, each image sequence consists of 256 images at a frame rate of one million frames per second, but only a select few frames from select experiments are shown here to highlight general details. The sliding velocity for each of the conditions was maintained at three meters per second. Observations made from these high speed images are based on the motion of the bulk material. Instances of large particulate and interface deformation are identified where possible. Lastly, only friction experiments were performed at Argonne National Laboratory, as the shear stress-strain experiments would not produce much material motion during an experiment.

For composites with high volume fractions of aggregate, such as polymer bonded explosives and their simulated materials, the number of interfaces may become overwhelming (Figure 4.20). Although the few images shown are not entirely enlightening, the full image sequence shows the deformation of the sample in both axial and torsional modes. In particular, the gaps between crystals, which are actually Sylgard (not voids), allow slightly higher penetration of x-rays than the crystals themselves. These regions can be enhanced and contrasted to show the motion of the material under loading. While some regions follow an observably straight line, other regions show local deformation different from the global mode. Some examples are: rotation and ejection of large crystals, collapse of voids as indicated by a loss of contrast at an interface, and localized slipping at the interface.

The material in this study includes some relatively large crystals that allow one to track their motion (Figures 4.21 and 4.22). However, as loading continued, the thin layers of binder were compressed and displaced around these larger crystals, eventually

(a) $t_0 + 4\mu s$

(b) $t_0 + 41\mu s$

(c) $t_0 + 79\mu s$

(d) $t_0 + 134\mu s$

(e) $t_0 + 160\mu s$

(f) $t_0 + 197\mu s$
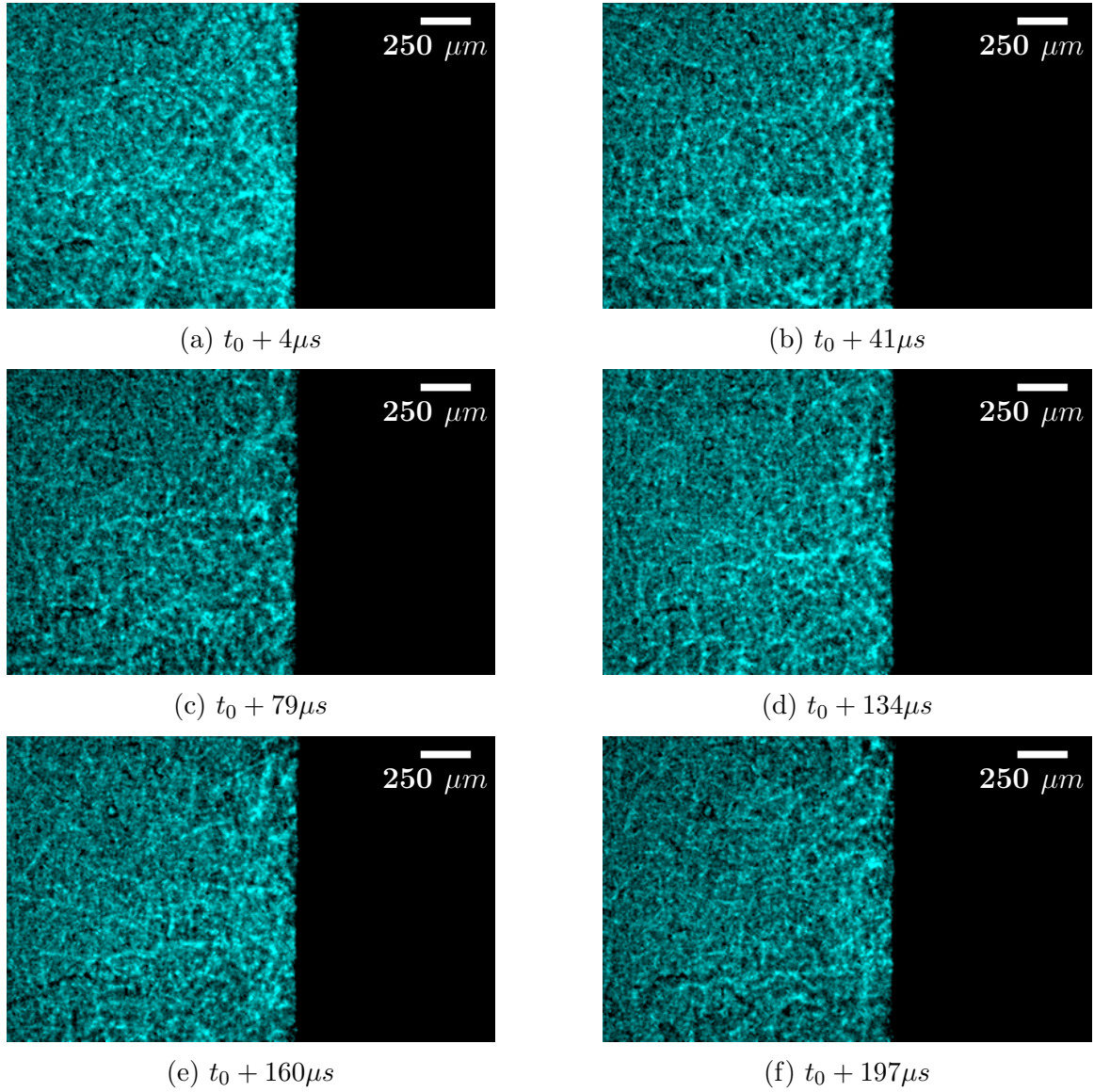
Figure 4.20. Friction experiment with a homogeneous field of view, the torque adapter angle of inclination was 45 degrees.

leading to loss of contrast, meaning the crystals essentially disappeared from view. Although not directly observable due to the large number of interfaces in these images, each of the crystals (whether large or small) are breaking up [12]. The presence of the Sylgard is quite irrelevant, as the specimen is a system of discrete particles that will ultimately fail during compression [11, 13, 14]. For these experiments, regions where the image appears to become less grainy are regions where the crystal aggregate has most likely become pulverized.

Other than the deformation of the material under loading, another region of interest is the interface experiencing sliding. Here, local deformation and sliding is clearly visible (Figures 4.21 and 4.22). While the few images in the figure appear to only show general motion, the full image sequence shows that the regions with localized sliding do so at different rates as compared to the rest of the interface. In the case of simulant sliding on simulant (Figure 4.23), both sides of the interface are deforming, and local sliding is also observable. It is clear that both sides of the interface are deforming in the same mode, except that the side fixed to the torque adapter is rotating faster as the opposing side is fixed to the transducer assembly.

4.2.4   Notes on Angle of Inclination and Friction

From an angular stand point, the torque adapter with a 45 degree incline is expected to provide equal parts of compression and rotation. This is clearly shown in the high speed images, where forward motion is observable as the material begins to rotate (Figure 4.20). However, this fact should not be confused with how the motion is determined by the torque adapter. In principle, the material response may be non-linear, meaning the motion of individual particles will not produce a 45 degree trace on the images. Furthermore, the high speed images also capture a portion of the unloading of the specimen. Although not entirely relevant in these sequences, the unloading period may reveal other phenomena, particularly if the sliding velocity remains high as the compression returns to zero.

(a) $t_0 + 6\mu s$

(b) $t_0 + 19\mu s$

(c) $t_0 + 32\mu s$

(d) $t_0 + 45\mu s$

(e) $t_0 + 58\mu s$

(f) $t_0 + 71\mu s$

(g) $t_0 + 84\mu s$

(h) $t_0 + 97\mu s$
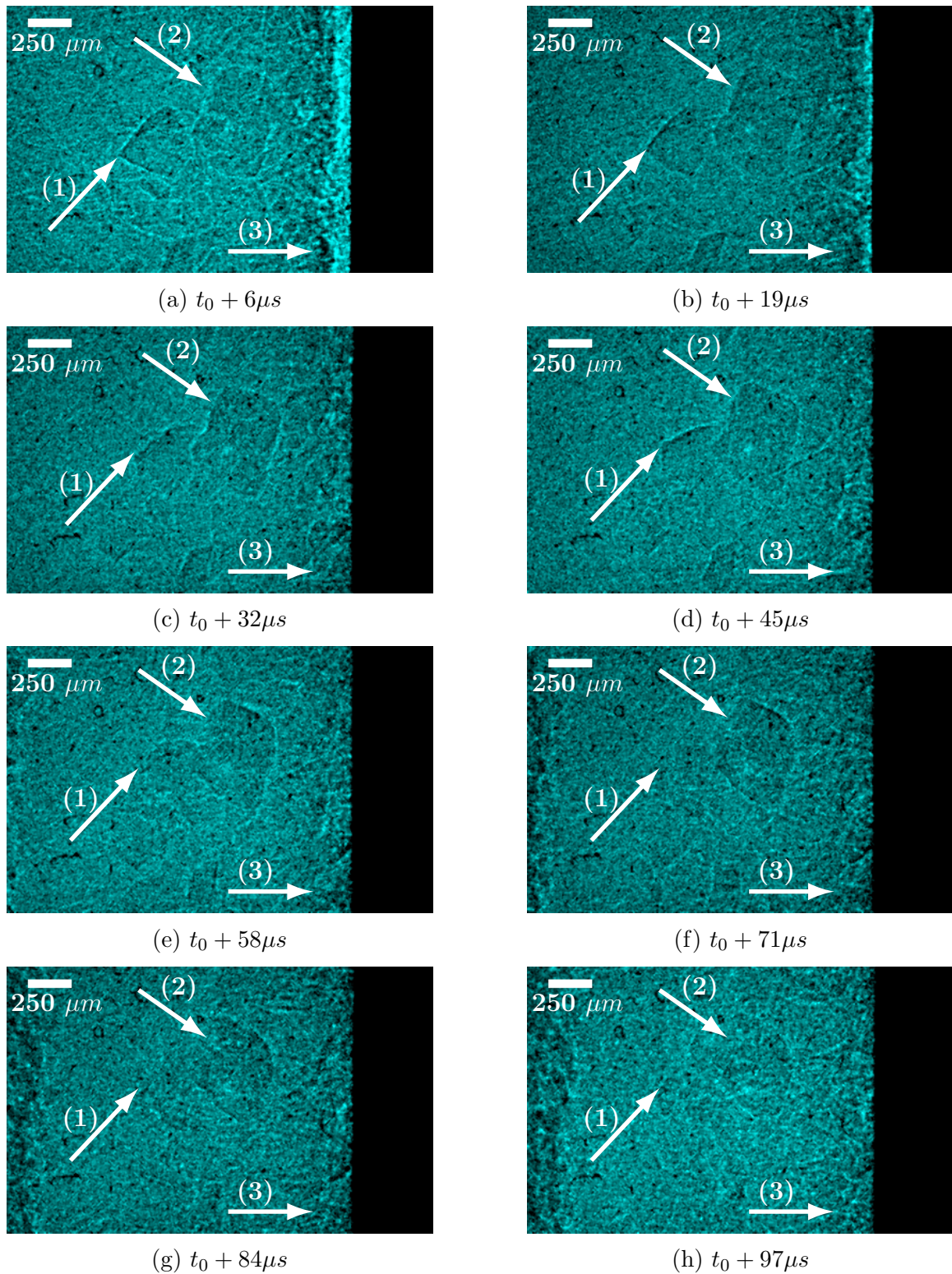
Figure 4.21. The motion of two large crystals is evident (1 & 2), local deformation at the interface may be tracked (3) during a friction experiment. The torque adapter angle of inclination was 60 degrees.

(a) $t_0 + 4\mu s$

(b) $t_0 + 20\mu s$

(c) $t_0 + 36\mu s$

(d) $t_0 + 52\mu s$

(e) $t_0 + 68\mu s$

(f) $t_0 + 84\mu s$

(g) $t_0 + 100\mu s$

(h) $t_0 + 116\mu s$
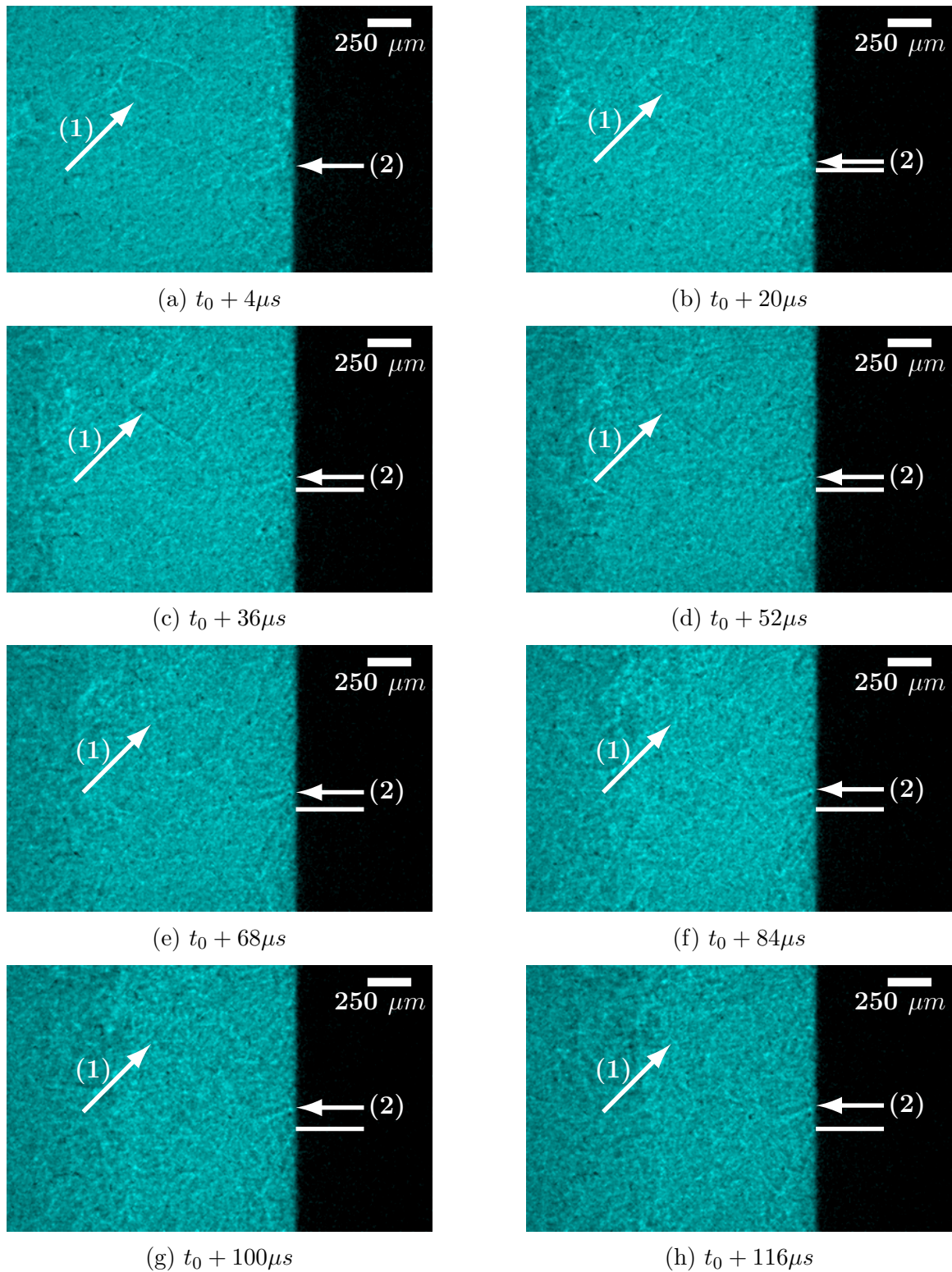
Figure 4.22. The motion and rotation of a large crystal can be followed (1) during a friction experiment. Features at the interface may be tracked (2), the angle of inclination was 75 degrees.

165

(a) $t_0 + 4\mu s$

(b) $t_0 + 20\mu s$

(c) $t_0 + 36\mu s$

(d) $t_0 + 52\mu s$

(e) $t_0 + 68\mu s$

(f) $t_0 + 84\mu s$

(g) $t_0 + 100\mu s$

(h) $t_0 + 116\mu s$
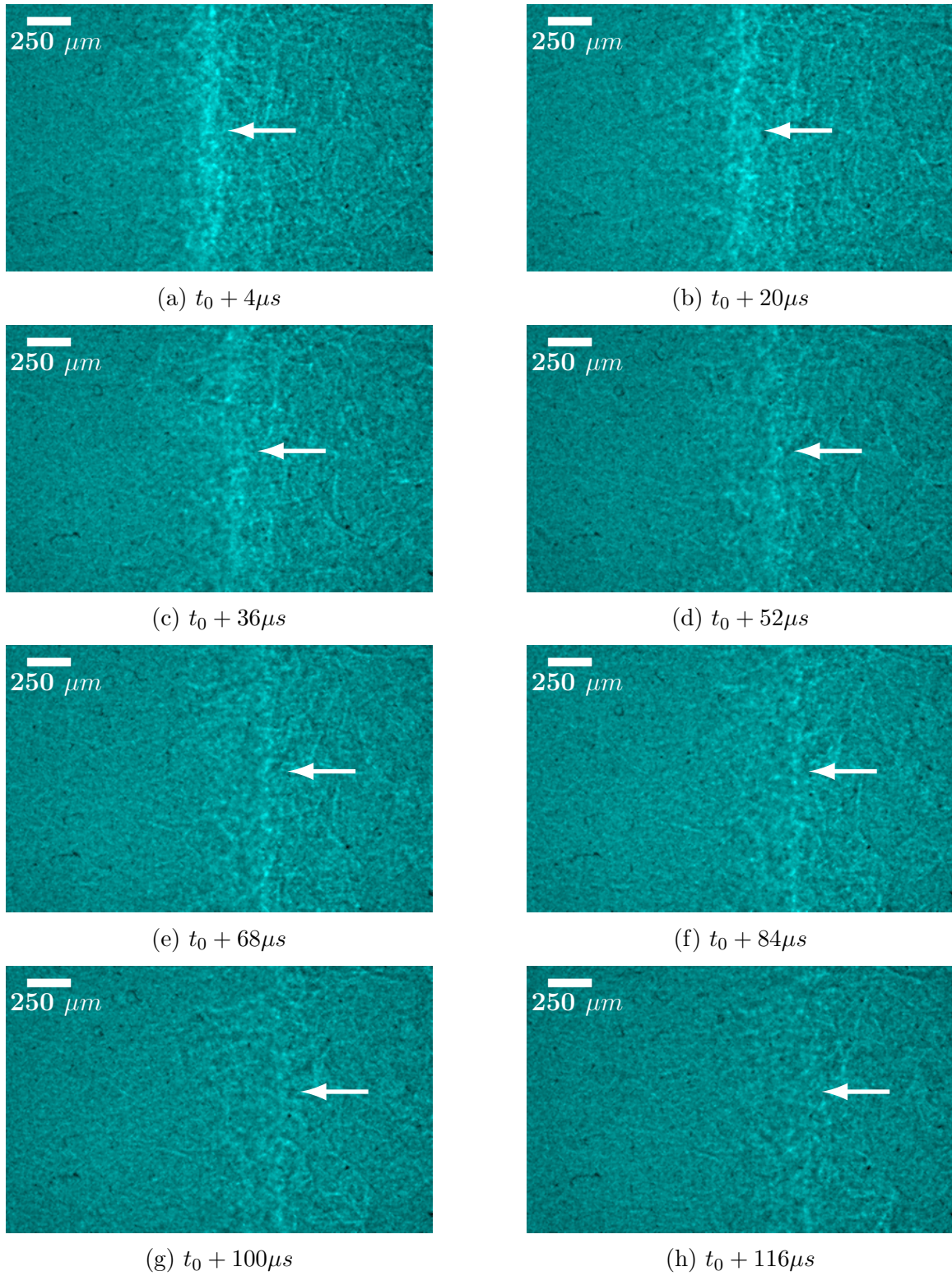
Figure 4.23. The composite sliding against itself. The angle of inclination was 60 degrees.

The torque adapters with a 60 degree incline are closer to a planar surface than the 45 degree inclines. As such, the angular velocity is expected to increase along with the axial force. However, the forward motion of the torque adapter should be less than the adapter with a 45 degree incline. Once the specimen has been compressed, most of the motion appears to be rotary in nature. For these particular experiments, this motion would imply the loading did not occur in the expected manner, and that the torque adapter was not in the correct position when the experiment occurred (i.e. the part of the adapter holding the sample moved slightly). Considering the environment, this situation is unavoidable, as the apparatus is in a sealed room and cannot be checked at the last second to verify that the torque adapter is in the correct position.

The torque adapters with a 75 degree incline are expected to have the fastest angular velocity of the thee adapters. However, due to the limited travel distance, the torque adapter quickly closes, producing an almost pure compressive stress state. This means that most of the motion captured in the high speed images does not involve a combined compression-torsion stress state, and insights drawn from these particular images should be compared carefully to the other cases. Interestingly, the particles in the samples tested with this torque adapter appear to trace a 45 degree line in the images. This motion is the most evident in Figure 4.22, where two large particles are within the view port.

5. DIRECTIONS FOR FUTURE RESEARCH

5.1 Side-Impact Torsion Kolsky Bar

The full potential of the side-impact torsion Kolsky bar has not been reached. The torsion Kolsky bar experiment in general is not widely utilized to study materials for either stress-strain or friction behavior. With a large selection of sufficiently soft materials (i.e. various types of rubber) for use as a pulse shaper, the side-impact torsion Kolsky bar is capable of generating rectangular, triangular, bi-linear, and many other shapes of incident torsion waves. The apparatus is also capable of creating fairly long incident torsion waves without the required space for storage of torsional deformation. However, the studies to date have been limited to friction of essentially two materials.

Shear and friction are responsible for many phenomena in engineering, with wear being a major contributor to the failure of mechanical systems. Wear is present in metallic, granular, and even polymer systems where surfaces are constantly exposed to mechanical loading and abrasion. In general, wearing takes time, but the same processes occur at higher rates during impact events that may lead to complete failure of a mechanical system. Applications range from local fracture of glass materials, debonding of granular materials, galling of metallic materials, and induced thermal responses in polymers.

Friction behavior need not be limited to the response at an entirely constant rate. While the development of a material model is greatly simplified by the availability of data at different rates (i.e. strain rate, sliding velocity, etc.), the models may not capture the true response under non-ideal dynamic conditions. One possible experiment to explore this behavior would be to use some form of non-rectangular incident wave, such as a triangular wave, which would expose an interface to a constantly changing
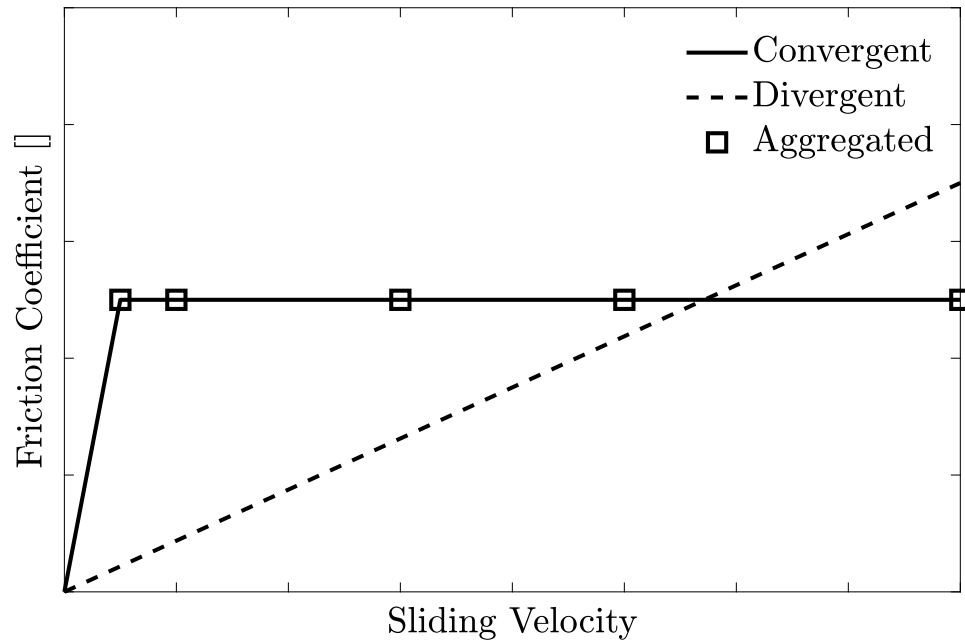
Figure 5.1. Hypothetical material response to a triangular incident wave. Would the response converge with the data at constant sliding velocities, or would the response take its own path?

sliding velocity. The question to answer would then be whether the aggregated data at constant sliding velocities corresponds to the response across a spectrum of sliding velocities (Figure 5.1). This is a direct analog to the stress-strain response at different strain rates: given a strain rate dependent material, if the strain rate jumps during loading, what does the response look like?

5.2   Compression-Torsion Torque Adapter

The combined compression-torsion Kolsky bar is not an ideal experiment. The torque adapter must begin in the opened position, which introduces problems relating to contact between the components. For a weak specimen response, the likelihood that the two halves of the torque adapter will separate is fairly high, as the motion begins from a fairly high state of potential energy once the incident wave arrives.

This issue could be resolved by using the torque adapter with a torsion Kolsky bar instead. Here, the torque adapter could begin from a closed position, and the incident torsion wave will induce torsion and compression in the specimen. Since the adapter is initially closed, the adapter always experiences resistance to keep the adapter in contact. This is in contrast to the compression Kolsky bar variant, where the adapter tends to reduce the resistance, resulting in loss of contact. Figure 2.5 in Section 2.2 illustrates the opened and closed states of the torque adapter.

Combined with the side-impact torsion Kolsky bar, the torque adapter could bring a new age to the study of dynamic behavior of materials. While it is desirable to remove as many variables as possible to simplify analysis, many applications involve complex stress states. For each application, it is reasonable to assume that there is a material being designed and studied specifically to fill that role. These new materials, as well as the current materials, need a suite of experiments tailored to more complex conditions in order to facilitate the development of material models and optimize for specific applications.

The concept of dually dynamic stress states is particularly important for granular materials, whose behavior drastically changes depending on the amount of stress within the system. A specific application of this experiment would be for geo-materials such as concrete and rock. Earthquake science has led to the development of many friction models to explain how the Earth's crust behaviors during an earthquake, which may induce compressive and shear stress in the giga-Pascal range. While the stresses are out of reach, the lower sliding velocities are entirely attainable. This concept also applies to concrete and other stiff and brittle particle composites, particularly those that may be involved in ballistic scenarios. Having the capability to induce large compressive and shear stresses simultaneously, in a dynamic manner, would be a huge benefit to developing material models of these materials.

The torque adapter may also benefit from further study. One flaw in the design is the use of inclined planes. As the opening angle of the adapter changes, the amount of converted stress changes due to the path tracing an ellipse (See Section 2.2.2). A

solution is to use an axisymmetric shape such as a screw or a double helix [16]. The benefit of these two types of geometry are that the tangent vector at the point of contact remains constant as a function of the opening angle. The difference between the screw and double helix is the number of contact points, which is one for the screw, and two for the double helix. Machining tolerances play an important role, and a single contact point is much easier to produce with consistency than two contact points. However, the effect of using a single contact point is yet unknown. It may be hypothesized that the double helix will perform better than the screw and inclined planes, but the mating parts of the torque adapter may not have a sufficient fit such that the helices are always in contact.

6. SUMMARY

The side-impact torsion Kolsky bar was developed to address several concerns with current torsion Kolsky bar methods. The ability to control the duration, amplitude, and shape of an incident wave is considered to be essential for Kolsky bar experiments. While the amplitude and duration are controlled by the components of the apparatus, the shape is controlled by a pulse shaper, a technique in itself that requires patience and experimentation. Being able to provide these three characteristics in torsion allows the torsion Kolsky bar to utilized in the development of material models in shear.

Early development of the side-impact torsion Kolsky bar was plagued by unknown interactions, leading to work on analytical and numerical solutions. The engineering analysis revealed several geometric constraints that should be applied to the apparatus. Artifacts in the torsion incident wave were identified and analyzed to optimize the apparatus. The artifacts set bounds on the material of pulse shapers, simplifying the selection of pulse shapers for various purposes.

The side-impact torsion Kolsky bar was applied to friction studies, where a simple rectangular waveform is often sufficient. However, small friction responses may be immeasurable, even with rather large levels of compression or incident shear. These cases require a modification to the apparatus: a transmission bar with a reduced torsional stiffness, resulting in a natural amplification of the waveforms.

Friction experiments between metal surfaces are expected to show a static friction peak before the onset of sliding. However, the rise time of the incident wave and the surface condition of the interfacial components may not result in a static friction peak. Similarly, the mechanical behavior and failure of adhesives involved in the experiment may result in the appearance of a false static friction peak. Soft particle composites show a static friction peak after a period of shear deformation. The onset

of sliding is relatively slow and is quickly followed by surface evolution, resulting in an evolving friction coefficient.

The development of the side-impact torsion Kolsky bar led to a new concept for combined compression-torsion. Using a torque adapter, an incident compression wave may be converted into compression and torsion just prior to interaction with a specimen. The dually dynamic state may be applied to shear and friction, just as a typical torsion Kolsky bar experiment. Function of the torque adapter was verified using high speed imagery, and x-ray phase contrasting imaging detailed the interior of a particle composite during this dually dynamic loading.

X-ray phase contrast imaging revealed the internal motion of the aggregate of the particle composite, ranging from rotation, compression, and fracture of particles. The shear number of particles in the composite masks the behavior of smaller particles, but the largest are clearly visible. The interface in a friction experiment may also be observed, with local slipping deformation visible as a function of time.

REFERENCES

[1] H Kolsky. An investigation of the mechanical properties of materials at very high rates of loading. *Proceedings of the Physical Society. Section B*, 62(11):676, 1949.

[2] WW Chen and B Song. *Split Hopkinson (Kolsky) bar: design, testing and applications.* Springer Science & Business Media, 2010.

[3] BD Sanborn. *An experimental investigation of radial deformation of soft materials in Kolsky bar experiments.* PhD thesis, Purdue University, 2011.

[4] S Nemat-Nasser, JB Isaacs, and JE Starrett. Hopkinson techniques for dynamic recovery experiments. *Proceedings of the Royal Society of London. Series A: Mathematical and Physical Sciences*, 435(1894):371–391, 1991.

[5] MC Hudspeth, BJ Claus, S Dubelman, J Black, A Mondal, N Parab, C Funnell, F Hai, ML Qi, K Fezzaa, et al. High speed synchrotron x-ray phase contrast imaging of dynamic material response to split hopkinson bar loading. *Review of Scientific Instruments*, 84(2):025102, 2013.

[6] W Chen, B Song, DJ Frew, and MJ Forrestal. Dynamic small strain measurements of a metal specimen with a split hopkinson pressure bar. *Experimental Mechanics*, 43(1):20–23, 2003.

[7] J Duffy, JD Campbell, and RH Hawley. On the use of a torsional split hopkinson bar to study rate effects in 1100-0 aluminum. *Journal of Applied Mechanics*, 38(1):83–91, 1971.

[8] WW Chen, MC Hudspeth, BJ Claus, ND Parab, JT Black, K Fezzaa, and SN Luo. In situ damage assessment using synchrotron x-rays in materials loaded by a hopkinson bar. *Phil. Trans. R. Soc. A*, 372(2015):20130191, 2014.

[9] L Lu, D Fan, BX Bie, XX Ran, ML Qi, N Parab, JZ Sun, HJ Liao, MC Hudspeth, B Claus, et al. Dynamic strain field mapping with synchrotron x-ray digital image correlation. *Review of Scientific Instruments*, 85(7):076101, 2014.

[10] ND Parab, JT Black, BJ Claus, MC Hudspeth, J Sun, K Fezzaa, and W Chen. Observation of crack propagation in glass using x-ray phase contrast imaging. *International Journal of Applied Glass Science*, 5(4):363–373, 2014.

[11] ND Parab, BJ Claus, MC Hudspeth, JT Black, A Mondal, J Sun, K Fezzaa, X Xiao, SN Luo, and W Chen. Experimental assessment of fracture of individual sand particles at different loading rates. *International Journal of Impact Engineering*, 68:8–14, 2014.

[12] ND Parab, ZA Roberts, MH Harr, JO Mares, AD Casey, IE Gunduz, MC Hudspeth, BJ Claus, T Sun, K Fezzaa, et al. High speed x-ray phase contrast imaging of energetic composites under dynamic compression. *Applied Physics Letters*, 109(13):131903, 2016.

[13] ND Parab, Z Guo, MC Hudspeth, BJ Claus, K Fezzaa, T Sun, and W Chen. Fracture mechanisms of glass particles under dynamic compression. *International Journal of Impact Engineering*, 106:146–154, 2017.

[14] ND Parab, Z Guo, MC Hudspeth, BJ Claus, K Fezzaa, T Sun, and W Chen. Dynamic fracture behavior of single and contacting poly (methyl methacrylate) particles. *Advanced Powder Technology*, 28(11):2929–2939, 2017.

[15] ND Parab, Z Guo, MC Hudspeth, BJ Claus, BH Lim, T Sun, X Xiao, K Fezzaa, and W Chen. In situ observation of fracture processes in high-strength concretes and limestone using high-speed x-ray phase-contrast imaging. *Phil. Trans. R. Soc. A*, 375(2085):20160178, 2017.

[16] B Claus, J Chu, M Beason, H Liao, B Martin, and W Chen. Dynamic experiments using simultaneous compression and shear loading. *Experimental Mechanics*, 57(9):1359–1369, 2017.

[17] JM Chu, BJ Claus, ND Parab, D OBrien, T Sun, K Fezzaa, and W Chen. Visualization of dynamic fiber-matrix interfacial shear debonding. *Journal of Materials Science*, 53(8):5845–5859, 2018.

[18] JM Chu, BJ Claus, ND Parab, D OBrien, K Fezzaa, T Sun, and W Chen. Visualization of fiber/matrix interfacial shear debonding mechanism at high rate loading. In *Proceedings of the American Society for CompositesThirty-second Technical Conference*, 2017.

[19] A Gilat. Torsional kolsky bar testing. *ASM handbook*, 8:505–515, 2000.

[20] DP Pope, T Vreeland Jr, and DS Wood. Machine for producing square torsion pulses of microsecond duration. *Review of Scientific Instruments*, 35(10):1351–1355, 2004.

[21] WE Baker and CH Yew. Strain-rate effects in the propagation of torsional plastic waves. *Journal of Applied Mechanics*, 33(4):917–923, 1966.

[22] JL Lewis and JD Campbell. The development and use of a torsional hopkinson-bar apparatus. *Experimental Mechanics*, 12(11):520–524, 1972.

[23] S Rajagopalan and V Prakash. A modified torsional kolsky bar for investigating dynamic friction. *Experimental mechanics*, 39(4):295–303, 1999.

[24] HD Espinosa, A Patanella, and M Fischer. A novel dynamic friction experiment using a modified kolsky bar apparatus. *Experimental Mechanics*, 40(2):138–153, 2000.

[25] H Huang and R Feng. Dynamic friction of sic surfaces: a torsional kolsky bar tribometer study. *Tribology Letters*, 27(3):329–338, 2007.

[26] F Yuan and V Prakash. Use of a modified torsional kolsky bar to study frictional slip resistance in rock-analog materials at coseismic slip rates. *International Journal of Solids and Structures*, 45(14):4247–4263, 2008.

[27] X Nie, R Prabhu, WW Chen, JM Caruthers, and T Weerasooriya. A kolsky torsion bar technique for characterization of dynamic shear response of soft materials. *Experimental mechanics*, 51(9):1527–1534, 2011.

[28] BJ Claus, X Nie, BE Martin, and W Chen. A side-impact torsion kolsky bar. *Experimental Mechanics*, 55(7):1367–1374, 2015.

[29] K Ogawa. Impact friction test method by applying stress wave. *Experimental Mechanics*, 37(4):398–402, 1997.

[30] JL Lewis and W Goldsmith. A biaxial split hopkinson bar for simultaneous torsion and compression. *Review of Scientific Instruments*, 44(7):811–813, 2003.

[31] JR Klepaczko. An experimental technique for shear testing at high and very high strain rates. the case of a mild steel. *International journal of impact engineering*, 15(1):25–39, 1994.

[32] Bratislav Lukić and Pascal Forquin. Experimental characterization of the punch through shear strength of an ultra-high performance concrete. *International Journal of Impact Engineering*, 91:34–45, 2016.

[33] S Philippon, G Sutter, and A Molinari. An experimental study of friction at high sliding velocities. *Wear*, 257(7):777–784, 2004.

[34] AM Bragov, AY Konstantinov, and AK Lomunov. Determining dynamic friction using a modified kolsky method. *Technical Physics Letters*, 34(5):439–440, 2008.

[35] B Sanborn, B Song, and E Nishida. Development of a new method to investigate the dynamic friction behavior of interfaces using a kolsky tension bar. *Experimental Mechanics*, 58(2):335–342, 2018.

[36] D Rittel, S Lee, and G Ravichandran. A shear-compression specimen for large strain testing. *Experimental Mechanics*, 42(1):58–64, 2002.

[37] J Zhao, WG Knauss, and G Ravichandran. A new shear-compression-specimen for determining quasistatic and dynamic polymer properties. *Experimental mechanics*, 49(3):427, 2009.

[38] PD Zhao, FY Lu, R Chen, YL Lin, JL Li, L Lu, and GL Sun. A technique for combined dynamic compression-shear test. *Review of Scientific Instruments*, 82(3):035110, 2011.

[39] Y Lin, J Qin, F Lu, R Chen, and X Li. Dynamic friction coefficient of two plastics against aluminum under impact loading. *Tribology International*, 79:26–31, 2014.

[40] AM Bragov, AK Lomunov, AY Konstantinov, and DA Lamzin. A modified kolsky method for determining the shear strength of brittle materials. *Technical Physics Letters*, 43(1):130–132, 2017.

[41] BH Lim, H Liao, W Chen, and MJ Forrestal. Effects of constant engineering and true strain rates on the mechanical behavior of 304 stainless steel. *Journal of Dynamic Behavior of Materials*, 3(1):76–82, 2017.

[42] BH Lim. Size and rate effects on mechanical behavior of ultra high performance concrete. 2013.

[43] MC Hudspeth, BJ Claus, ND Parab, BH Lim, W Chen, T Sun, and K Fezza. In situ visual observation of fracture processes in several high-performance fibers. *Journal of Dynamic Behavior of Materials*, 1(1):55–64, 2015.

[44] MC Hudspeth, A Agarwal, B Andrews, BJ Claus, F Hai, C Funnell, J Zheng, and W Chen. Degradation of yarns recovered from soft-armor targets subjected to multiple ballistic impacts. *Composites Part A: Applied Science and Manufacturing*, 58:98–106, 2014.

[45] JM Chu, BJ Claus, and W Chen. Mechanical properties of transgenic silkworm silk under high strain rate tensile loading. *Journal of Dynamic Behavior of Materials*, 3(4):538–547, 2017.

[46] W Chen, B Zhang, and MJ Forrestal. A split hopkinson bar technique for low-impedance materials. *Experimental mechanics*, 39(2):81–85, 1999.

[47] Peter J Blau. *Friction science and technology: from concepts to applications.* CRC press, 2008.

[48] A Schallamach. Friction and abrasion of rubber. *Rubber Chemistry and Technology*, 31(5):982–1014, 1958.

[49] A Schallamach. A theory of dynamic rubber friction. *Wear*, 6(5):375–382, 1963.

[50] BNJ Persson. Theory of rubber friction and contact mechanics. *The Journal of Chemical Physics*, 115(8):3840–3861, 2001.

[51] K Vorvolakos and MK Chaudhury. The effects of molecular weight and temperature on the kinetic friction of silicone rubbers. *Langmuir*, 19(17):6778–6787, 2003.

[52] E Rabinowicz. The intrinsic variables affecting the stick-slip process. *Proceedings of the Physical Society*, 71(4):668, 1958.

[53] H Yoshizawa, P McGuiggan, and J Israelachvili. Identification of a second dynamic state during stick-slip motion. *Science*, 259(5099):1305–1308, 1993.

[54] TS Chow. The effect of particle shape on the mechanical properties of filled polymers. *Journal of Materials Science*, 15(8):1873–1888, 1980.

[55] RM Christensen. A critical evaluation for a class of micro-mechanics models. In *Inelastic Deformation of Composite Materials*, pages 275–282. Springer, 1991.

[56] JD Eshelby. The determination of the elastic field of an ellipsoidal inclusion, and related problems. In *Proceedings of the Royal Society of London A: Mathematical, Physical and Engineering Sciences*, volume 241, pages 376–396. The Royal Society, 1957.

[57] R Hill. A self-consistent mechanics of composite materials. *Journal of the Mechanics and Physics of Solids*, 13(4):213–222, 1965.

[58] RM Christensen and KH Lo. Solutions for effective shear properties in three phase sphere and cylinder models. *Journal of the Mechanics and Physics of Solids*, 27(4):315–330, 1979.

[59] T Mori and K Tanaka. Average stress in matrix and average elastic energy of materials with misfitting inclusions. *Acta metallurgica*, 21(5):571–574, 1973.

[60] R Christensen, H Schantz, and J Shapiro. On the range of validity of the mori-tanaka method. *Journal of the Mechanics and Physics of Solids*, 40(1):69–73, 1992.

[61] EM Mas, BE Clements, WR Blumenthal, CM Cady, and GT Gray. Applying micro-mechanics to finite element simulations of split hopkinson pressure bar experiments on high explosives. In *AIP Conference Proceedings*, number 1, pages 539–542. IOP Institute of Physics Publishing Ltd, 2002.

[62] EM Mas, BE Clements, and DC George. Direct numerical simulations of pbx 9501. In *Shock Compression of Condensed Matter-2003: Proceedings of the Conference of the American Physical Society Topical Group on Shock Compression of Condensed Matter*, volume 706, pages 389–392. AIP Publishing, 2004.

[63] S Dartois, C Nadot-Martin, D Halm, A Dragon, A Fanget, and G Contesse. Micromechanical modelling of damage evolution in highly filled particulate composites–induced effects at different scales. *International Journal of Damage Mechanics*, 22(7):927–966, 2013.

[64] L Richard Simpson and M Frances Foltz. Llnl small-scale friction sensitivity (bam) test. Technical report, Lawrence Livermore National Lab., CA (United States), 1996.

[65] FP Bowden, MFR Mulcahy, RG Vines, and A Yoffe. The detonation of liquid explosives by gentle impact. the effect of minute gas spaces. *Proceedings of the Royal Society of London. Series A. Mathematical and Physical Sciences*, 188(1014):291–311, 1947.

[66] FP Bowden, MA Stone, and GK Tudor. Hot spots on rubbing surfaces and the detonation of explosives by friction. *Proceedings of the Royal Society of London. Series A. Mathematical and Physical Sciences*, 188(1014):329–349, 1947.

[67] FP Bowden and OA Gurton. Initiation of explosions by grit particles. *Nat. Lond*, 162:654, 1948.

[68] FP Bowden and OA Gurton. Birth and growth of explosion in liquids and solids initiated by impact and friction. *Proceedings of the Royal Society of London. Series A. Mathematical and Physical Sciences*, 198(1054):350–372, 1949.

[69] Nicholas E Kerschen. *Investigation into high explosive particle dynamics under impact loading.* PhD thesis, Purdue University, 2018.

[70] KS Jaw and JS Lee. Thermal behaviors of petn base polymer bonded explosives. *Journal of Thermal Analysis and Calorimetry*, 93(3):953–957, 2008.

VITA

Benjamin J. Claus

Education

- Ph.D., Aeronautical Engineering, Purdue University, December 2018. "Controlling Dynamic Torsion Loading"

- M.S., Aeronautical Engineering, Purdue University, May 2014. "Characteristics of Fibrous Tissue at High Rates of Tensile Loading"

- B.S., Aeronautical Engineering, Purdue University, May 2012.

First Author Publications

- Claus, B., Nie, X., Martin, B. E., & Chen, W. (2015). A Side-Impact Torsion Kolsky Bar. Experimental Mechanics, 55(7), 1367-1374.

- Claus, B., Chu, J., Beason, M., Liao, H., Martin, B., & Chen, W. (2017). Dynamic Experiments using Simultaneous Compression and Shear Loading. Experimental Mechanics, 57(9), 1359-1369.

Co-Author Publications

- Hudspeth, M., Claus, B., Dubelman, S., Black, J., Mondal, A., Parab, N., ... & Luo, S. N. (2013). High Speed Synchrotron X-Ray Phase Contrast Imaging of Dynamic Material Response to Split Hopkinson Bar Loading. Review of Scientific Instruments, 84(2), 025102.

- Chen, W., Hudspeth, M., Claus, B., Parab, N., Black, J., Fezzaa, K., & Luo, S. (2014). In Situ Damage Assessment Using Synchrotron X-Rays in Materials Loaded by a Hopkinson Bar. Phil. Trans. R. Soc. A, 372(2015), 20130191.

- Hudspeth, M., Agarwal, A., Andrews, B., Claus, B., Hai, F., Funnell, C., ... & Chen, W. (2014). Degradation of Yarns Recovered from Soft-Armor Targets

Subjected to Multiple Ballistic Impacts. Composites Part A: Applied Science and Manufacturing, 58, 98-106.

- Lu, L., Fan, D., Bie, B., Ran, X., Qi, M., Parab, N., Sun, J., Liao, H., Hudspeth, M., Claus, B., & Fezzaa, K. (2014). Note: Dynamic Strain Field Mapping with Synchrotron X-Ray Digital Image Correlation. Review of Scientific Instruments, 85(7), 076101.

- Parab, N., Black, J., Claus, B., Hudspeth, M., Sun, J., Fezzaa, K., & Chen, W. (2014). Observation of Crack Propagation in Glass Using X-Ray Phase Contrast Imaging. International Journal of Applied Glass Science, 5(4), 363-373.

- Parab, N., Claus, B., Hudspeth, M., Black, J., Mondal, A., Sun, J., ... & Chen, W. (2014). Experimental Assessment of Fracture of Individual Sand Particles at Different Loading Rates. International Journal of Impact Engineering, 68, 8-14.

- Hudspeth, M., Claus, B., Parab, N., Lim, B., Chen, W., Sun, T., & Fezza, K. (2015). In Situ Visual Observation of Fracture Processes in Several High-Performance Fibers. Journal of Dynamic Behavior of Materials, 1(1), 55-64.

- Parab, N., Roberts, Z., Harr, M., Mares, J., Casey, A., Gunduz, I., Hudspeth, M., Claus, B., ... & Son, S. (2016). High Speed X-Ray Phase Contrast Imaging of Energetic Composites under Dynamic Compression. Applied Physics Letters, 109(13), 131903.

- Chu, J., Claus, B., & Chen, W. (2017). Mechanical Properties of Transgenic Silkworm Silk Under High Strain Rate Tensile Loading. Journal of Dynamic Behavior of Materials, 3(4), 538-547.

- Chu, J., Claus, B., Parab, N., O'Brien, D., Fezzaa, K., Sun, T., & Chen, W. (2017). Visualization of Fiber/Matrix Interfacial Shear Debonding Mechanism

at High Rate Loading. In Proceedings of the American Society for Composites - Thirty-Second Technical Conference.

- Parab, N., Guo, Z., Hudspeth, M., Claus, B., Fezzaa, K., Sun, T., & Chen, W. (2017). Fracture Mechanisms of Glass Particles under Dynamic Compression. International Journal of Impact Engineering, 106, 146-154.

- Parab, N., Guo, Z., Hudspeth, M., Claus, B., Fezzaa, K., Sun, T., & Chen, W. (2017). Dynamic Fracture Behavior of Single and Contacting Poly (Methyl-Methacrylate) Particles. Advanced Powder Technology, 28(11), 2929-2939.

- Parab, N., Guo, Z., Hudspeth, M., Claus, B., Lim, B., Sun, T., ... & Chen, W. (2017). In Situ Observation of Fracture Processes in High-Strength Concretes and Limestone using High-Speed X-Ray Phase-Contrast Imaging. Phil. Trans. R. Soc. A, 375(2085), 20160178.

- Chu, J., Claus, B., Parab, N., O'Brien, D., Sun, T., Fezzaa, K., & Chen, W. (2018). Visualization of Dynamic Fiber-Matrix Interfacial Shear Debonding. Journal of Materials Science, 53(8), 5845-5859.

Conferences

- 2013 Society of Experimental Mechanics Annual Conference "Soft Tissue Injury Development under Dynamic Tension"

- 2013 American Society of Mechanical Engineers Annual Meeting "Microscopic Damage/Injury Development under Dynamic Loading in Soft Tissues Damage Development of the Medial Collateral Ligament Under Dynamic Loading"

- 2014 National Congress for Theoretical and Applied Mechanics "Microscopic Damage Development of the Medial Collateral Ligament Under Dynamic Loading"

- 2014 Society of Experimental Mechanics Annual Conference "Development of a Side-Impact Pulse-Shaping Torsional Kolsky Bar"

- 2014 Purdue Society of Engineering Science "Development of a Side-impact Pulse-shaping Torsional Kolsky Bar"

- 2015 Society of Experimental Mechanics Annual Conference "Transmission of Torsional Waves within a Torsion Kolsky Bar"

- 2016 Purdue Global Security and Defense Innovation Symposium "Effect of Manufacturing Method on Dynamic Friction of Energetic Simulants"

- 2016 Purdue Global Security and Defense Innovation Symposium "Effect of Manufacturing Method on Dynamic Friction of Energetic Simulants"

- 2017 Society of Experimental Mechanics Annual Conference "Dynamic Friction Studies of Soft Composite Materials"